HIGH-TEMPERATURE LM CATHODE ION THRUSTERS

FINAL REPORT

5 FEBRUARY 1968 THROUGH 15 APRIL 1969

CONTRACT JPL 952131

BY

J. HYMAN, JR., W. O. ECKHARDT, J. R. BAYLESS

J. A. SNYDER, AND J. W. PFEIFER

HUGHES

HUGHES AIRCRAFT COMPANY

RESEARCH LABORATORIES

MALIBU, CALIFORNIA

90265

H U G H E S R E S E A R C H L A B O R A T O R I E S
M a l i b u, C a l i f o r n i a

a division of hughes aircraft company

HIGH-TEMPERATURE LM CATHODE ION THRUSTERS

Final Report
5 February 1968 through 15 April 1969
Contract No. JPL 952131

J. Hyman, Jr., W.O. Eckhardt,
J.R. Bayless, J.A. Snyder, and
J.W. Pfeifer
Plasma Physics Department

Performed for

Jet Propulsion Laboratory
California Institute of Technology

Sponsored by

National Aeronautics and Space Administration
Contract NAS 7-100 (Task Order No. RD-26)

This work was performed for the Jet Propulsion Laboratory, California Institute of Technology, sponsored by the National Aeronautics and Space Administration under Contract NAS7-100.

"This report contains information prepared by the Hughes Research Laboratories under JPL subcontract. Its content is not necessarily endorsed by the Jet Propulsion Laboratory, California Institute of Technology, or the National Aeronautics and Space Administration."

ABSTRACT

A thermally integrated 30-cm LM cathode thruster and a 20-cm thruster employing an externally cooled LM cathode have been developed under Contract JPL 952131 along with an LM cathode neutralizer and components of a liquid-mercury feed system. Over-all efficiency η_T = 72.6% is achieved by the 30-cm LM cathode thruster system at beam current I_B = 1.155 A and specific impulse $I_{sp,eff}$ = 3990 sec. The system includes a single-capillary-fed thermally integrated LM cathode, a liquid-mercury high-voltage isolator, an EM pump, and an LM cathode neutralizer. When fully optimized, the thruster achieves a mass utilization efficiency η_m = 84% with a total source energy per ion V_S = 250 eV/ion. The LM cathode reaches normal operating temperature ($\sim$ 200°C) by a balance between discharge heating and cooling by radiation from the thruster body. The LM cathode neutralizer operates at a mass flow fraction $\sim$ 3% with a total coupling voltage to the beam collector $\sim$ 30 V. (No trace of erosion due to the neutralizer has been observed after 50 hours of operation.) With the 20-cm thruster, neutral flow-rate equivalent (I_a) was throttled (at a beam voltage V_B = 2 kV) from 760 mA to 414 mA with a fixed ratio of discharge current to beam current I_K/I_B = 10. Mass utilization efficiency varied with neutral flow rate within the range 78% < η_m < 92%, and η_m reached its maximum at I_a = 540 mA. In a radial-field configuration, the 20-cm thruster generated a beam I_B = 1 A at V_B = 2 kV with V_S = 356 eV/ion at η_m = 98%.

TABLE OF CONTENTS

LIST OF ILLUSTRATIONS

SECTION I

INTRODUCTION AND SUMMARY

Upon completion of the subject contract effort, a major milestone has been reached with the demonstration of efficient operation of a 30-cm thermally integrated liquid-mercury (LM) cathode thruster. In its thermally integrated configuration, the LM cathode is maintained at normal operating temperature by a balance between discharge heating and cooling by radiation from the thruster body. The level of technology demonstrated under the current effort has been established during a continuing program of LM cathode research and development which started with the invention of this cathode type in 1962.* The current program benefitted extensively from prior experimental advances in the operation of thrusters with oxide-coated cathodes at the Jet Propulsion Laboratory (JPL) and the Lewis Research Center (LeRC), and from earlier work at the Hughes Research Laboratories (HRL) with ion thrusters employing both oxide-coated and LM cathodes.

The LM cathode is a force-fed liquid-metal pool cathode which is gravity independent. The volume of liquid metal which is exposed to the discharge is sufficiently small that it is able to maintain its integrity by cohesive forces, and it is held in place by adhesive attachment to a pool-keeping structure which is placed within the solid metal cathode body. In the ion thruster application of this cathode, removal of mercury atoms from the liquid mercury surface is used to feed expellant into the discharge chamber. The most favorable results have been obtained with molybdenum pool-keeping structures of divergent-nozzle geometry. A major advantage of the divergent geometry is that it automatically stabilizes the liquid metal surface at that level in the pool-keeping structure at which the rate of removal of metal atoms from the pool surface is exactly balanced by the expellant feed rate to the pool, which is set at the value desired for thruster operation. Should the surface move downstream of its equilibrium position, the increased area of the pool surface results in an increased rate

*W.O. Eckhardt, "Liquid-Metal Arc Cathode with Maximized Electron/Atom Emission Ratio," U.S. Patent pending.

evaporation of metal atoms, thereby returning the exposed surface toward its equilibrium position. Should the level recede from its equilibrium value, the resultant decreased rate of evaporation likewise acts to stabilize the level.

During preceding contracts, components of the thruster system have each undergone separate development. Under Contract NAS 3-6262 the feasibility of LM cathode thruster life in excess of 10^4 hours was demonstrated at HRL, where a 20-cm thruster equipped with a circular LM cathode was successfully tested for an accumulated 4,000 hours. Following this test, no erosion of the molybdenum cathode structure was evident, and no degradation of cathode performance had occurred. Furthermore, remarkable time invariance of cathode and thruster characteristics was demonstrated. In a 500-hour extension of the same life test, the LM cathode neutralizer demonstrated a lifetime capability much in excess of that period of time.

Development of high-temperature LM cathodes began at HRL under Contract NASW-1404 after it became apparent from thermal analysis that combining thrusters in peripheral or clustered arrays results in the requirement for an equilibrium thruster-shell temperature on the order of 200°C for the operation of any electron-bombardment ion thruster where heat rejection is accomplished by radiation from the thruster shell alone. Thus, LM thruster cathodes rejecting waste heat from the thruster shell must operate at a temperature on the order of 200°C. Operation of LM cathodes at high temperature has stressed the use of an annular rather than circular geometry for the pool-keeping structure. The ratio of the mercury pool perimeter to the discharge current is much greater for the former geometry than for the latter, so that the annular cathode can more easily dissipate discharge heat losses from the mercury pool. An annular LM cathode developed under Contract NASW-1404 was capable of operating at a cathode body temperature T_K = 300°C with a specific heat load from the discharge $V_{K,th} = 7.5\ W \cdot A^{-1}$.

Under the subject contract, the magnetic field configuration of an already existing 20-cm diameter thruster was modified to resemble (to a first approximation) that of the 15-cm diameter LeRC SERT II thruster. Using the existing low-perveance ion extraction system, the modified thruster has been operated at a beam voltage V_B = 6 kV ($I_{sp,eff}$ = 6,600 sec) typically at a beam current I_B = 550 mA with a total source energy per ion V_S = 250 eV/ion* at a mass utilization efficiency η_m = 85%.

*V_S, the total source energy per ion, is the discharge energy per ion, because no heater, vaporizer, or keeper power is required with the LM cathode.

Without further modification, the same 20-cm thruster has also been operated at a beam voltage V_B = 2 kV ($I_{sp,eff}$ = 3590 sec) typically at a beam current I_B = 480 mA with the total source energy per ion V_S = 280 eV/ion at a mass utilization efficiency η_m = 80%.

For interplanetary missions utilizing solar-electric-propulsion, it is necessary to vary the power consumption of individual thrusters to match the solar panel output. At a given specific impulse, the magnitude of the beam current can be throttled below its nominal value by decreasing the mercury flow rate. Under this contract, the capability of ion-beam throttling has been demonstrated with the 20-cm LM cathode thruster. At a beam voltage V_B = 2 kV, the ion beam current (I_B) was throttled from I_B = 580 mA to I_B = 320 mA. With the ratio of discharge to beam current held constant at I_K/I_B = 10 throughout this variation, the beam current increased with increasing neutral flow-rate equivalent (I_a) such that the mass utilization efficiency ($\eta_m = I_B/I_a$) varied between 78% and 92%, with the maximum η_m occurring at I_a = 540 mA.

On the basis of the operating experience gained with the 20-cm thruster, sufficient information was generated for the development of a 30-cm LM cathode thruster which combines the proven experimental advances in discharge chamber efficiency with the features of thermal integration of the LM cathode, low specific impulse operation, and low over-all weight. This thruster weighs approximately 6 kg and incorporates a high-temperature LM cathode, a thermally conductive aluminum backplate, and a 0.076 cm thick screen electrode with 68% open area; the accel electrode is 0.254 cm thick. In the thermally integrated configuration, the LM cathode body temperature is maintained at 200°C by a balance between discharge heating and cooling by radiation from the thruster shell. Operating at a beam voltage V_B = 2 kV (I_{sp} = 3800 sec), typical performance is characterized by a source energy per ion V_S = 250 eV/ion at a mass utilization efficiency η_m = 85% and a beam current I_B = 1.35 A.

Under a previous contract (Contract NAS 3-9703) a 15-cm hollow-cathode thruster was operated with a predominantly radial magnetic field configuration. On the basis of the performance of that thruster, a 20-cm radial-field thruster using an LM cathode was assembled and tested as part of the current effort. The ion extraction electrodes, electromagnets, and outer body of the existing 20-cm thruster served as a basic structure, which was modified by the addition of suitable components to establish

the radial-field configuration. At a beam voltage V_B = 2 kV ($I_{sp,eff}$ = 4,400 sec), a beam current I_B = 1 A was obtained at a mass utilization efficiency of η_m = 98% with a total source energy per ion V_S = 353 eV/ion.

Development of LM cathode thrusters has been complemented by a program of research and development of the other components necessary for a complete thruster system. An LM cathode neutralizer has been operated (under laboratory conditions) at an electron-to-atom ratio $K_e/K_a \sim 200$ with a current of 1.9 A and a diode discharge voltage $<^a$30 V. In conjunction with thruster operation, the LM cathode neutralizer has been operated typically with a mass flow fraction of $\sim$ 3% and a total coupling voltage (i.e., coupling voltage to the beam collector) of 30 V. No trace of erosion of either the neutralizer or the accel electrode has been observed after 50 hours of thruster operation. Techniques have been firmly established for the design and fabrication of high-temperature annular LM cathodes for discharge chamber applications. At a cathode body temperature T_K = 200°C, the quantity of heat delivered by the discharge to such cathodes is sufficiently small (3.8 W/A discharge) to permit its radiant dissipation from the shell of a light weight thruster. Using a liquid-mercury high-voltage isolator, satisfactory LM cathode discharge operation has been demonstrated under conditions of high voltage isolation at up to 4.5 kV. A single-capillary mercury flow impedance has been developed; liquid mercury flow-rate equivalent can be varied continuously from 50 mA to 5 A by changes in mercury driving pressure.

SECTION II

THERMAL INTEGRATION OF THE LM CATHODE

Within the past several months, a major milestone in the development of LM cathode thrusters has been reached with the demonstrated efficient operation of a 30-cm thruster with a thermally integrated LM cathode. The basic features of a 30-cm thermally integrated LM cathode thruster design are displayed schematically in Fig. 1. When thermally integrated with the body of the thruster, the LM cathode achieves thermal equilibrium through a balance between discharge heating and cooling by radiation from the thruster body.

A quantity of thermal power ($P_{K,th}$) is lost to the LM cathode from the discharge in normal operation. This power has been measured and found to be proportional to discharge current (I_K), a relationship which gives rise to the definition of a quantity $V_{K,th} = P_{K,th}/I_K$, the specific thermal load. As shown in Fig. 2 the specific thermal load of a typical high-temperature LM cathode varies with the operating temperature (T_K) of the cathode body. For an electron-to-atom ratio $K_e/K_a = 6.3$ (corresponding to a ratio of discharge to beam current $I_K/I_B = 7$, typical of that required to operate the 30-cm LM cathode thruster at a mass utilization efficiency $\eta_m = 90\%$), the specific thermal load has a value $V_{K,th} = 3.8$ W/A at a cathode body temperature $T_K = 200°C$. For the thruster operating at a beam current $I_B = 1$ A, the cathode heating power is $P_{K,th} = 27$ W. Since this thermal power is small compared with the total source power of 270 W (resulting from the source energy per ion $V_S = 270$ eV/ion at $\eta_m = 90\%$), radiant dissipation to space of cathode heat is accomplished readily so long as the thruster surfaces which radiate this cathode heat are not coupled too strongly with those radiating the remaining loss portion of the source power. The design shown in Fig. 1 accomplishes the goal of decoupling the separate heat sources by collecting the bulk of the source power on thermally conducting anode surfaces and dissipating the anode heat directly by radiation to space from an external anode connector which has only weak thermal coupling with the remainder of the thruster body.

The anode is attached to an external connector by a series of leadthroughs consisting of short aluminum rods which pass through insulating ceramic sleeves. These leadthroughs serve

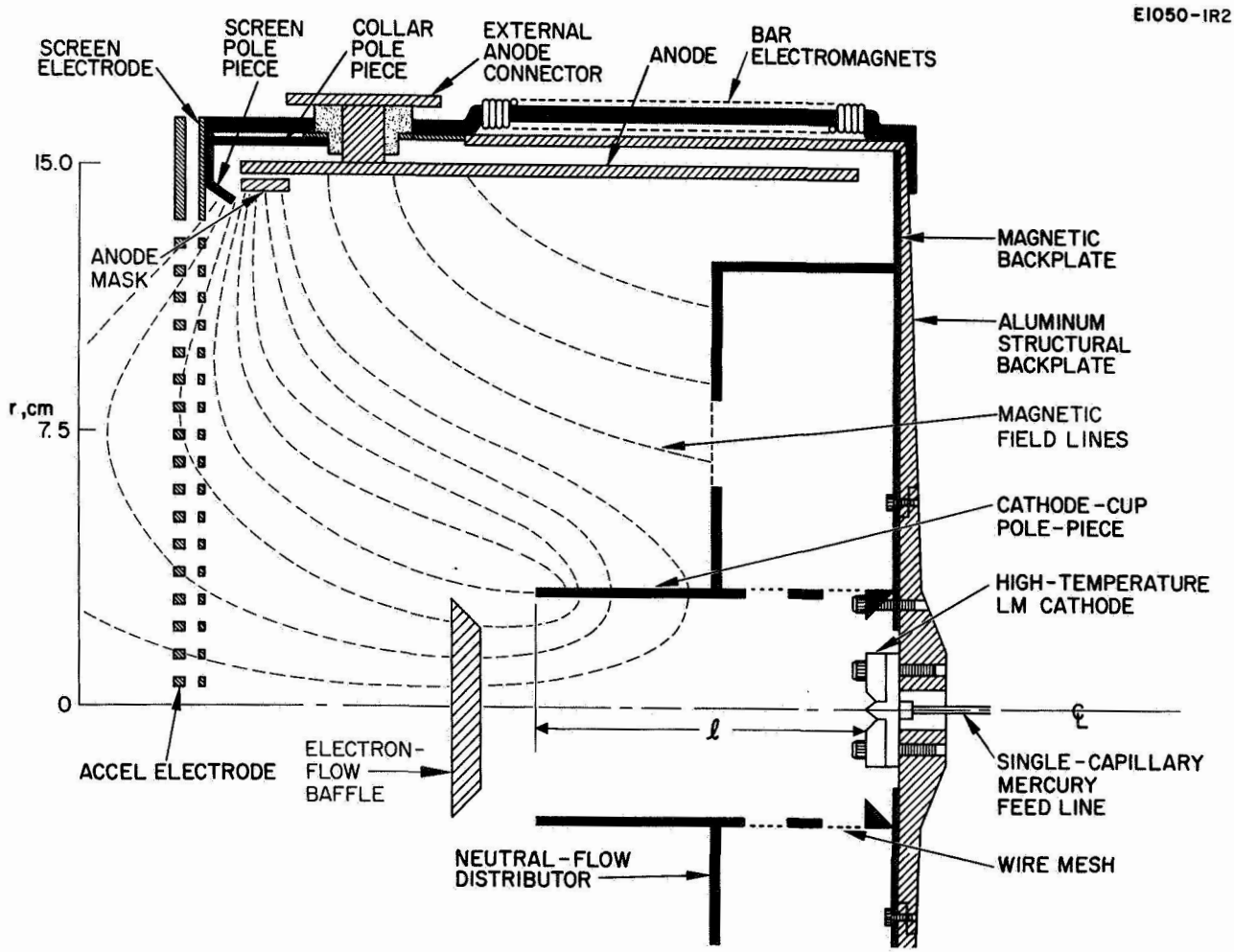

Fig. 1. Schematic drawing of the 30-cm thermally integrated LM cathode thruster.

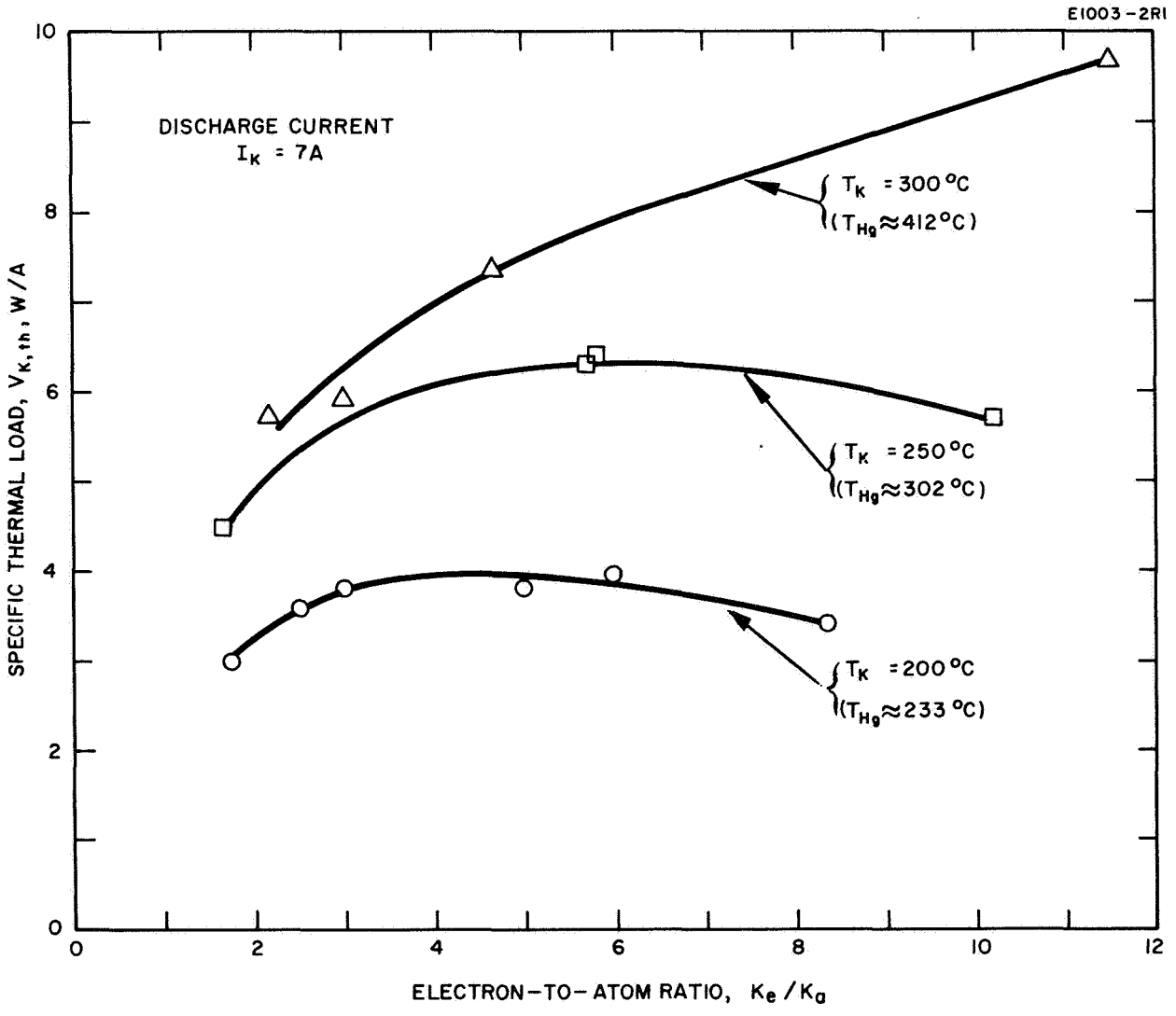

Fig. 2. Dependence of the specific thermal load ($V_{K,th}$) on cathode temperature (T_K) for high-temperature LM cathode K-25-V.

the dual purpose of connecting the anode to the external electrical circuits, while also passing on to the external connector the discharge heat which is delivered to the anode. The anode heat ($P_{A,th}$) (which has been assumed to constitute the major fraction of the total source power) is dissipated by radiation to space from the outer surface of the external anode connector and through the apertures of the ion extraction system.

The cathode heat ($P_{K,th}$) passes from the molybdenum body of the LM cathode directly into the aluminum backplate of the thruster. This backplate is tapered to present a uniform thermal resistance per unit radial length for heat flow from the cathode to the cylindrical aluminum side wall of the thruster which continues the thermal path forward to the upstream edge of the external anode connector. Downstream of this position, the thruster body is constructed of a thin cross section to reduce the conductive coupling between the cathode and anode thermal circuits. A light weight iron backplate lies over the inner surface of the aluminum structural backplate to complete the magnetic circuit from the cathode-cup pole piece to the bar electromagnets. Rather than employ a single iron sheet of the minimum thickness required to link the magnetic flux, the magnetic backplate consists of several thinner iron sheets. These sheets provide heat shielding to further reduce the radiant coupling between the anode and cathode thermal circuits. As requirements dictate, the coupling can be reduced still further by placing heat shields between the anode and the inside surfaces of the aluminum thruster body.

The thickness of the aluminum structure was chosen as a compromise between the opposing requirements for good thermal conduction between cathode and thruster side wall on the one hand, and a desire for light weight on the other hand. In the case of the 30-cm thruster, the cylindrical wall was fabricated to a thickness of 0.150 cm. The aluminum backplate has a thickness of 0.150 cm where it joins with the cylindrical wall, and increases in thickness inversely with the radius (to maintain uniform thermal resistance per unit radial length) up to the point of attachment of the LM cathode. With this design, the weight of the total thruster, including its ion-extraction system, is about 6 kg.

It is apparent that the heat flux to the cathode ($P_{K,th}$) is reduced by improvements in discharge chamber performance. This can be illustrated by noting the dependence of discharge current (I_K) on beam current (I_B), discharge voltage (V_D), and total source energy per ion (V_S):

$$I_K = \frac{I_B}{V_D} V_S .$$

Combining this expression with the power relationship quoted earlier in this section, we have

$$P_{K,th} = \left(\frac{V_{K,th} I_B}{V_D} \right) V_S .$$

If all parameters within the brackets remain constant, the cathode heating power decreases directly in proportion to reductions in the total source energy per ion.

In addition, recent discharge-chamber performance improvements with the LM cathode thruster have been accompanied by increases in V_D and (because of the resulting reduction in discharge current demand) by decreases in T_K and hence $V_{K,th}$. Both effects lead to further reductions of $P_{K,th}$. All these decreases in cathode heating permit proportional decreases in the thickness of the conducting aluminum thruster shell, thus leading to reductions in over-all thruster weight.

SECTION III

LM CATHODE THRUSTER DEVELOPMENT

A. INTRODUCTION

The expected value of source energy per ion (V_S) is a determining parameter in the structural design of a thermally integrated LM cathode thruster, because (as explained in the preceding section) the weight of the thermally conductive structure scales with the value of this performance parameter. Prior to the onset of the present effort, no program of LM cathode thruster optimization had been pursued since November 1966. Meanwhile, programs conducted at the LeRC to optimize the 15-cm SERT II thruster[1] for operation with the oxide cathode[2] and the hollow cathode[3] had both achieved significant success in reducing discharge-chamber losses. Because no equivalent data were available for operation of the LM cathode in a similarly optimized thruster, a program of research and development was undertaken at HRL to optimize the electron-bombardment thruster for operation with the LM cathode.

Previously, as reported in Ref. 4, a 20-cm LM cathode thruster had been operated typically at a beam voltage V_B = 6 kV. With a beam current I_B = 680 mA, a mass utilization efficiency η_m = 87% was achieved with a total source energy per ion of V_S = 400 eV/ion. At the discharge voltage V_D = 33 V (typical of operation at that time), this data point corresponds to a ratio of discharge current to thruster beam current $I_K/I_B \sim 12$, and to a specific thermal load $V_{K,th} \sim 5.8$ W/A at T_K = 250°C.

With the present 30-cm LM cathode thruster, the source energy per ion has been reduced to $V_S \sim 250$ eV/ion at η_m = 84% and the optimum discharge voltage has risen to a value $V_D \sim$ 40 V. The ratio of discharge current to beam current therefore has been reduced to a value $I_K/I_B \sim 6$, while T_K has dropped to 200°C and $V_{K,th}$ to $\sim$ 3.8 W/A. With this higher level of optimization only about one-third of the previous power per unit beam current is delivered to the cathode.

B. 20-CM THRUSTER

As a first step in the program to optimize the performance of the electron-bombardment thruster for operation with the LM cathode, the existing 20-cm diameter thruster[4] was modified to conform (in first approximation) to the magnetic field geometry of the LeRC 15-cm SERT II thruster. The modified configuration of this thruster is shown schematically in Fig. 3, which is drawn approximately to scale. It was equipped with a magnetic collar and with both screen and cathode-cup pole pieces to reproduce the desired magnetic field profile. A baffle was placed downstream of the cathode pole piece at a variable axial distance (d). The exact configuration of this baffle was modified in a series of separate experiments. The cathode was placed at a variable axial distance (ℓ) behind the mouth of the cathode pole piece. All of the propellant was fed through the cathode, in contrast to the technique used in the SERT II thruster.

1. Zone-Baffle Design

The design of the baffle configuration was guided by the magnetic shadow technique which was enunciated during the previous effort in thruster optimization[5] in which the use of a zone baffle was introduced for the purpose of selectively distributing the electron and atomic flux within the discharge chamber. With the magnetic shadow technique, a disk baffle (with or without apertures) is placed downstream of the cathode, so that electrons streaming around the baffle perimeter or through the apertures emerge on and follow magnetic field lines which intersect the screen electrode at radii selected to yield maximum over-all thruster performance. A further function served by the baffle (which became clear in other studies[3,4] and during the current effort) is to constrict the passage of electron flux from the cathode to the discharge chamber. Within certain limits (to be discussed later), this permits the discharge voltage to be raised to any desired level, thus allowing an independent choice of discharge voltage as a parameter in thruster optimization.

2. Discharge-Chamber Optimization

The program of discharge-chamber optimization with the 20-cm thruster was brief but successful. Only two changes were made in the baffle design prior to choosing a zone-baffle

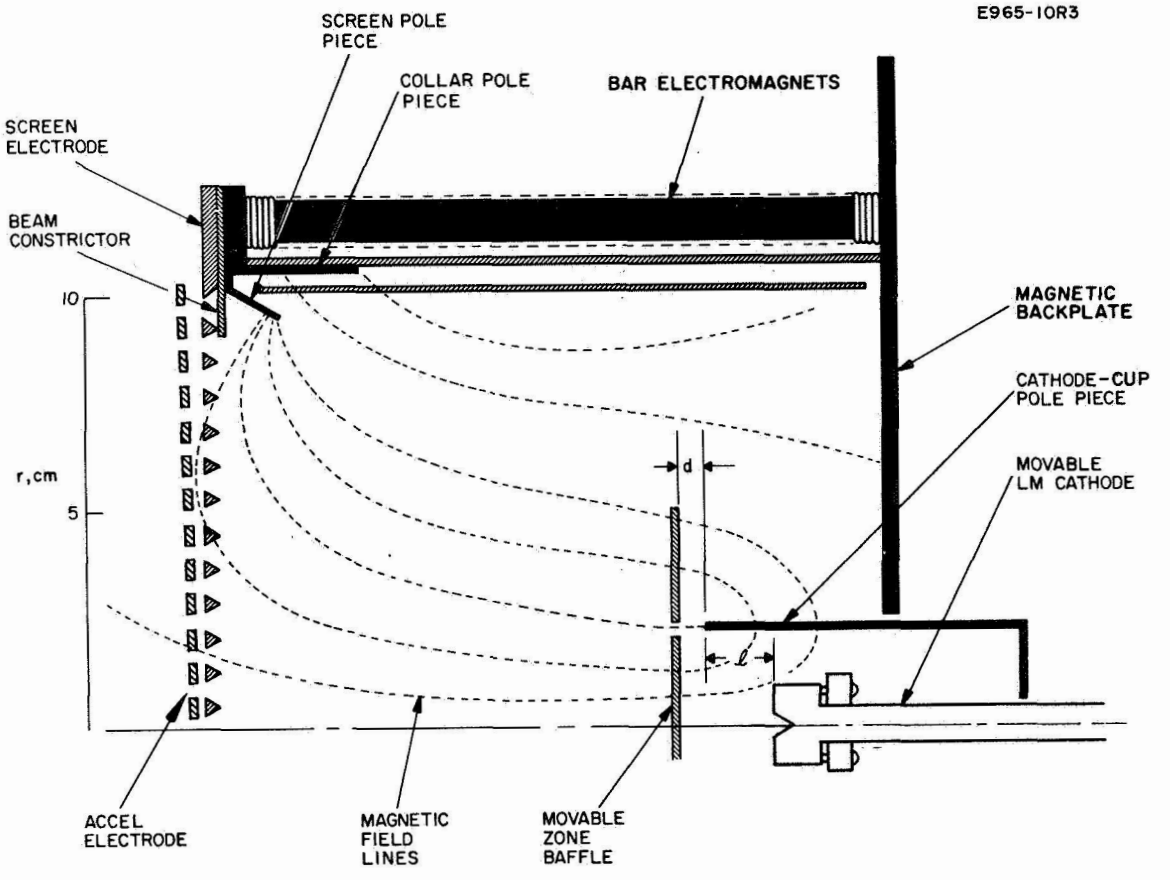

Fig. 3. Modified 20-cm LM cathode thruster.

configuration which was considered to provide a sufficiently high level of performance. The zone baffle consisted of a central circular disk surrounded by a coaxial and coplanar annular disk. Both disks were fabricated from 0.152 cm thick, nonmagnetic stainless steel. The central disk had a diameter of 4.42 cm, which was 0.3 cm smaller than the inside diameter of the cathode-cup pole piece. The annular outer zone of the baffle had an inside diameter equal to that of the cathode-cup pole piece, and an outer diameter of 10 cm. The purpose of the central disk is to define the radial position and cross-sectional area for electron escape from the cathode-cup pole piece, whereas the outer annular zone of the baffle serves to better distribute the neutral particle flow. This design permits some independent variation of the flow conductances (between cup region and main discharge chamber) for electrons on the one hand and for propellant atoms on the other hand; the electrons, constrained by the magnetic field, pass predominantly through the radial gap between cup and baffle, while the propellant atoms flow also behind the outer annular zone to the mid-radius of the discharge chamber.

The only other thruster modification which led to a significant enhancement of thruster performance was the installation of a nonmagnetic beam mask. This was placed upstream of the screen electrode, to restrict the beam diameter to 18 cm in order to reduce the loss of neutral particles from the outermost apertures of the ion beam extraction system. These apertures were partially shielded from the plasma by the screen pole piece and could not be expected to produce intense beamlets, but were nonetheless able to permit a significant escape of neutral particles from the discharge chamber. This modification alone resulted in a 3-1/2% increase in the maximum obtainable propellant utilization efficiency.

Optimum performance was observed with the baffle placed 1 to 2 mm downstream of the lip of the cathode pole piece. The discharge voltage was maintained at an optimum value $V_D \sim 35$ V, which was set by adjustments of the baffle position and of the magnetic field intensity. Within the range $1 \text{ cm} < \ell < 3 \text{ cm}$, performance was not critically dependent on the position of the cathode within the cathode-cup pole piece, but degraded significantly beyond those limits. For optimum performance the magnetic field intensity had a value $B \sim 30$ G on the axis at the midplane of the discharge chamber.

3. Thruster Performance

As a result of the modifications described above, the discharge-chamber performance was improved significantly above the level reported in Ref. 4, as can be seen by inspection of the data in Fig. 4. To provide a comparison with earlier data, the newly modified 20-cm thruster was initially operated at a beam voltage V_B = 6 kV. At a beam current I_B = 510 mA with a mass utilization efficiency η_m = 87% the total source energy per ion was reduced to V_S = 260 eV/ion. Still using the existing low-perveance ion extraction system, the beam voltage was reduced to V_B = 2 kV ($I_{sp,eff}$ = 3,590 sec). With the accel electrode biased at $V_{Ac} \cong -3$ kV, a beam current I_B = 480 mA was produced at a source energy per ion V_S = 280 eV/ion with a mass utilization efficiency η_m = 80%. Ion beam interception by the accel electrode was less than 1%.

On the basis of these preliminary data the design was judged to be sufficiently improved to warrant further documentation of the performance characteristics over a range of thruster operating conditions. Beam voltage was the first parameter to be varied from V_B = 6 kV to V_B = 1.5 kV, while holding the mercury flow-rate equivalent constant at a value $I_a \sim 600$ mA. Next the beam voltage was set at V_B = 3 kV while the mercury flow-rate equivalent was varied from $I_a \simeq 370$ mA to $I_a \simeq 750$ mA. Performance obtained under both of these variations was optimized point by point with respect to baffle position (d) and the magnetic field intensity (B). When the overall operating characteristics of the modified thruster were established, the beam voltage was set at V_B = 2 kV, and the baffle position and magnetic field intensity were set at fixed values which optimized thruster performance over a wide range of mercury flow rate. Under these fixed conditions, the mercury flow rate equivalent was throttled from I_a = 760 mA to I_a = 410 mA while the ratio of discharge current to ion beam current was held at a fixed value I_K/I_B = 10. The results of these variations are described below.

a. Variation of the Beam Voltage

An interaction exists between thruster discharge-chamber performance and the conditions of ion beam extraction. As discussed by Hyman, et al.,[6] the interaction should depend on the total ion accelerating voltage $V_T = (|V_B| + |V_{Ac}|)$, rather than on the beam voltage alone. An experiment was performed to demonstrate this characteristic of the interaction. Using the same beam extraction system, thruster performance

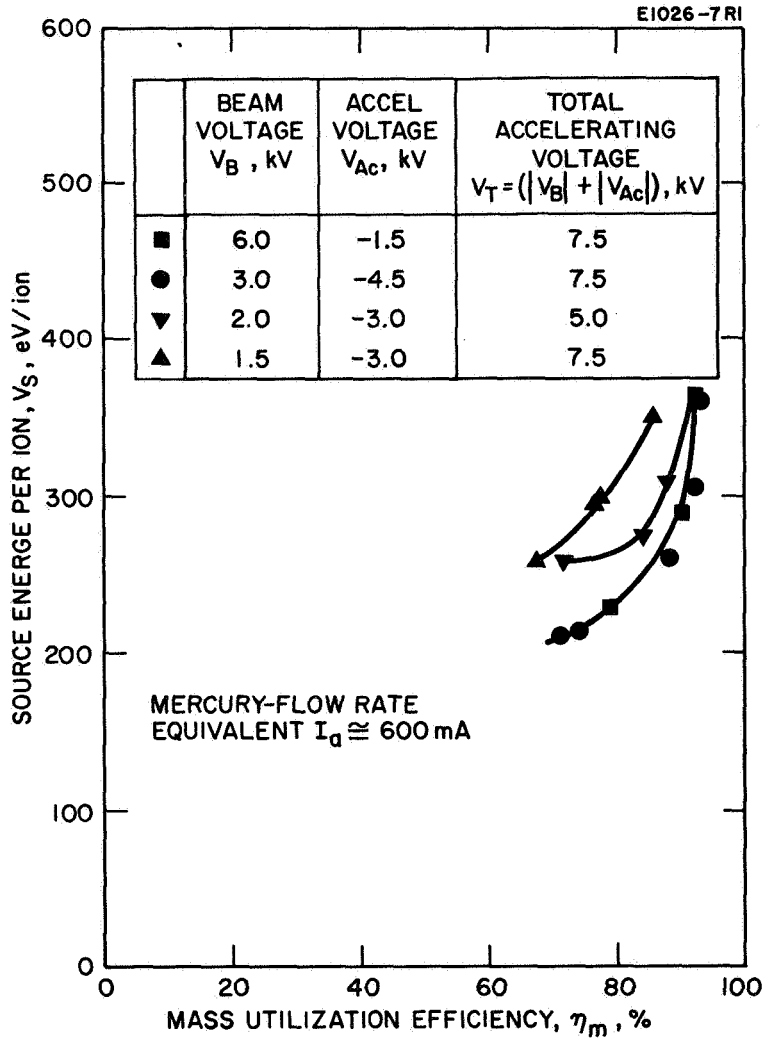

Fig. 4. Discharge-chamber performance of the 20-cm LM cathode thruster for four sets of ion-accelerating potentials.

was compared for two different conditions of ion beam extraction which both utilize a total accelerating voltage V_T = 7.5 kV: first for a beam voltage V_B = 6 kV ($I_{sp,eff} \leq$ 8,050 sec) with an accel voltage V_{Ac} = - 1.5 kV, and then for V_B = 3 kV ($I_{sp,eff} \leq$ 5,500 sec) with V_{Ac} = - 4.5 kV. In both cases the source energy per ion (V_S) was measured as a function of the mass utilization efficiency (η_m) with the mercury flow-rate equivalent set at $I_a \sim$ 600 mA. The data (shown in Fig. 4) demonstrate that, as anticipated, thruster performance was nearly identical for the two conditions of ion-beam extraction. Other data shown in Fig. 4 illustrate the manner in which discharge-chamber performance does vary with variations in the total accelerating potential. In general a given value of mass utilization efficiency is achieved with lower discharge-chamber power expenditures as the total ion-accelerating potential is increased. At a beam voltage V_B = 2 kV ($I_{sp,eff}$ = 3,590 sec) with a total accelerating voltage V_T = 5 kV, the discharge losses rise to V_S = 280 eV/ion at a mass utilization efficiency η_m = 80% and a beam current I_B = 480 mA. Thus, for a constant electrode geometry the total accelerating potential appears to be the major parameter which affects thruster efficiency.

No data were taken below a beam voltage V_B = 1.5 kV, because the ion current drawn to the accel electrode increased to slightly greater than 1% of I_B when V_B was reduced to 1.5 kV with V_{Ac} = -3.0 kV. To hold accel interception at less than 1% while maintaining high thruster efficiency, operation of the 20-cm thruster with its low-perveance ion extraction system was limited to $I_{sp,eff} \gtrsim$ 3,590 sec at η_m = 80%.

b. Variation of the Mercury Flow Rate

To indicate the influence of ion beam throttling on discharge-chamber performance, the source energy per ion was measured as a function of the mass utilization efficiency over a range of mercury flow rate at a beam voltage V_B = 3.0 kV and an accel electrode voltage V_{Ac} = - 4.5 kV. The experimental results are plotted in Fig. 5. At a mass utilization efficiency η_m = 80%, discharge losses vary over a range of 70 eV/ion when I_a is changed from 370 mA to 750 mA (throttled by a factor of two). The departure from the best performance V_S = 230 eV/ion (which is achieved at I_a = 600 mA) may reflect the fact that the initial optimization of this thruster had been carried out near that neutral flow rate.

To obtain the data presented above, both the magnetic field intensity and baffle position were reoptimized for each of the data points presented in Figs. 4 and 5. Throttling characteristics

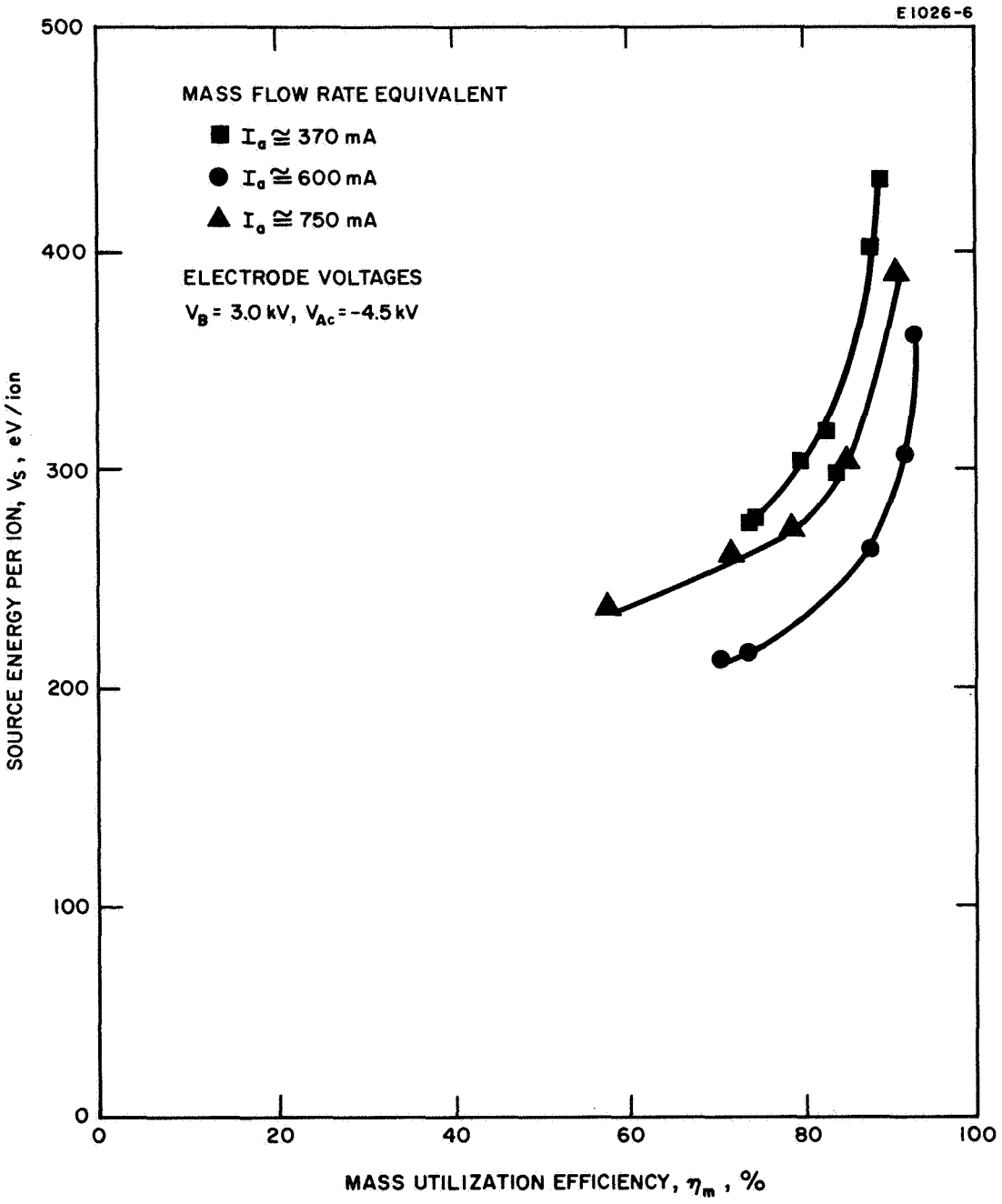

Fig. 5. Discharge-chamber performance of the 20-cm LM cathode thruster for three values of neutral mercury flow rate.

for the LM cathode thruster are presented below with the magnetic field intensity and the baffle position set at fixed values which were chosen to optimize thruster performance over a wide range of mercury flow rate.

c. Throttling Characteristics

In preparation for establishing the throttling characteristics of the 20-cm LM cathode thruster, optimum values B_o and d_o were obtained for the axial magnetic field intensity (B), measured on the axis at a point midway between the screen electrode and the lip of the cathode-cup pole piece, and for the baffle position (d). Values were chosen which were shown to be consistent with good thruster performance over a range of neutral flow-rate equivalent (I_a) from approximately 370 to 740 mA. Initial trial values of B and d were chosen first on the basis of previously obtained thruster data. Then, for several values of I_a in the desired range, the beam current was measured as the magnetic field current and baffle position were varied about their initial values. This procedure was repeated for several values of the ratio I_K/I_B. The beam current was generally very sensitive to changes in the magnetic field intensity and in baffle position; beyond certain maximum values of (B) or of (d), the beam current dropped abruptly. The results of these preliminary measurements yielded values B_o = 21 G and d_o = 2.2 mm, both of which were used for all measurements thereafter.

The throttling characteristics of the 20-cm LM cathode thruster are shown in Fig. 6 where the ion-beam current (I_B) and the discharge voltage (V_D) are plotted as functions of the mercury flow-rate equivalent (I_a), for a fixed ratio of discharge to beam current I_K/I_B = 10. Data were obtained throughout a range of neutral flow-rate equivalent from 414 to 760 mA. Within this range, the beam current (I_B) increases with increasing neutral flow rate equivalent such that the mass utilization efficiency ($\eta_m = I_B/I_a$) lies between 78% and 92%, with the maximum η_m occurring at I_a = 540 mA. The discharge voltage decreases with increasing mercury flow from V_D = 44 V at I_a = 414 mA to V_D = 32 V at I_a = 760 mA. Below the mercury flow-rate equivalent I_a = 414 mA, the discharge is difficult to maintain, and above I_a = 760 mA the beam current saturates and I_B no longer increases with increasing I_a. Operating at a higher ratio of discharge to beam current (I_I/I_B > 10) does little to increase I_B.

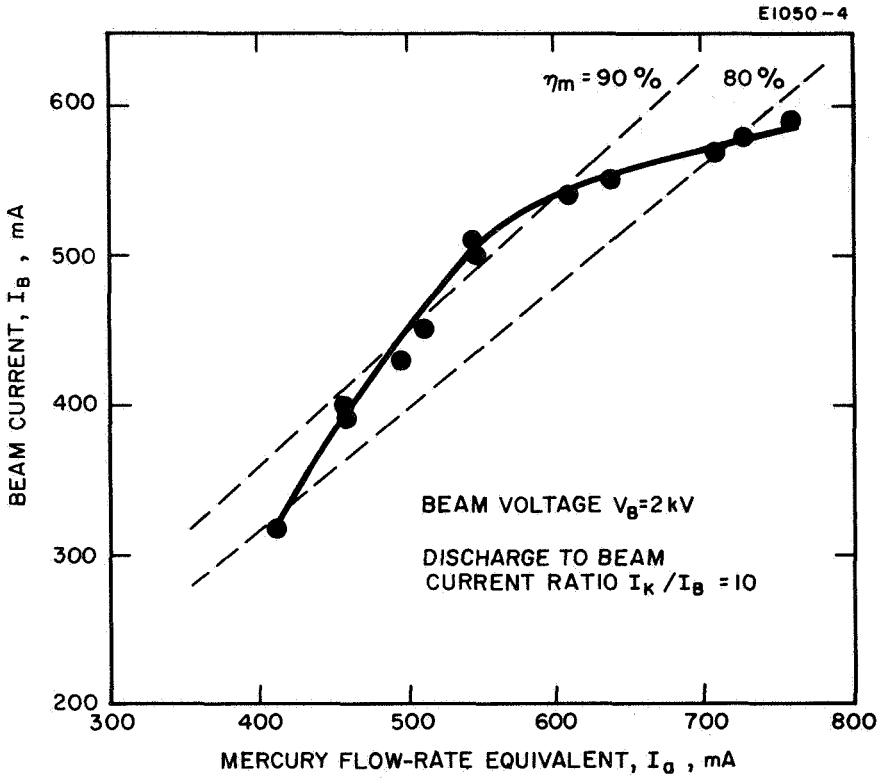

(a)

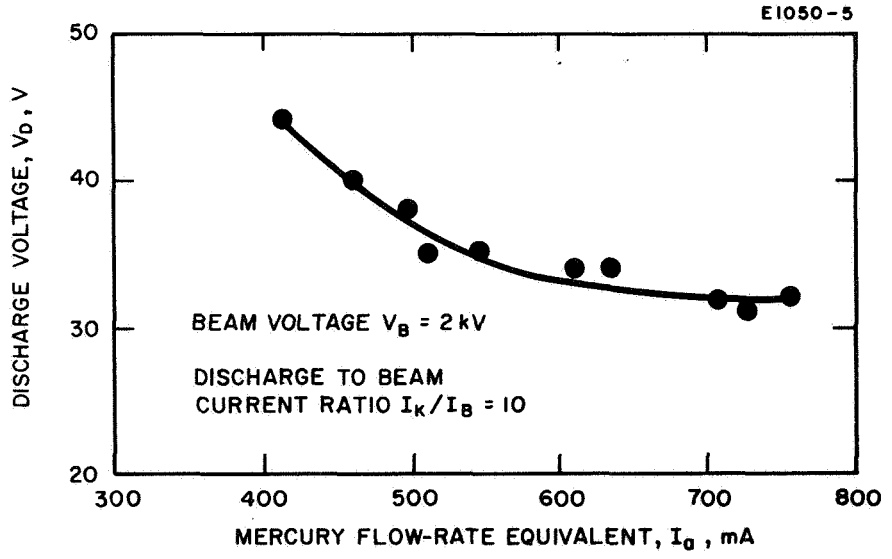

(b)

Fig. 6. Throttling characteristics of the 20-cm LM cathode thruster.

A partial explanation for the apparent saturation of ion beam current is given below in the description of the development of the 30-cm LM cathode thruster. In that development, an apparent saturation of beam current was overcome by a change in the design of the cathode-cup pole piece.

C. 30-CM THERMALLY INTEGRATED THRUSTER

The basic thermal design of the 30-cm thruster has already been described in Section II of this report. In the present section, the design is described in greater detail, particularly with respect to the choice of materials and the design of the ion extraction system. A technique is described by which an apparent saturation in beam intensity (similar to that encountered with the 20-cm thruster) was overcome by modifications in the cathode-cup pole piece. The operating characteristics of the 30-cm thruster are also reported.

1. Design of the 30-cm Thruster

a. Discharge Chamber

The design of the discharge chamber of the 30-cm LM cathode thruster borrows heavily from geometrical criteria evolved in the optimization[2,3] of the NASA 15-cm SERT II thruster at LeRC. The initial baffle geometry and operating technique were derived from the experimental development utilizing the modified 20-cm LM cathode thruster, and were then optimized by operation of the 30-cm thruster itself. A design drawing of the 30-cm thruster is shown in Fig. 7. Table I lists the thruster component parts and gives the weight of each. The total thruster weight (including LM cathode, ion extraction, electrodes, and magnets) is 6.157 kg. The anode diameter of 30 cm is twice the value used for the SERT II thruster. The cathode-cup pole piece and magnetic back plate are scaled up by the same factor. The separation between the anode and the thruster shell was not increased from the SERT II dimension. The cross section of the screen and collar pole pieces were left at the same cross-sectional dimensions used in SERT II. The decision to retain the original SERT II dimension for the screen and collar pole pieces was based on the belief that the effect of the shape of these pole pieces is significant only in the close proximity. Close to these pole pieces the curvature of the magnetic field is not significantly affected by

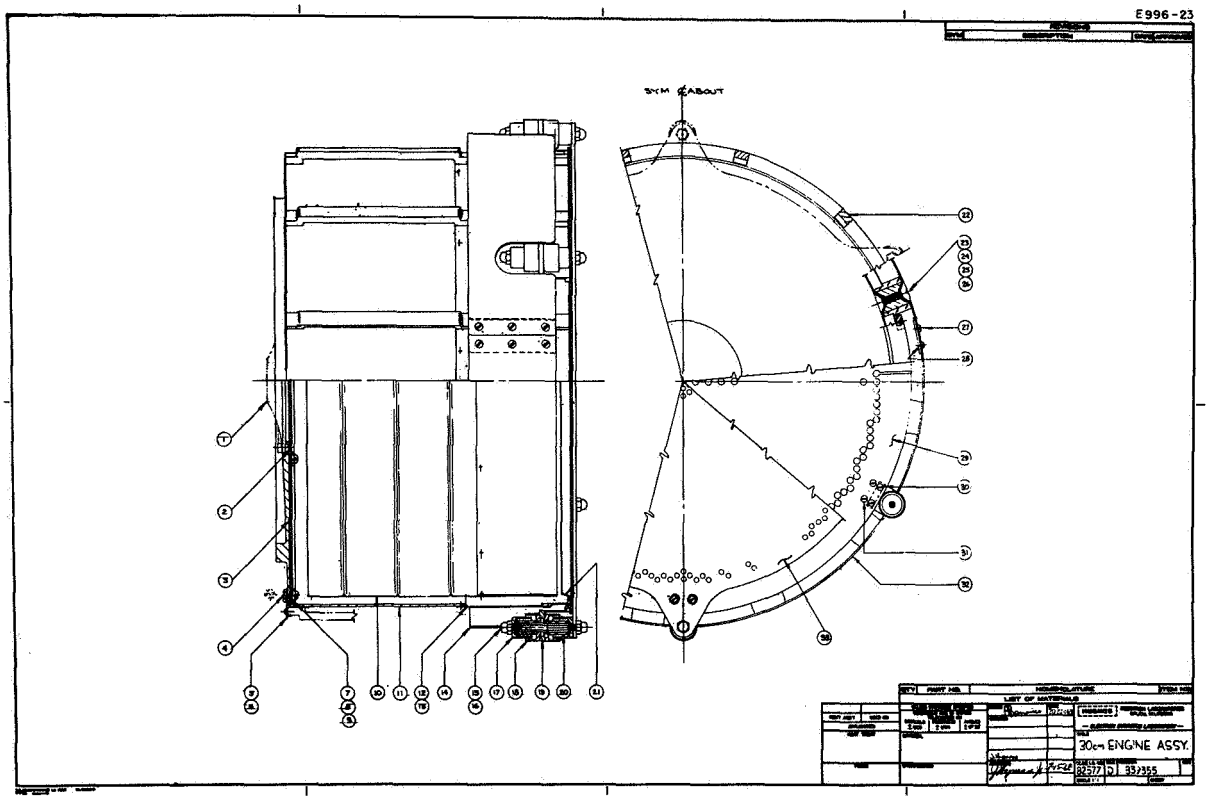

Fig. 7. Design of the 30-cm LM cathode thruster.

TABLE I

Component Weights for the 30-cm Thruster

Part Number	Title	No. Req.	Total Weight, kg
B-837977	Stud	6	0.020
B-837982	Spacer	12	0.021
D-839331	Screen electrode	1	(0.134 est.)
D-839312	Accel electrode	1	1.362
D-839313	Pole piece	1	0.299
D-839314	Back plate	1	0.650
D-839315	Anode	1	0.149
C-839316	Rear anode	1	0.257
C-839319	Lower housing	1	0.532
C-839320	Upper housing	1	0.133
B-839321	Bushing	12	0.092
B-839322	Insulator	12	0.158
D-839356	Anode connector	1	0.166
C-839357	Splice	1	0.006
C-839358-99	Outer shield	12	0.078
C-839358-98-1	Inner shield	6	0.037
C-839358-98-3	Inner shield	6	0.037
C-839359	Insul. support	6	0.066
C-839366-1	Aft pole piece	1	0.181
C-839366-3	Aft pole piece	1	0.183
C-839367	Pole piece back plate	1	0.048
C-839368-98 -99	Mounting nut Mounting screw } per set	12	0.111
C-839369	Magnet	12	1.022
--------	Hardware, screws, etc.	--	0.074
--------	Cathode plate	1	0.194
--------	LM cathode	1	0.109
--------	Cathode-plate pole piece	--	0.038
Total	30-cm Thruster	1	6.157 kg

the thruster diameter, and thus the cross-section dimensions of the pole pieces should not be a function of the thruster diameter so long as the thruster diameter is much larger than these dimensions.

Initially the discharge chamber was designed to a length of 20 cm, even though this was 6 cm shorter than would be indicated by a direct scaling of the 15-cm LeRC SERT II design. The choice of a shorter discharge-chamber length was based on the assumption that the optimum thruster length should remain essentially constant in spite of changes in thruster diameter. The length was not set at the SERT II dimension of 12.9 cm,[2] however, to allow for some increase in the axial length of the discharge chamber which might be required to assure radial uniformity of the flow of neutral mercury into the discharge chamber. At the time this decision was made, all of the propellant was passed through the mouth of the cathode-cup pole piece of the LM cathode thruster.

As explained in Section II, the design of the 30-cm thruster employs aluminum as the major structural material. This metal was chosen for the application because of its combination of light weight and high thermal conductivity, which together have resulted in the design of a light-weight thermally integrated thruster. The decision to employ aluminum for fabrication of the 30 cm thruster was made with the understanding that under certain conditions in air mercury is known to attack aluminum in a highly destructive manner. The literature[7] indicates, however, that alloys of aluminum with low silicon content have shown good resistance to such attack. Experience at HRL[8-10] led to the choice of low silicon content 6061 aluminum alloy as the major structural material for thruster fabrication. To date, no mercury attack has been observed in the 30-cm thruster after 100 hours of operation and 4,000 total hours of exposure to mercury.

b. Ion Extraction System

Design of the 30-cm ion extraction system was based on information derived from various sources. Kramer and King[11] reported on an ion optical system suitable for extracting dense ion beams from gas discharges. Using the technique described by Hyman, et al.,[6] they studied the beam-forming characteristics of their chosen geometries by using an automatic charged-particle trajectory tracer with space-charge simulation. These studies were confirmed by experimental measurements which showed that several of the ion extraction systems being studied operated satisfactorily over a wide range of mercury-ion beam

current densities with accelerating voltages ranging from 3 to 7 kV. In the experimental studies, the screen electrode hole diameter was 0.460 cm. Both cylindrical and countersunk screen holes were tested. The highest perveance was achieved with a pair of electrodes, separated by 0.250 cm, employing a countersunk screen electrode and an accel electrode having cylindrical holes of the same diameter.

Subsequently, Masek and Pawlik[12] operated an ion-extraction system of similar hole size with a total accelerating voltage ranging from 3.2 to 4.6 kV. The nominal screen-to-accel spacing was 0.178 cm, though data were reported for spacings as small as 0.102 cm. Initially, a screen electrode thickness of 0.254 cm was used, but significant decreases in discharge chamber losses were realized by reducing the thickness to 0.076 cm. The 0.462-cm diameter holes in the screen were not countersunk. Accel electrodes were tested with hole diameters of 0.462 cm, 0.374 cm, and 0.318 cm, with a thickness of 0.254 cm. It was found that accel impingement current increased only slightly in changing from an accel hole diameter of 0.462 cm to an accel hole diameter of 0.374 cm, whereas discharge chamber efficiency improved by 20 eV/ion. Moreover, this slight increase in impingement current was more than offset by the increase in accel electrode mass, so that the over-all electrode lifetime was expected to be a maximum at the 0.374 cm diameter.

Variations of this same basic geometry have been analyzed in a detailed computer study carried out at HRL.[13] A screen electrode with counter-sunk holes of 0.475 cm diameter was paired with an accel electrode with a hole diameter of 0.360 cm. The design value of 0.228 cm for the interelectrode spacing was varied in order to analyze the effect of stress-induced perturbation of this spacing from the design value, as it may occur during thruster operation. In one variation the electrodes were separated by a distance of 0.178 cm, the nominal separation used in the JPL studies. At this separation, the particle flow remained essentially laminar (very little crossover) and all trajectories cleared the accel electrode by a considerable margin. From this observation, it appears that considerable leeway exists for the reduction of the interelectrode spacing before direct accel interception becomes a problem, a fact which had already been demonstrated by the studies at JPL.

The configuration of the 30-cm ion-extraction system was designed on the basis of the evidence listed above. Satisfactory performance of this configuration with an LM cathode

thruster has now been demonstrated. The specifications of this design are given in Table II. Six insulating supports, mounted on the outer rim of the screen electrode, hold the accel electrode at a distance of 0.127 cm from the screen electrode.

TABLE II

Design Specifications of Ion Extraction System

Electrode	Material	Thickness, cm	Hole Diameter cm	Distance Between Hole Centers, cm	Hole Shape
Screen	Molybdenum	0.076	0.475	0.535	Cylindrical
Accel	Molybdenum	0.254	0.365	0.535	Cylindrical

c. Magnetic Circuit

The magnetic field for the 30-cm thruster can be provided either by 12 permanent bar magnets or by 12 bar electromagnets; the latter were used throughout this program in order to retain the magnetic field intensity as a parameter to be optimized. The bar electromagnets are fabricated from iron and are 20-cm long with a 1 cm x 0.5 cm cross section. The rear two-thirds section of each bar was wound with 100 turns of 20 gauge nickel-clad stranded copper wire. The electrical resistance of the 12 electromagnets connected in series is approximately 2 Ω, and for typical thruster operating conditions the joule heating amounted to 40 W. (This power loss can be reduced considerably with further optimization of the electromagnetic design.) Other elements of the magnetic circuit, illustrated in Fig. 1, are constructed from ASTM-A-7 steel and have thicknesses of approximately 0.15 cm.

The longitudinal magnetic field was measured as a function of the coil current. For typical thruster operating conditions the electromagnet coil current I_M is about 4.5 A, which results in a magnetic field intensity of approximately 14 G on the discharge chamber axis and 5 cm upstream from the screen electrode. It was also determined that the residual induction is ± 2.5 G at $I_M = 0$.

2. Thruster Performance

The 30-cm thruster is shown in Fig. 8 mounted on the vacuum chamber end plate and surrounded by a water-cooled structure which is also used to support the thruster ground screen. The thruster is thermally coupled to this structure by radiation only, while it is thermally isolated from its mounting supports. Thermal isolation from the supports is achieved by mounting the thruster on a thermal guard ring, which in turn is mounted on the vacuum chamber end plate. During thruster operation this thermal guard ring can be heated (by means of a resistance heater) to the same temperature as that attained by the thruster back plate; this assures that no heat is conducted either to or from the thruster. The thruster achieves thermal equilibrium by radiation alone, as may be required in the actual spacecraft environment.

The thruster has been operated for the most part at a beam voltage V_B = 2 kV and an accel electrode voltage V_{Ac} = -3 kV, yielding a total accelerating voltage of 5 kV. The current intercepted by the accel electrode is less than 1% of the beam current and decreases with increasing mass utilization efficiency, indicating that most of the accel electrode current arises from charge-exchange scattering rather than from direct interception. Thruster operation has been notably free of problems associated with breakdown or shorting between the screen and accel electrodes. Initially, a zone baffle was used which was similar to that shown schematically in Fig. 3 for use with a 20-cm thruster. This baffle consisted of two parts: a central disk of a diameter somewhat less than the inside diameter of the cathode-cup pole piece, and a coplanar annular piece concentrically surrounding the central disk. The annular piece had an inside diameter equal to that of the cathode-cup pole piece and an outside diameter which extended to about half of the thruster diameter. During thruster operation, the zone baffle could be moved axially to an optimum position (d) downstream of the lip of the cathode-cup pole piece.

In initial experiments, the annular gap width (g) between the baffle parts was set at $g = 0.127$ cm, a value close to that in use with the 20-cm thruster. Performance improved slightly in subsequent experiments when g was changed from 0.127 cm to 0.254 cm and finally to 0.508 cm. Typical performance was characterized by a discharge voltage V_D = 38 V,

M 6330

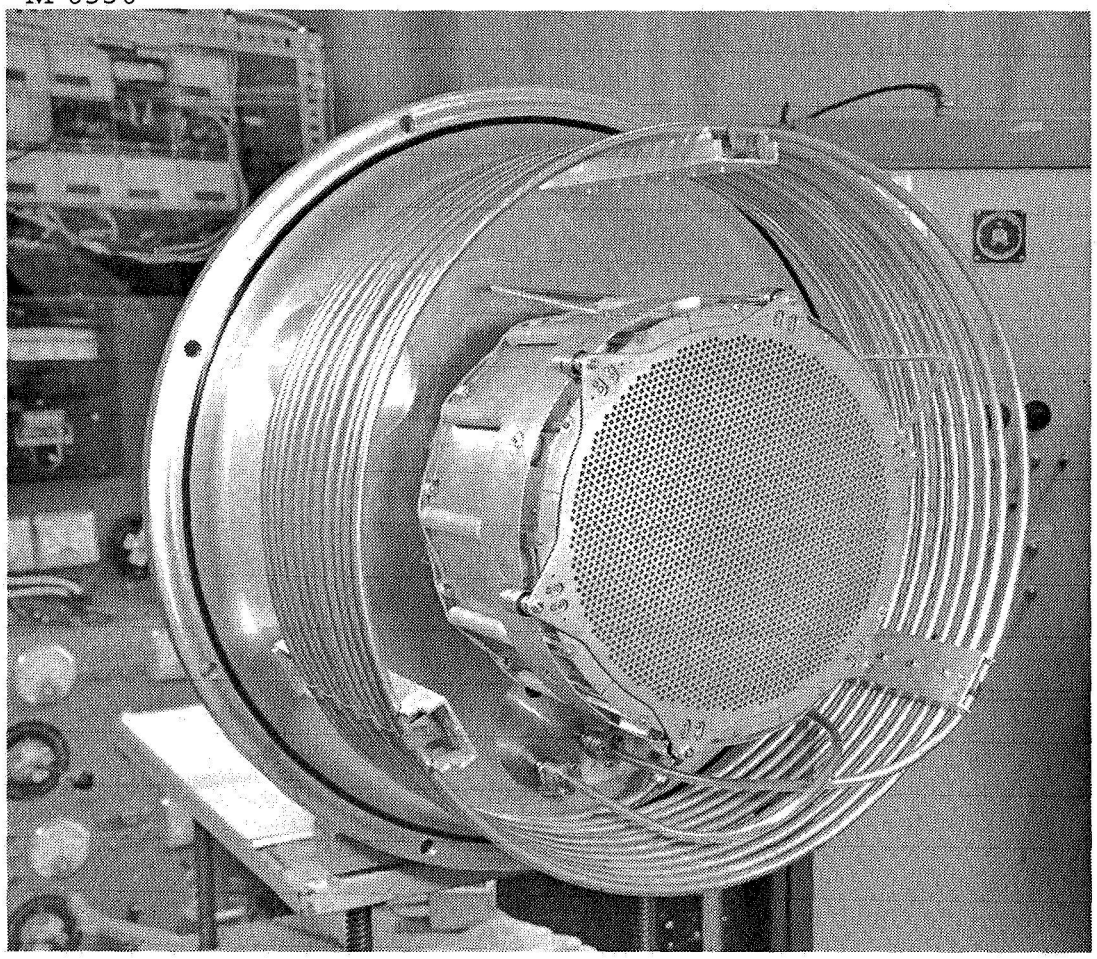

Fig. 8. Photograph of the 30-cm LM cathode thruster. (The thruster is mounted on the vacuum chamber end plate.)

and an axial magnetic field intensity B = 25 G as measured at the thruster midplane. The source energy per ion was V_S = 450 eV/ion* at a mass utilization efficiency η_m = 80%.

In a subsequent experiment, a 30-cm diameter, 1.27 cm long, stainless steel cylinder was placed over the most downstream section of the anode and was insulated from it to serve as an anode mask. This cylindrical strip could be operated at either anode or cathode potential. When at cathode potential it had the effect of electrically moving the anode away from the screen electrode by 1.27 cm. The anode mask was installed with the aim of increasing the lifetime of high-energy electrons between their emergence from the baffle gap and their capture by the anode. With a baffle having a 0.254-cm annular gap and with the anode mask operated at anode potential, as much as 70% of the discharge current was collected by the anode mask. When the mask was operated at cathode potential, the current to it dropped essentially to zero, and the characteristics of the discharge were significantly changed. In particular, the discharge voltage rose above its previous value or could be held at a given value with about 75% (B $\sim$ 14 G) of the magnetic field intensity required when the anode mask was at anode potential.

With the anode mask at cathode potential the source energy per ion was reduced to a value V_S = 330 eV/ion at a mass utilization efficiency η_m = 80%. Near this set point, performance data were obtained for three values of mercury flow-rate equivalent: I_a = 600, 750, and 1000 mA. For higher values of mercury flow rate, the ion beam showed definite signs of saturation, similar to those observed with the 20-cm thruster. This apparent saturation of the ion beam current has since been overcome, and thruster performance has been enhanced significantly by an over-all modification of the discharge chamber to the configuration shown in Fig. 1.

Several innovations from the previous discharge chamber configuration were incorporated in the design shown in Fig. 1. The over-all magnetic length of the discharge chamber has been reduced from 20 cm to 15 cm. Reduction in over-all length of the LM cathode thruster to a value close to the SERT II value[2] of 12.9 cm was made feasible by an additional modification

*V_S, the total source energy per ion, is equal to the discharge energy per ion because no heater, vaporizer, or keeper power is required with the LM cathode.

which permitted extensive post-cathode diversion of neutral mercury flow. Both modifications were accomplished without major changes in structure by the expedient of placing a thin-wall hollow iron pill-box at the upstream end of the discharge chamber. The iron pill-box is 25.4 cm in diameter and 5 cm high with a circular center cutout of 6.6 cm diameter to permit the cathode-cup pole piece to protrude through. The length of the cathode-cup pole piece was increased by 5 cm so that it projected into the active region of the discharge chamber by the same length as before. Inside the pill-box on the side walls of the elongated cathode-cup pole piece, two bands of 12 holes (each 1.19 cm diameter) were provided. These holes were covered with a 20 wire/cm stainless steel mesh which is 50% transparent for neutral particle flux. The effective open area of one band of holes could be varied continuously by a movable shutter sleeve. The other band was always operated fully open. Eight holes of 2.5 cm diameter were placed equally spaced on a 12.7-cm diameter circle surrounding the cathode-cup pole piece on the downstream surface of the hollow iron pill-box. These holes were also covered by 20 wire/cm stainless steel mesh. A movable disk baffle was provided downstream of the lip of the cathode-cup pole piece. This baffle had a conical edge (see Fig. 1) to permit continuous variation in the width of the baffle gap. The decision to reduce the over-all length of the discharge chamber toward that of the SERT II thruster was initiated by the belief that the optimum thruster length should remain essentially constant in spite of changes in thruster diameter. This belief was strongly reinforced by reports from LeRC[14,15] concerning development there of a 30-cm hollow-cathode bombardment thruster.

Although the diversion of a large fraction of the neutral mercury flow was necessary from the standpoint of uniform expellant distribution, the use of post-cathode propellant diversion is felt to have served an even more important purpose with respect to elimination of the apparent saturation in ion beam current. Both at HRL and elsewhere[3,12] a tendency has been noted for the discharge voltage to decrease as the cathode propellant flow increases while the geometrical parameters of the discharge chamber are kept constant. This reduction of the discharge voltage is accompanied by a degradation of the discharge chamber performance. With fixed geometry of the openings which connect the cathode-cup region with the main discharge chamber, an increased propellant flow through the cathode results in an increased particle density within the cup region as well as within those openings, and — without reference to a specific mechanism — it must be concluded that

the observed performance degradation is a result of this density increase. In the initial configuration of the 30-cm thruster, all of the neutral flow was directed through the mouth of the cathode-cup pole piece, and when the baffle was in its optimum axial position, most of the propellant flow could escape from the cathode cup only through the radial gap between the inner and the outer part of the baffle. With the cylindrical disk baffle which was then in use, the optimum position was such that the open area of the axial gap between cathode cup and baffle was considerably smaller than the open area of the radial gap (see Fig. 3 for a similar example with the 20-cm thruster).

In its 15-cm long configuration the 30-cm thruster was operated at a beam current I_B = 830 mA with a mass utilization efficiency η_m = 93% at a source energy per ion V_S = 338 eV/ion. As before, a beneficial effect resulted from totally uncovering the screened holes in the cylindrical walls of the cathode-cup pole piece. Since, in this configuration, one band of holes was always open, the effect of uncovering the second band was not as dramatic as before, although it did have the effect of increasing the discharge voltage by about 3 V and increasing the mass utilization efficiency by about 3%. In its optimum position, the baffle was located at a distance d = 0.5 cm from the tip of the cathode-cup pole piece. Best performance was achieved with the anode mask operated at cathode potential.

In an additional modification, a third band of screened holes was placed on the cylindrical side wall of the cathode-cup pole piece to increase performance gains beyond those which were realized by opening the movable shutter sleeve covering the second set of holes. To further increase the flow of neutral particles through the pill-box, a second ring of eight screened holes of 2.54 cm diameter was placed on its downstream face.

In this configuration, the 30-cm thruster, operating with high-temperature LM cathode K-25-V, yielded a source energy per ion V_S = 248 eV/ion at a mass utilization efficiency η_m = 85% and an ion beam current I_B = 1.13 A (mercury flow-rate equivalent I_a = 1.35 A). Also, a source energy per ion V_S = 270 eV/ion was achieved at a mass utilization efficiency η_m = 90% with I_B = 1.22 A (I_a = 1.35 A). With I_B = 1.44 A (I_a = 1.55 A) a source energy per ion V_S = 292 eV/ion was obtained at a mass utilization efficiency η_m = 93%. As before the baffle was provided with a conical edge to permit continuous variation of the baffle gap for electron flow. The thruster achieved its best performance when it was operated with the screened holes in the cylindrical wall of the cathode-cup pole piece opened

fully, with the anode mask biased at cathode potential, and with a baffle position d = 0.5 cm. Experimental data for 30-cm thruster performance are shown in Fig. 9. A dashed curve has been drawn connecting two of the data points, because they were obtained at different values of the mercury flow rate.

3. Thruster System Performance

Discharge-chamber performance with the 30-cm thruster reached its highest level of optimization during operation of the configuration described in the preceding section. Several new baffle configurations were tried afterward in an effort to further optimize 30-cm thruster performance, but no improvement was realized. No other attempts were made to further optimize performance; in fact, several changes which were made thereafter actually resulted in a slight decrease in discharge-chamber efficiency from that reflected by Fig. 9. These changes occurred in the process of converting the 30-cm LM cathode thruster into a fully compatible integrated thruster system with a thermally integrated single-capillary-fed LM cathode, with high-voltage isolation of the thruster from the mercury storage reservoir, and with an LM cathode neutralizer.

The only modification which might reasonably be expected to result in a change in discharge-chamber performance was the fact that LM cathode K-51 is physically smaller and was therefore located at a different axial location from LM cathode K-25-V which was used in the previous experiment. When attached to the removable portion of the 30-cm thruster's aluminum backplate, the pool-keeping structure of LM cathode K-51 is located at a position $\ell = 9.17$ cm from the mouth of the cathode-cup pole piece, whereas $\ell = 7.08$ cm in the case of LM cathode K-25-V.

Discharge-chamber performance of the 30-cm thruster, operated as part of the total thruster system, is shown in Fig. 10. Discharge-chamber losses exceed those displayed by the same thruster at its highest level of optimization by about 15%, but otherwise the performance characteristics are similar.

An ion beam profile measured 11.1 cm downstream from the accel electrode is illustrated in Fig. 11. The dashed curve is the beam profile extrapolated to the accel electrode plane. In order to draw the maximum ion current from an ion-optical system it is necessary that the plasma density be radially uniform. The extent to which this ideal is approached by a given thruster can be measured in terms of the quantity

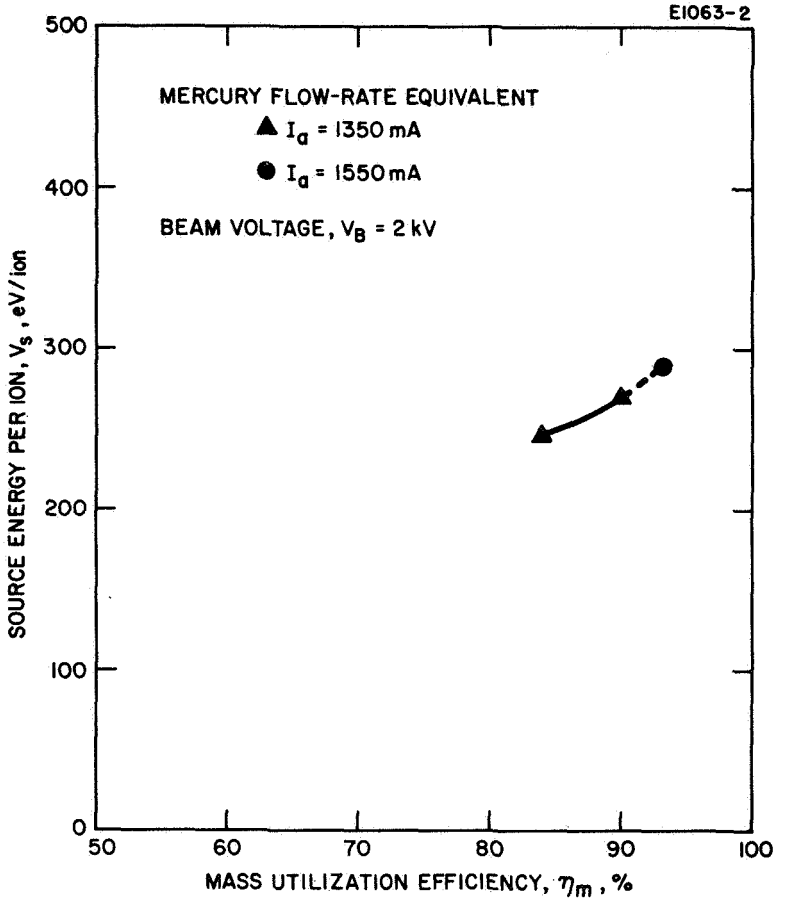

Fig. 9. Discharge-chamber performance of the 30-cm LM cathode thruster (highest level of optimization).

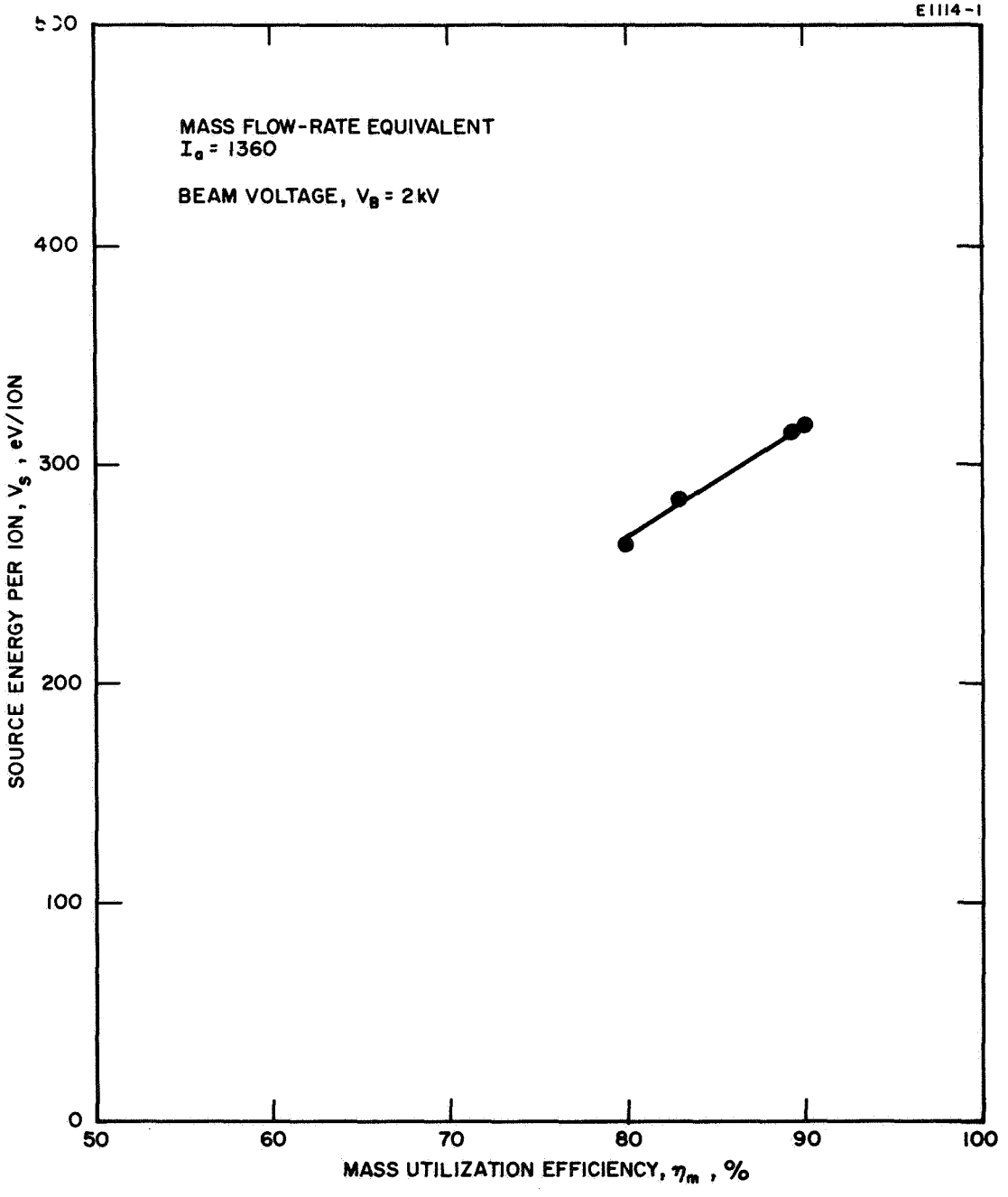

Fig. 10. Discharge-chamber performance of the 30-cm LM cathode thruster, operated as part of a total thruster system.

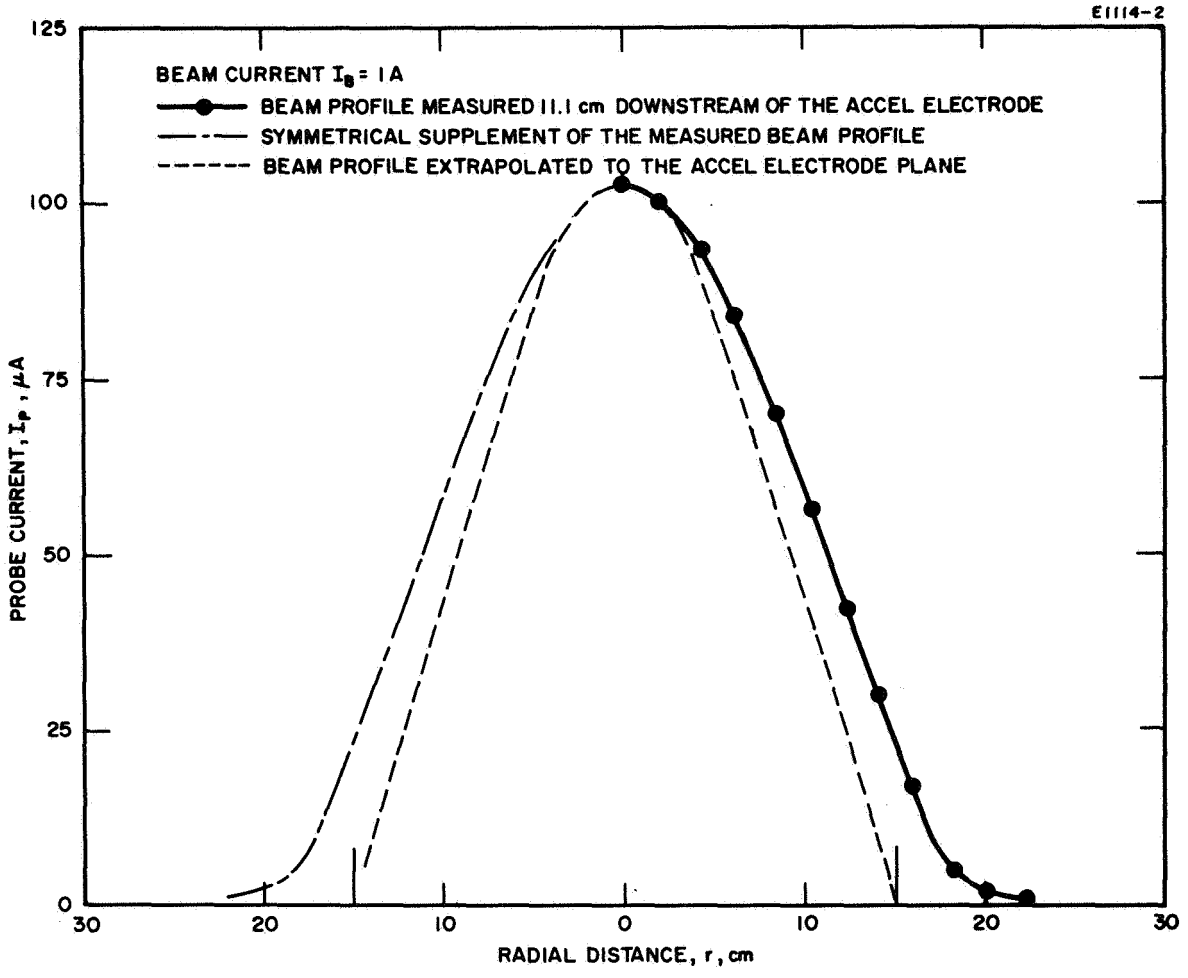

Fig. 11. Beam profiles of the 30-cm LM cathode thruster.

$$\varepsilon = \frac{2\pi \int_0^{r_b} J(r)\, r\, dr}{\pi\, r_b^2\, J_{max}}$$

(sometimes called the "perveance efficiency")[16] where $J(r)$ is the current density at the accel electrode at radius r, J_{max} is the maximum current density, and r_b is the outer ion beam radius at the accel electrode. Based on the dashed curve in Fig. 11 one obtains $\varepsilon = 33\%$ for the 30-cm thruster. The system was operated with the thruster electrically isolated from the mercury storage reservoir by a hydrogen-bubble high-voltage isolator which is described in Section V-C. The single-capillary flow impedance (described in Section V-B) served as a reliable and highly repeatable element of the feed system. Under typical operating conditions, with the thruster cooled by radiation alone, the following equilibrium temperatures were measured: cathode body temperature = 195°C, thruster back plate temperature = 145°C, and external anode-connector temperature = 205°C. The LM cathode neutralizer (described in Section IV-B) operated with a ratio of neutralizer mass flow to total mass flow ($\eta_{m,N}$) of 3.0 ... 3.3% and a total coupling voltage between the neutralizer and the beam collector $V_{N-C} = 30$ V. After approximately 50 hours of operation, during which the neutralizer provided complete ion beam neutralization, there was no observable sputter erosion of either the neutralizer or the extraction electrodes. Ion beam interception by the accel electrode remained constant at less than 1% irrespective of whether the neutralizer was used.

Data obtained from operation of the thruster system provide a basis for its comparative evaluation. The total efficiency of the over-all system is evaluated in Table III and compared in Fig. 12 with performance predicted[17] for operation of other electron-bombardment thruster types in the year 1970. The data points lie close to the curve marked "1970 Projection." This performance represents a level of efficiency which is highly competitive with other electrical propulsion systems currently under development.

While using the same ion extraction system, the 30-cm thruster system (with single-capillary-fed LM cathode K-51 and LM cathode neutralizer K-48) has also been operated successfully at a beam voltage $V_B = 1$ kV, corresponding to a specific impulse $I_{sp,eff} = 2750$ sec. The thruster operated with a source energy per ion $V_S = 362$ eV/ion at a mercury flow-rate equivalent

TABLE III

Total Efficiency of the 30-cm Thermally Integrated LM Cathode Thruster

Effective specific impulse, $I_{sp,eff}$	3,580 sec	3,710 sec	3,990 sec
Beam voltage, V_B	2,000 V	2,000 V	2,000 V
Beam current, I_B	1,110 mA	1,120 mA	1,155 mA
Discharge losses, V_S	264 eV/ion	283 eV/ion	314 eV/ion
Beam mass utilization efficiency, η_m	80%	83%	89.3%
Total neutralizer coupling voltage V_{N-C}	30 V	30 V	30 V
Neutralizer mass flow fraction, $\eta_{m,N}$	3.0%	3.0%	3.3%
Accel interception current, I_{Ac}	12 mA	11 mA	10 mA
Thruster Power:			
Beam power, $P_B = I_B V_B$	2,220 W	2,245 W	2,310 W
Discharge power, $P_S = I_B V_S$	293 W	318 W	362 W
Neutralizer power, $P_N = I_B V_{N-C}$	33.3 W	33.7 W	35 W
Accel electrode power, $P_{Ac} = I_{Ac} V_B$	24 W	22 W	20 W
Isolator power, P_{IS}	3 W	3 W	3 W
EM pump power,[a] P_{EM}	2 W	2 W	2 W
Total thruster system power,[b] P_T	2,575.3 W	2,623.7 W	2,732 W
Total Power Efficiency, $\eta_{P,T} = P_B/P_T$	86.2%	85.5%	84.5%
Total mass utilization efficiency, $\eta_{m,T} \sim \eta_m - \eta_{m,N}$	77%	80%	86%
Total thruster efficiency, $\eta_T = \eta_{P,T}\eta_{m,T}$	66.3%	68.4%	72.6%

[a] This is the maximum EM pump power and is obtained when the pump is developing its full head. The average value of P_{EM} over an entire mission will be considerably less than the given value.

[b] This value has been determined assuming the use of permanent magnets. During experimentation, electromagnets were used to achieve greater operating flexibility; approximately 50 W was consumed by these magnets.

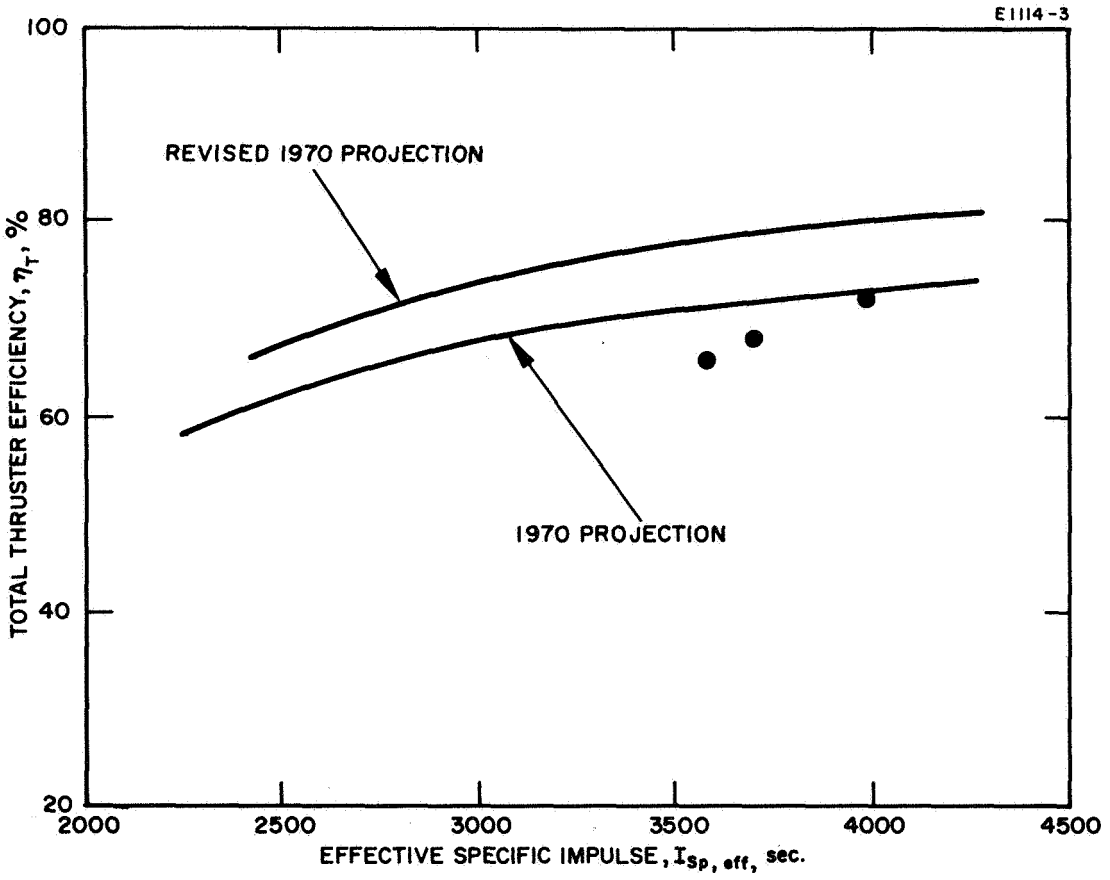

Fig. 12. Comparison of the present 30-cm LM cathode thruster system with system performance projected for other electron-bombardment thruster types.

I_a = 1250 mA (beam current I_B = 1160 mA) with a mass utilization efficiency η_m = 86.5%. As usual, the accel voltage was V_{Ac} = -3 kV and the accel interception was less than 1% of the beam current.

D. LM CATHODE THRUSTER IN RADIAL-FIELD CONFIGURATION

A 15-cm diameter radial-field thruster configuration was devised and tested under a separate effort carried out at HRL. As stated in the final report[16] of that contract, "This geometry was chosen with the intension of replacing the diffusion-controlled, centrally-peaked density profile with a distribution rendered radially uniform by unobstructed motion of electrons along radial field lines." In the above effort, a hollow cathode was used, housed within a soft-iron center post which served to establish a radial magnetic field. In operation, this configuration has yielded the following performance: Discharge chamber losses (disregarding cathode power) were less than 190 eV/ion at a mass utilization efficiency η_m = 90%. With a total accelerating voltage $V_T = (|V_B| + |V_{Ac}|) = 5$ kV, an ion beam current in excess of 400 mA was extracted with a SERT II ion-optical system. The beam profile was quite uniform, the current density being essentially constant over a central region of 12 cm diameter.

Encouraged by the performance exhibited by the radial-field thruster using a hollow cathode, a similar radial-field thruster was constructed using an LM cathode. The ion-extraction electrodes, bar electromagnets, and outer body of the existing 20-cm thruster served as a basic structure which was modified by the addition of suitable components to convert it to an LM cathode radial-field thruster.

A schematic drawing of this thruster is shown in Fig. 13. In the new configuration, the magnetic field extends radially outward from a central 5-cm diameter hollow soft-iron post to a cylindrical pole piece at the side wall of the discharge chamber. An LM cathode is placed within the central post. During thruster operation the cathode can be moved axially in order to seek an optimum position within the cathode-post pole piece at distance ℓ upstream of the electron exit holes; alternatively, the cathode can be fixed with relation to the cathode post and the entire cathode assembly moved to an optimum position L relative to the screen electrode. An annular disk-shaped anode extends radially across the upstream face of

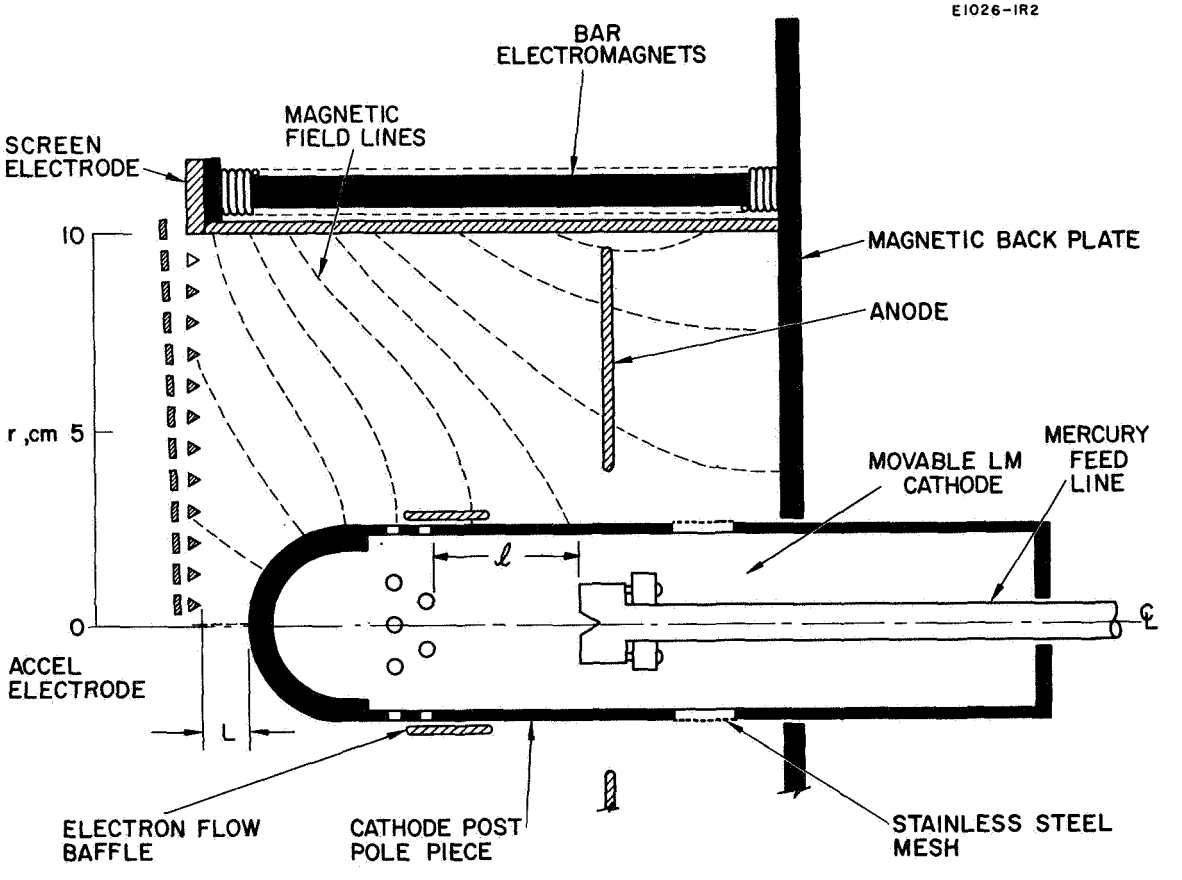

Fig. 13. Schematic drawing of the 20-cm LM cathode thruster in radial-field configuration.

the discharge chamber from 1.4 cm beyond the central cathode post to near the cylindrical walls of the discharge chamber. The electron flux emerges from 24 holes of 0.475 cm diameter, located 4 cm from the tip of the cathode post. The cross-sectional area for electron-escape through these holes can be varied by movement of an electron-flow baffle. The magnetic field configuration is such as to guide energetic electrons from the exit holes in the central post across the entire face of the extraction screen before they are collected by the anode in the rear of the discharge chamber. Six screened holes of 1.57 cm diameter, located 11.5 cm from the tip of the cathode post, provide an alternate path for flow of neutral particles from the cathode region into the discharge chamber. This serves to reduce the neutral particle number density within the cathode post and to better distribute the neutral particle flux.

In operation, the thruster performance does not appear to depend critically on either the position L of the cathode post relative to the screen electrode or to position ℓ of the LM cathode within the cathode-post pole piece. However, a slight increase in performance does result from thruster operation at minimum values of L and for a value ℓ which locates the cathode at a position midway between the two sets of holes in the cathode post. Thruster performance depends critically on the position of the electron flow baffle, with the best performance occurring with approximately 5% of the total hole area open for transmission of electron flux. The thruster was found to operate stably over the range of neutral flow-rate equivalent from I_a = 600 mA to 1,100 mA. As shown in Fig. 14, total source energies per ion V_S = 302 and 356 eV/ion were required for mass utilization efficiencies of η_m = 85 and 98%, respectively, at a neutral flow-rate equivalent I_a = 1,050 mA.

The beam current profile measured 8.8 cm downstream from the accel electrode as illustrated in Fig. 15. The nonsymmetrical nature of the profile is probably the result of a misalignment of the electron flow baffle which covered 95% of the total hole area for electron escape. In any future operation of the radial-field configuration, either fewer or smaller holes would be used so that optimum performance would be achieved with the holes more fully exposed. Position of the baffle would then not be so critical, and misalignment could easily be avoided. A major characteristic of the radial-field configuration is its ability to produce a radially uniform plasma, which is important if the maximum ion current density is to be drawn from each aperture of the ion-optical system. The uniformity of the plasma

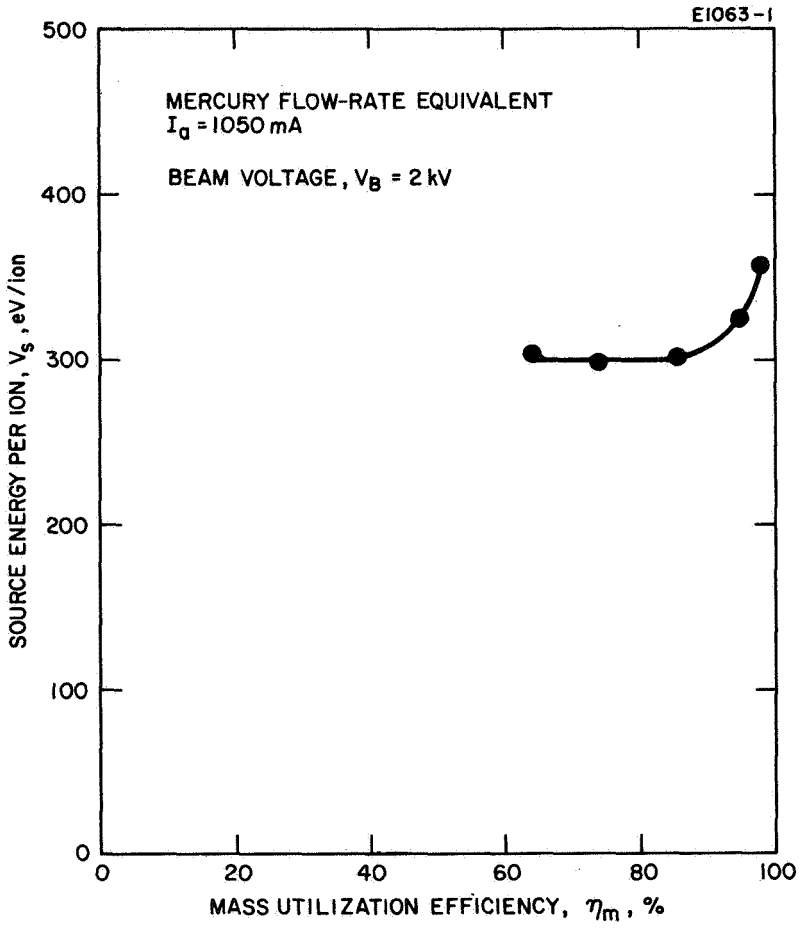

Fig. 14. Discharge-chamber performance of the 20-cm LM cathode thruster in radial-field configuration.

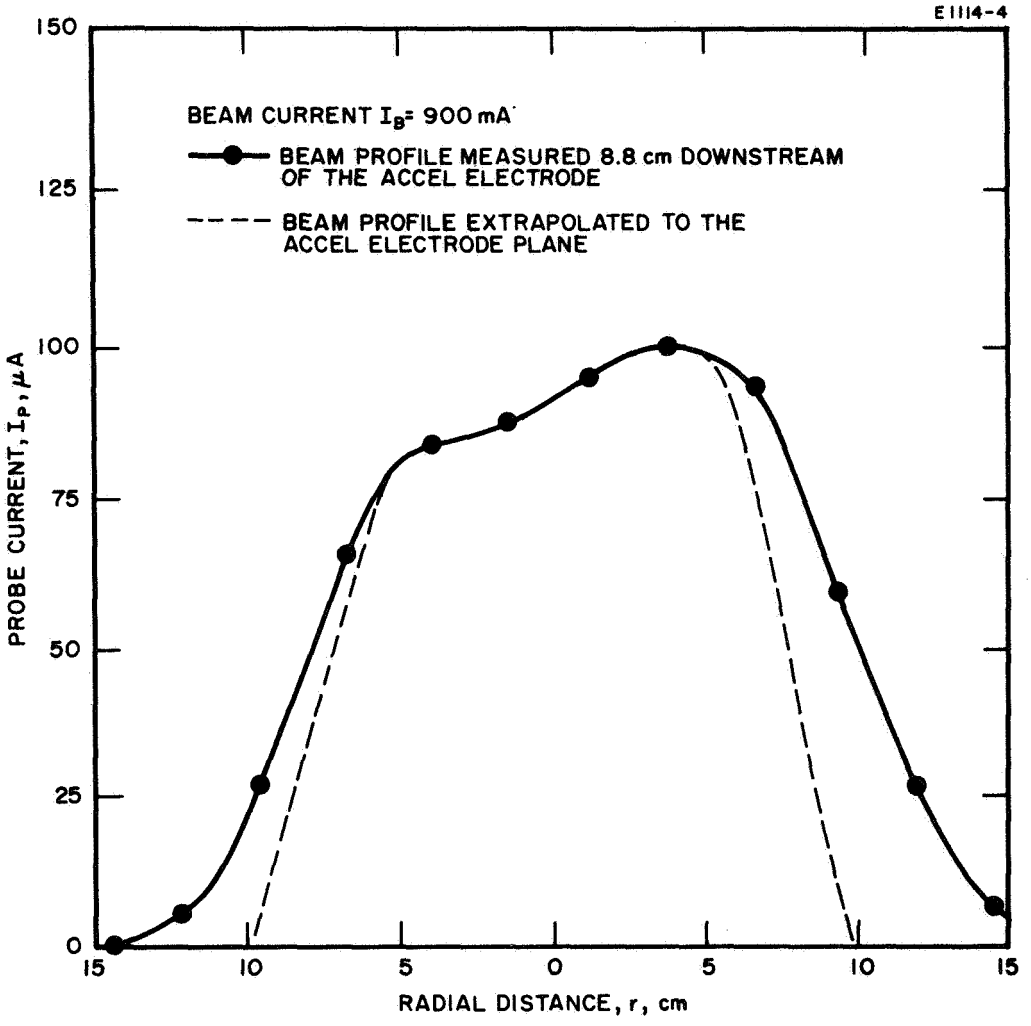

Fig. 15. Beam profiles of the 20-cm cathode thruster in radial-field configuration.

density can be assessed quantitatively in terms of the quantity ε defined earlier. Based on the dashed curve in Fig. 14, one obtains $\varepsilon = 54\%$, a significant increase over the value of $\varepsilon = 33\%$ obtained with the 30-cm thruster.

Performance reported here for the LM cathode thruster in the radial-field configuration gives only a preliminary indication of the capability of this thruster type. The time which was available under the subject contract permitted only a very brief effort to optimize discharge-chamber performance, and only a cursory examination of the thruster's operating characteristics. The results which have been obtained indicate, however, that thruster performance is sufficiently promising to warrant further research at a later date into this mode of operation.

SECTION IV

LM CATHODE RESEARCH AND DEVELOPMENT

A. MAIN THRUSTER-CATHODE DEVELOPMENT

1. Introduction

The LM cathode is a force-fed liquid-metal pool cathode which is gravity independent. The volume of liquid metal which is exposed to the discharge is sufficiently small that it is able to maintain its integrity by cohesive forces, and it is held in place by adhesive attachment to a pool-keeping structure placed within the solid metal cathode body. In the ion thruster application of this cathode, removal of mercury atoms from the liquid mercury surface is used to feed the expellant into the discharge chamber. The most favorable results have been obtained with molybdenum pool-keeping structures of divergent-nozzle geometry. A major advantage of the divergent geometry is that it automatically stabilizes the liquid metal surface at that level in the pool-keeping structure at which the rate of removal of metal atoms from the pool surface is exactly balanced by the expellant feed rate to the pool, which is set at the value desired for thruster operation.

Under the previous contract (Contract NASW-1404) the annular cathode design was adopted for high-temperature applications, in preference to the circular geometry, because it distributes the thermal cathode load $P_{K,th}$ over the circumference of the annulus (independent of the area of the mercury pool A_K) rather than around the much smaller perimeter of the corresponding circular pool. This distribution of the thermal load in the annular design serves to increase its over-all thermal conductance, and operation can be achieved with a much lower temperature drop between the vicinity of the mercury pool and the body of the cathode.

Fabrication of the annular configuration is nontrivial because a feed channel with an annular gap of 2 ... 12 μm ($\sim$ 0.1 ... 0.5 x 10^{-3} in.) is required. Maintaining the required tolerances on the conical surfaces employed in the annular design has proved somewhat difficult, so that the annular cathodes in existence prior to the subject contract effort were fabricated with annular gaps of no less than 5 μm. As a consequence,

the required electron-to-atom ratios could be obtained at elevated temperature only by operating these cathodes in a mode (referred to as the retracted arc mode) which differs from that employed at low temperatures. The mode change is indicated by the observation that the specific thermal loading ($V_{K,th}$) of the cathode* is not constant as the mercury pool temperature (T_{Hg}) is increased. For an electron-to-atom emission ratio $K_e/K_a \sim 10$, values for $V_{K,th}$ had been measured previously as low as 2.5 W A^{-1} for $T_{Hg} \lesssim 130°C$, and up to 12 W A^{-1} for $T_{Hg} \gtrsim 300°C$ (Ref. 4).

The necessary electron-to-atom emission ratio (K_e/K_a) for a thruster application is determined by the required beam current (I_B), mass utilization efficiency (η_m), and cathode discharge current (I_K), by the relationship $K_e/K_a = \eta_m I_K/I_B$. Because it is necessary to preserve the same electron-to-atom emission ratio K_e/K_a when T_{Hg} is raised as for lower temperatures, the area A_K of the mercury from which evaporation takes place must be reduced (Fig. 16(a) and (b)). At the same time, the annular diameter must be made as large as possible to aid in the removal of discharge power ($P_{K,th}$) from the cathode matrix, and therefore the width of the mercury surface must become small. When the width of the ring of mercury is reduced to the width of the feed channel ($\sim$ 5 μm), further operation occurs with the cathode arc spots retracted into the feed channel itself (Fig. 16(c)) or, in fact, on the surface of the mercury in the major supply channel (Fig. 16(d)). In the latter case, when A_K is again large, excessive evaporation is prevented by the feed channel itself, which acts as a vapor flow constrictor but at the same time introduces an additional voltage drop (due to the plasma losses in the channel) which is clearly detrimental to thruster performance.

A second area of continuing LM cathode development deals with the reduction of the amplitude of fluctuations in the mercury flow rate which occur as the mercury enters the pool-keeping structure. Flow fluctuations result in corresponding fluctuations of the liquid mercury level in the pool-keeping structure. When LM cathodes are operated at high temperature or at high values of the electron-to-atom ratio K_e/K_a, the equilibrium position of the liquid level is close to the upstream end of the pool-keeping structure where the mercury surface area A_K (and therefore the rate of mercury evaporation) is minimized. In this condition, fluctuations in liquid level

*$V_{K,th}$ is the ratio of (thermal power received by the LM cathode from the discharge) to (electron current delivered by the LM cathode to the discharge): $V_{K,th} = P_{K,th}/I_K$.

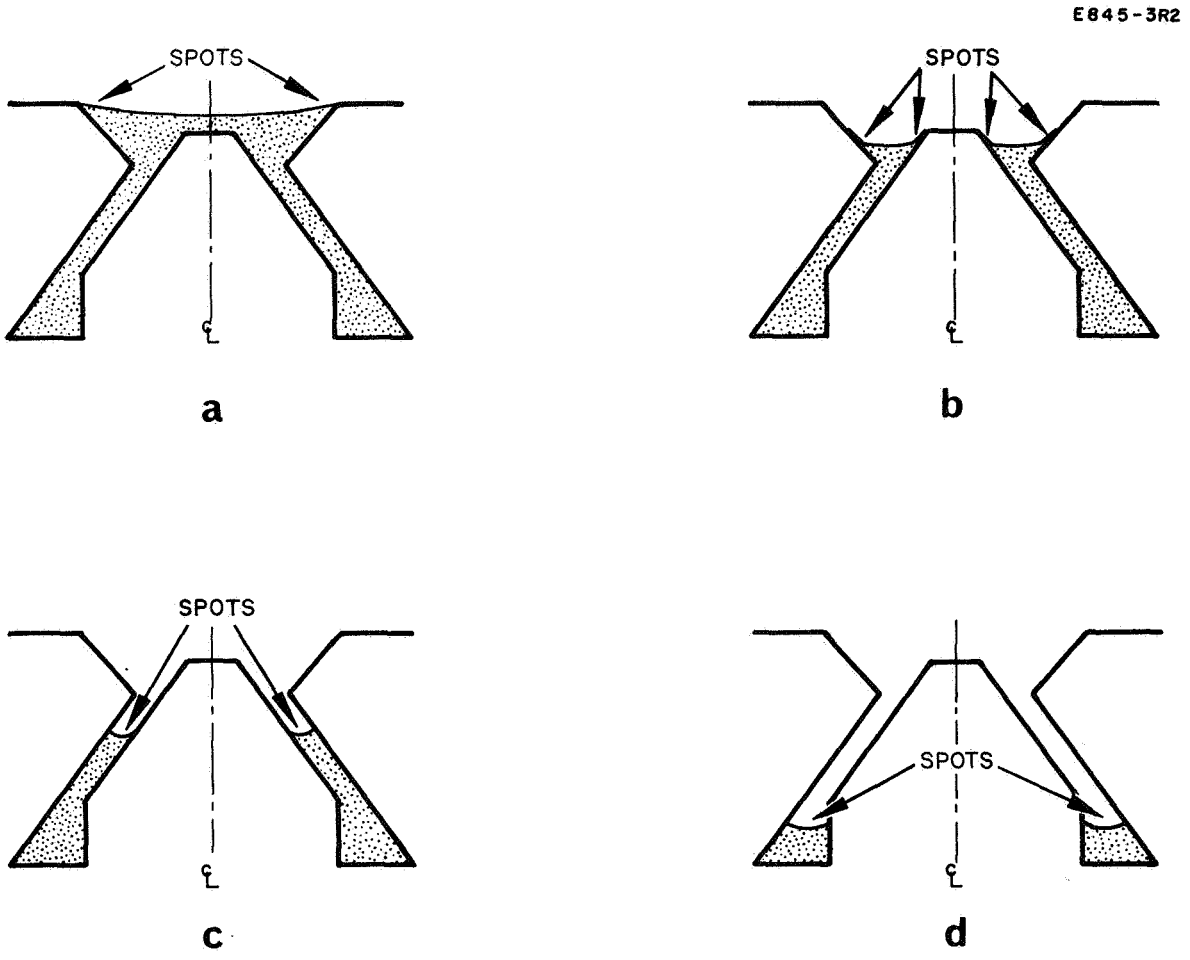

Fig. 16. Positions of the mercury pool surface for an annular LM cathode.

cause the mercury surface to recede momentarily out of the pool keeping structure and into the feed channel, which results in momentary operation in the retracted arc mode. Fluctuations of the mercury flow rate result either from thermal fluctuations (which in turn are driven by the flow fluctuations, resulting in nonlinear oscillations with a period of $\sim$ 1 sec), or from a surface-tension instability which may occur whenever a nonwetting fluid passes through a narrow flow constriction (as explained in Section V-B). Using techniques described in Ref. 5, suitable thermal design of the pool-keeping structure and reduction in the volume of the mercury plenum (which exists between the porous tungsten flow impedance and the pool-keeping structure) have already greatly reduced the amplitude of thermally induced fluctuations.

Research and development of the liquid-mercury-fed LM cathode has concentrated both on the design and fabrication of LM cathodes with feed-channel gaps which are sufficiently narrow to avoid the necessity of discharge operation in the retracted arc mode, and on reduction of the amplitude of flow-rate fluctuations which result either from the action of thermal fluctuations on a mercury plenum or from surface-tension instabilities. The ability of the LM cathode to successfully meet the requirements for high-temperature thruster operation has been enhanced further by the fact that the required value of the electron-to-atom ratio (K_e/K_a) has been relaxed from $\gtrsim$ 10 to $\sim$ 7. This is a consequence of the reduction in the ratio of discharge current to beam current (I_K/I_B) which was realized by discharge-chamber optimization.

Two LM cathodes were designed, fabricated, and tested in which a 2.5 μm tantalum shim was used to establish a uniformly narrow feed channel: an annular cathode designated K-25-V, and a linear-slit cathode K-45. Both cathodes were tested at high temperature in a diode discharge. The specific thermal load of annular cathode K-25-V was found to vary with cathode temperature as expected, and at a cathode body temperature T_K = 200°C the specific thermal load was found to be $V_{K,th}$ = 3.8 W/A for electron-to-atom emission ratios typical of those required for thruster operation. Linear-slit LM cathode K-45 has also undergone high-temperature testing in a diode discharge to determine its thermal loading characteristics. The specific thermal load of the linear-slit cathode was found to vary with temperature in a manner similar to that exhibited by annular cathode K-25-V.

Under a previous effort (Contract No. NASW-1404) an annular high-temperature LM cathode K-26-III was operated in a purely vapor-fed mode, with a vapor feed system replacing the conventional

liquid feed system.[4] Although only limited data were obtained at that time, the specific thermal loading of K-26-III in the vapor-fed mode was found to be somewhat less than that observed in liquid-fed operation with the same cathode. As part of the LM cathode research, diode testing has been undertaken to generate additional data for a full evaluation of the performance characteristics of the vapor-fed mode of operation. The data indicate no significant difference between the specific thermal loading of the vapor-fed LM cathode K-26-III and that of the liquid-fed LM cathode K-25-V. The vapor-fed LM cathode has also been operated satisfactorily in a thruster.

All LM cathodes which have been introduced previously employ a porous-tungsten impedance for the regulation of mercury flow. A new annular LM cathode (K-51) has been designed, fabricated, and tested which utilizes a single-capillary flow impedance to reduce the amplitude of flow-rate fluctuations (see Section IV-B-3); this cathode also employs a cylindrical (rather than conical) geometry of the cathode structure to permit more accurate fabrication of the critical annular feed channel. After its initial check-out in a diode discharge, LM cathode K-51 was thermally integrated with the thruster and operated satisfactorily as part of the 30-cm LM cathode thruster system.

2. Annular LM Cathode K-25-V

During the preceding contract (Contract NASW-1404), two annular cathodes were fabricated and designated K-25 and K-26. Their mean annular radii were 0.635 mm and 0.91 mm, respectively. As part of the past research effort[4] the flow passage geometry of both cathodes was modified in several steps, the most recent of which was chosen to optimize operation in the vapor-fed mode. In their final stages of modification neither cathode was suitable for operation in the liquid-fed mode.

Under the subject contract effort the smaller of the two annular cathodes (K-25) was reworked to return it to liquid-fed operation. In its present configuration the cathode is designated K-25-V. The mean annular radius has been enlarged to a value of 1.27 mm. The technique of assembly indicated schematically in Fig. 17 is similar to that used previously, but with one significant change which resulted in a considerable increase in the facility with which the critical dimension of the narrow annular gap could be controlled. As before, the two conical walls of the annular gap are machined separately

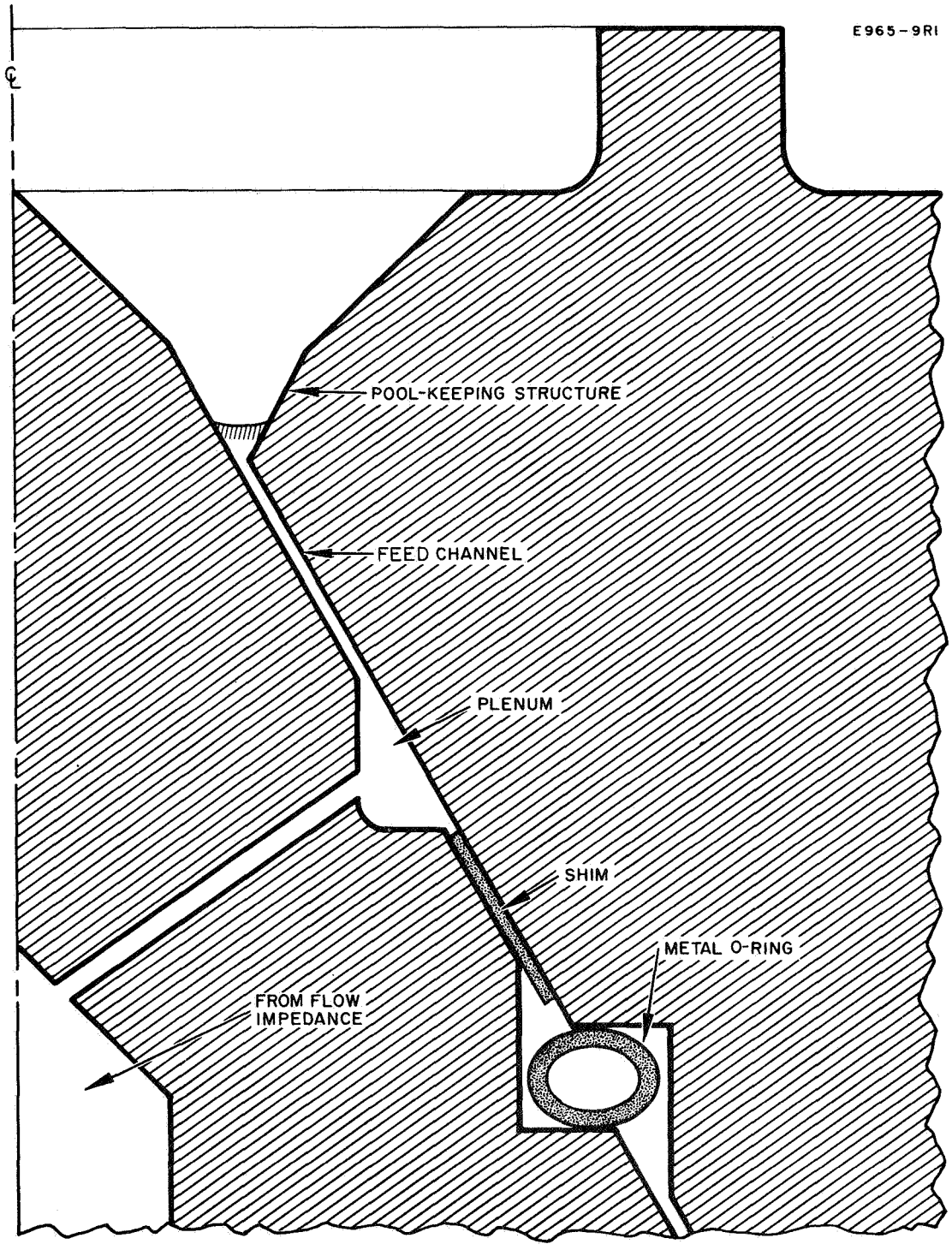

Fig. 17. Annular LM cathode (K-25-V) using a tantalum shim to establish the feed channel width.

and placed in the proper relative position by their own self-centering geometry. Next, the two cones are lapped together to a perfect match. The required annular feed channel separation is then established by mating the two cones together with only a narrow tantalum shim (2.5 μm thick) separating them (this is the new part in the assembly procedure).

Mercury is fed under pressure to a small annular plenum machined near the tip of the positive cone. It flows forward toward the tip through the narrow feed channel, into the annular pool-keeping structure which is formed by the tip of the positive cone and a small reversed negative cone which is machined in the front face of the part containing the mating negative cone. Mercury is prevented from flowing in the other direction by a metal O-ring placed midway down the positive cone. (During assembly this O-ring is crushed sufficiently that the mating conical surfaces are separated only by the tantalum shim.)

Annular cathode K-25-V was operated in a diode discharge at high temperature. The specific thermal load ($V_{K,th}$) was measured at a discharge current I_K = 7 A for cathode body temperatures T_K = 200°C, 250°C, and 300°C as a function of the electron-to-atom ratio K_e/K_a. The data were plotted in Fig. 2. The cathode ran stably at all temperatures, operating all day without spontaneous extinctions. The variations of $V_{K,th}$ were in accord with expectations based on our analytical model of the behavior of the arc spots.[4]

At constant discharge current, either an increase in cathode temperature or a decrease in the mercury feed rate resulted in a shrinking of the exposed annular mercury surface. The width of the arc-spot pattern was observed to decrease with the mercury surface; in the extreme limit, both the liquid surface and the arc spots receded into the 2.5 μm wide feed channel as the discharge shifted to the retracted-spot mode. This mode is characterized by an increase in $V_{K,th}$, the thermal power delivered to the cathode per unit discharge current.

The cathode was operated at high temperature over a period of several days in the range of interest for the 30-cm thruster. Anticipating operation at a beam current I_B = 1 A, mass utilization efficiency η_m = 90%, discharge voltage V_D = 35 V, and a source energy per ion of V_S = 250 eV/ion, the cathode was operated with a discharge current I_K = 7 A and a neutral mercury flow rate I_a = 1.11 A; thus, K_e/K_a = 6.3. At a cathode body temperature T_K = 200°C a specific thermal load $V_{K,th}$ = 3.8 W/A was measured. By calculating the temperature drop required

to drive the heat from the mercury surface to the thermocouple location at a radius of 0.44 cm, the mercury surface temperature was estimated to be $T_{Hg} \sim 233°C$ under the above conditions. At a calculated mercury surface temperature $T_{Hg} \sim 355°C$ (corresponding to a measured $T_K = 250°C$) the specific thermal load was $V_{K,th} = 6$ W/A, and at a surface temperature $T_{Hg} \sim 480°C$ ($T_K = 300°C$) the specific thermal load was $V_{K,th} = 8$ W/A. The heat delivered to the cathode under any of these three operating conditions can be accommodated by the thermal design of the 30-cm thruster.

The same annular cathode was also evaluated at high temperature in a diode discharge over a range of current suitable for operation in a 20-cm electron-bombardment thruster. Anticipating a beam current $I_B = 600$ mA, mass utilization efficiency $\eta_m = 90\%$, discharge voltage $V_D = 35$ V, and a source energy per ion $V_S = 280$ eV/ion, the cathode was operated at a discharge current $I_K = 5$ A and a neutral mercury flow rate $I_a = 666$ mA. As in the measurements in the range of interest for the 30-cm thruster, at a cathode body temperature $T_K = 200°C$ (corresponding to $T_{Hg} \sim 232°C$ for $I_K = 5$ A), a specific thermal load $V_{K,th} = 3.8$ W/A was measured. Similarly, at $T_K = 250°C$ (corresponding to $T_{Hg} \sim 340°C$) the specific thermal load was $V_{K,th} = 7$ W/A. The quantity of heat delivered to the cathode under either of these conditions is sufficiently small to permit radiant dissipation from either the 30-cm thruster or from a similarly designed thruster of 20-cm diameter.

The two lower-temperature curves in Fig. 2 show a maximum in the value of $V_{K,th}$ at an electron-to-atom flux ratio $K_e/K_a \sim 4 \ldots 6$. This is caused by partial utilization of the cathode's thermal conductance, as a result of operation with arc-spot patterns covering only part of the circumference of the cathode annulus at low electron-to-atom ratios. When the cathode is operated at electron-to-atom ratios above 4 ... 6 (at the particular current of 7 A), a larger fraction of the circumference becomes utilized and $V_{K,th}$ decreases. Past experiments have shown that when a full-circle spot pattern is established, a minimum is reached beyond which $V_{K,th}$ rises monotonically. The $T_K = 300°C$ curve does not show a maximum because at this temperature the spot pattern was always a full circle within the range of observation. The range of K_e/K_a in Fig. 2 is limited to the present range of interest for bombardment thruster cathodes which are designed to pass all of the mercury flow through the LM cathode. Higher values of the ratio K_e/K_a are of interest only for thrusters designed to operate with some degree of pre-cathode expellant diversion.

3. Linear-Slit LM Cathode K-45

Interest in a linear-slit LM cathode results from the accuracy with which a uniformly narrow mercury feed channel can be established in the linear geometry. In a high-temperature LM cathode, a narrow feed channel is necessary to avoid operation in the retracted arc mode (this mode results in high thermal power delivery to the cathode). Uniformity of the feed channel leads to uniformity of the linear arc spot pattern, and thus to full utilization of the cathode's thermal conductance.

The design of the linear-slit cathode is shown schematically in Fig. 18. It is based on a variation of the annular cathode concept which uses the distribution of the thermal load $P_{K,th}$ over the perimeter of a narrow rectangular mercury pool, rather than over the inner and outer perimeters of an annular mercury pool. The length of the rectangular pool in this particular cathode is 0.32-cm. Similar to the technique described above for the assembly of annular LM cathode K-25-V, the feed-channel separation of the linear-slit cathode is established by inserting a 2.5 μm thick tantalum shim between the walls on either side of the pool-keeping structure which is formed by pressing together the two cathode halves. The cathode halves are pressed together in an experimental cathode mounting clamp. This clamp also contains a porous-tungsten flow impedance, flow channels, seals, etc.

The cathode has been operated in a diode discharge at temperatures from 26 to 314°C at discharge currents in the range of interest for operation of the 20-cm and 30-cm thrusters. Within this temperature range, stable operation was achieved at electron-to-atom ratios typical for normal thruster operation. For the electron-to-atom ratios of interest, at temperatures $\lesssim$ 26°C mercury would overflow the pool-keeping structure (a problem which could easily be overcome by simply enlarging the pool-keeping structure), while at temperatures $\gtrsim$ 314°C the discharge could not be maintained; thus, stable operation at these temperature extremes required a deviation of the electron-to-atom ratio from the range of interest.

The data listed in Table IV show the variation of the specific thermal load with cathode body temperature, and Fig. 19 compares the measurements of $V_{K,th}$ obtained with linear-slit cathode K-45 with those obtained with annular cathode K-25-V. The results do not differ appreciably in the high-temperature region which is of particular interest.

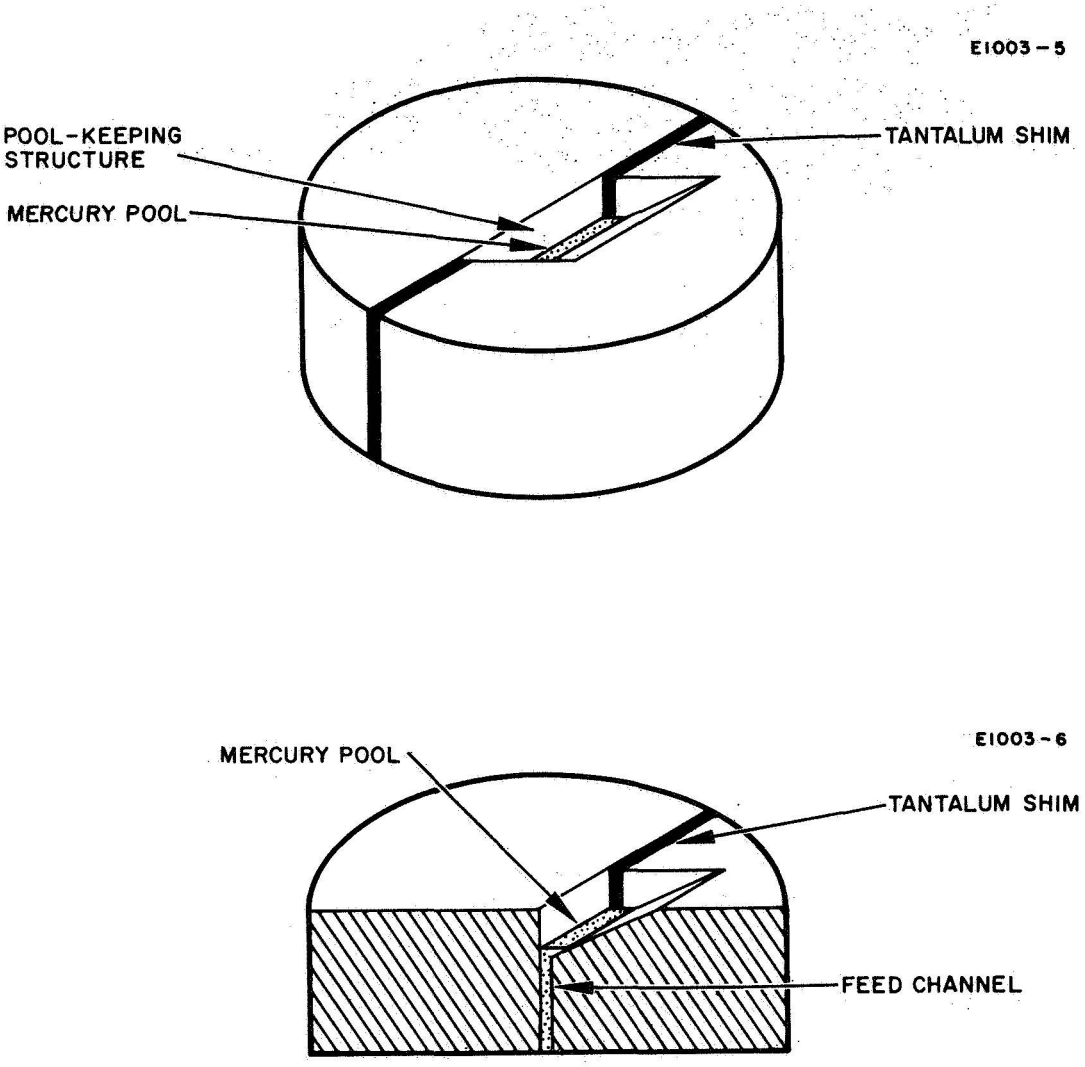

Fig. 18. Experimental linear-slit LM cathode K-45.

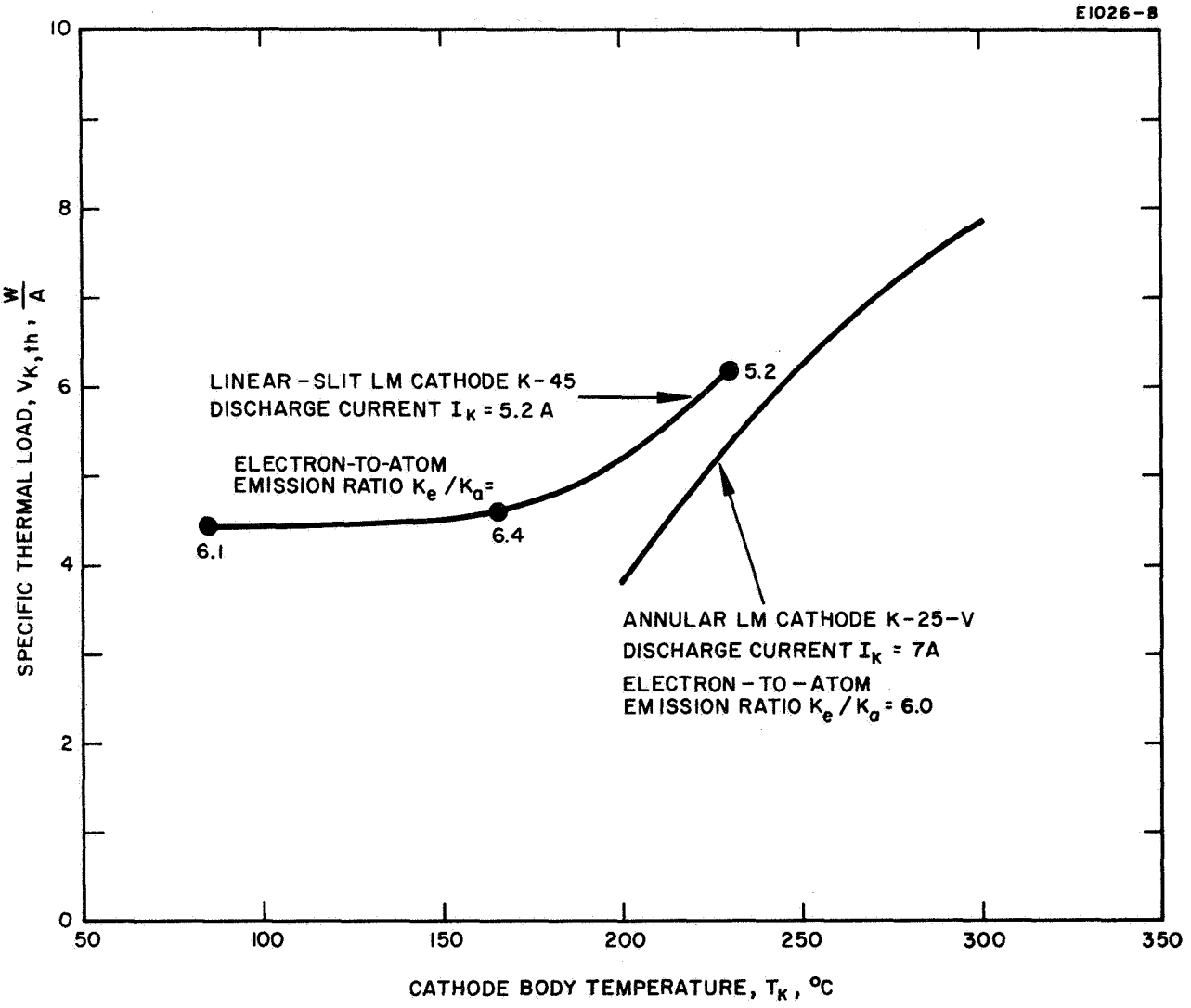

Fig. 19. Dependence of the specific thermal load ($V_{K,th}$) on cathode body temperature (T_K) for linear-slit LM cathode K-45 and annular LM cathode K-25-V.

TABLE IV

Operating Characteristics of Linear-Slit Cathode K-45

Cathode Body Temperature, T_K, °C	Discharge Current, I_K, A	Electron-to-Atom Ratio, K_e/K_a	Specific Thermal Load, $V_{K,th}$, W/A
26	5.5	19	1.3
84	5.2	6.1	4.4
165	5.0	6.4	4.6
233	5.3	5.1	6.2
314	6.0	2.3	7.5

After the linear-slit cathode discharge had been operated for approximately 10 hours, it was noted that the tantalum shim nearest to the discharge appeared to be partially eroded. This does not occur with the annular cathode K-25-V which also uses a tantalum shim to establish the narrow feed channel, because in that case the shim is totally recessed away from the pool-keeping structure. Because no increased performance capabilities were exhibited by linear-slit LM cathode K-45, no further effort was directed toward its development.

4. Vapor-Fed LM Cathode K-26-III

Observations of LM cathode operation in the retracted arc mode indicate that as the mercury contained in the pool-keeping structure shrinks to the size of the feed channel, the arc-spot pattern becomes diffuse (i.e., the cathode glow is distributed uniformly over an area at the mouth of the feed channel rather than concentrated along the line of intersection of the mercury and molybdenum surfaces). In this mode, the mercury surface is below the mouth of the channel, but copious evaporation keeps the mouth of the feed channel supplied with vapor, and the arc spots are believed to exist by virtue of transient condensation of this vapor on the walls of the feed channel.[4]

Under a previous effort (Contract No. NASW-1404) an annular high-temperature LM cathode K-26-III was operated in a purely vapor-fed mode, with a vapor feed system replacing the conventional liquid feed system.[4] In this way, it was possible to demonstrate complete spatial separation between the region where the vapor is evolved from the liquid mercury surface, and the region at the mouth of the molybdenum feed channel where the mercury vapor serves to sustain a diffuse arc-spot pattern.

To generate sufficient data with which to properly evaluate the performance characteristics of the vapor-fed mode of high-temperature LM cathode operation, measurements have been performed on cathode K-26-III in a diode discharge. In its present configuration, vapor-fed annular cathode K-26-III is joined to a liquid mercury feed system by means of a mercury vaporizer which is heated independently from the cathode. Performance of the vaporizer was first established by operating it without the cathode attached. For typical neutral mercury flow rates, all the mercury which passed through the vaporizer was fully evaporated when the vaporizer body temperature was held at a temperature greater than 180°C. To assure complete evaporation in diode operation, the vaporizer temperature was maintained at approximately 420°C. The specific thermal load of the cathode, $V_{K,th}$, was measured as a function of the cathode body temperature T_K for an electron-to-atom emission ratio of interest for 20- and 30-cm thrusters. The neutral mercury flow-rate equivalent I_a was approximately 1.45 A.

Figure 20 compares the results obtained with high-temperature annular LM cathodes K-25-V (liquid-fed) and K-26-III (vapor-fed). For cathode temperatures below about 260°C, mercury vapor was observed to condense permanently (rather than transiently) at the cathode throat, and the discharge was difficult to maintain at the noted electron-to-atom emission ratio and discharge current. For cathode temperatures above approximately 340°C the discharge could not be maintained at the desired electron-to-atom ratio. The latter result confirms the previously postulated theory of operation,[4] which emphasizes the requirement for transient condensation of mercury vapor to occur on the cathode surfaces in order to permit the formation of arc spots.

The performance of the vapor-fed cathode K-26-III does not differ appreciably from that of the liquid-fed cathode K-25-V so far as thermal loading is concerned. It should be noted, however, that initially a vapor-fed LM cathode must be heated

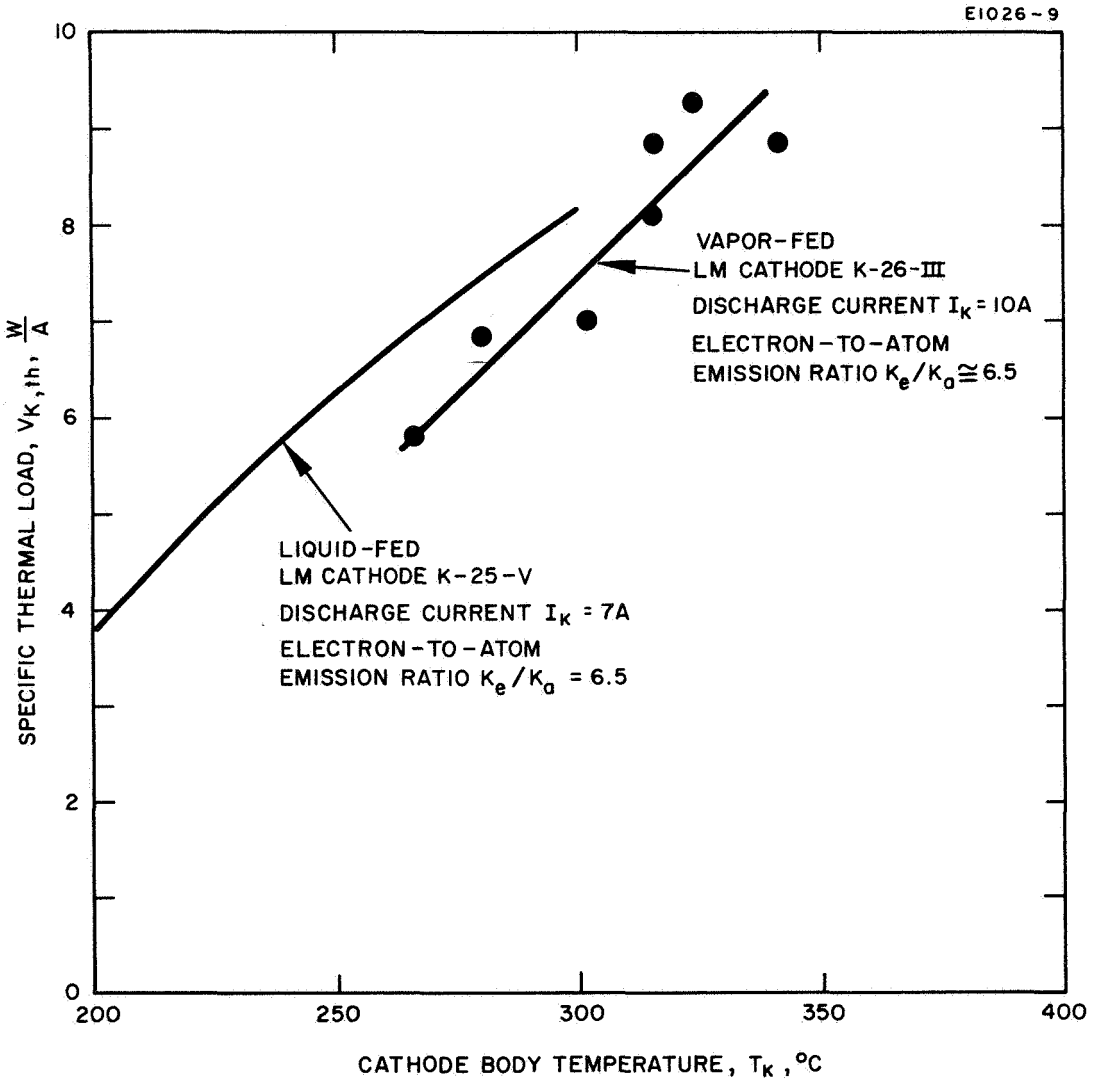

Fig. 20. Dependence of the specific thermal load ($V_{K,th}$) on cathode body temperature (T_K) for vapor-fed LM cathode K-25-V.

externally to temperatures within the operating range before a discharge can be maintained. For a given application, the vapor-fed and liquid-fed modes can be expected to give similar performance, and the choice between them should be made according to the needs of the over-all thruster system.

To demonstrate that vapor-fed LM cathodes represent a practical alternative to liquid-fed LM cathodes in thruster applications, the 20-cm thruster was operated briefly with vapor-fed LM cathode K-26-III. With a neutral flow-rate equivalent I_a = 731 mA, a mass utilization efficiency η_m = 88% was obtained with a total source energy per ion V_S = 560 eV/ion. The cathode body and vaporizer temperatures were 292°C and 313°C, respectively. These results demonstrate adequately the feasibility of thruster operation with a vapor-fed LM cathode, and no thruster optimization with this cathode type was carried out.

Discharge losses with the vapor-fed LM cathode were significantly greater than those encountered with the liquid-fed LM cathode which had been used throughout the program to optimize the performance of the 20-cm thruster. The less-than-optimum performance obtained with the vapor-fed LM cathode can be understood for the following reasons: (1) the cathode could not conveniently be placed with the existing cathode-cup pole piece at the previously established optimum position, (2) the lowest value of the neutral flow rate at which vapor-fed LM cathode K-26-III was designed to be operated is considerably above the value for optimum performance of the 20-cm thruster discharge chamber in the configuration employed, and (3) the distribution of plasma density may be considerably different with the vapor-fed LM cathode from that obtained with the liquid-fed LM cathode used in the thruster optimization.

5. Annular LM Cathode K-51

A light-weight annular LM cathode was fabricated for use with the 30-cm thruster; it is designated as K-51. This LM cathode is shown schematically in Fig. 21, attached directly to the removable portion of the aluminum backplate of the thermally integrated 30-cm thruster. The design of this LM cathode differs from that of previous high-temperature LM cathodes in that the annular feed channel is cylindrical rather than conical in shape. With the cylindrical geometry, it is possible to more accurately fabricate the critical dimensions of the feed channel which is necessary for efficient high-temperature operation. This LM cathode was designed specifically to take full advantage of operation with a single-capillary feed system (see Section V-B).

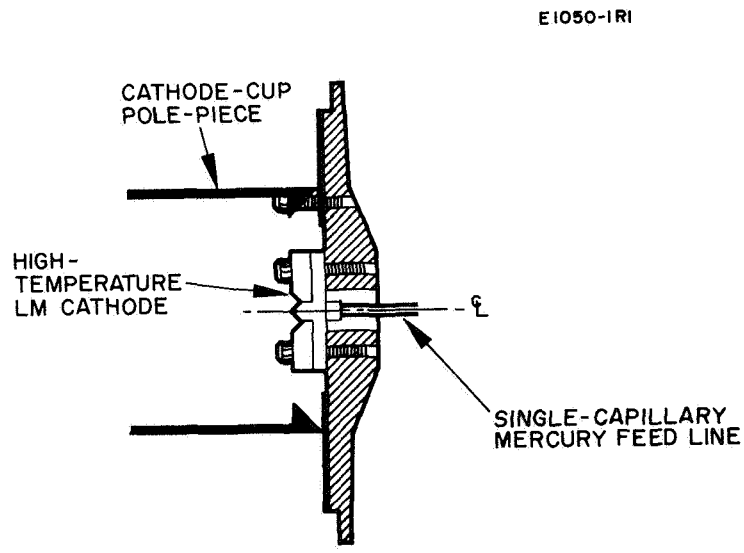

Fig. 21. Schematic drawing of single-capillary-fed annular LM cathode K-51. (The cathode is shown attached to the removable portion of the thruster's thermally conductive aluminum back plate.)

Figure 22 is a photograph showing this cathode mounted for testing in a diode discharge. A gas-cooled metal heat sink is attached to the outer edge of the removable section of the thruster's aluminum backplate as a substitute for the heat sink normally provided by the thruster itself. Diode tests with this LM cathode were limited to the demonstration that satisfactory operation was achieved over the range of interest for operation of the 30-cm thruster. Sufficient time was not available within the subject contract to establish the temperature dependence of the specific thermal load ($V_{K,th}$); however, a value of $V_{K,th} \sim$ 4 W/A at 200°C is indicated by the equilibrium temperature attained by the cathode during thruster operation.

LM cathode K-51 has been thermally integrated with the 30-cm LM cathode thruster. Under typical operating conditions (see Section III-C) the cathode body temperature was measured at T_K = 220°C, while the temperature of the thruster backplate was 200°C.

B. LM CATHODE NEUTRALIZERS

1. Introduction

The LM cathode was intended originally to serve as a cathode for the main discharge of electron-bombardment thrusters. After proving its durability and low power consumption in this application, the LM cathode was adapted for use also as a neutralizer cathode. Tests conducted to date have demonstrated that the LM cathode is well suited as a neutralizer, and that it has the potential for better performance than may be possible with other approaches. After the conclusion of a 500-hour LM cathode neutralizer test in conjunction with the 4,000-hour life test of a 20-cm LM cathode thruster in 1966, no measureable increase in accelerator erosion was observed which could be attributed to the use of the neutralizer.* The body of the LM cathode neutralizer was similarly free of any evidence of arc erosion.[5] LM cathode neutralizers possess additional attractive

*A possible reason for this observed absence of neutralizer-induced accelerator erosion is the highly directional emission of the mercury atoms and ions which emanate from an LM cathode together with the emitted electrons. This directionality, in conjunction with appropriate aiming of the neutralizer axis relative to the beam axis, is believed to prevent the impingement on the accel electrode of ions originating in the neutralizer plasma jet.

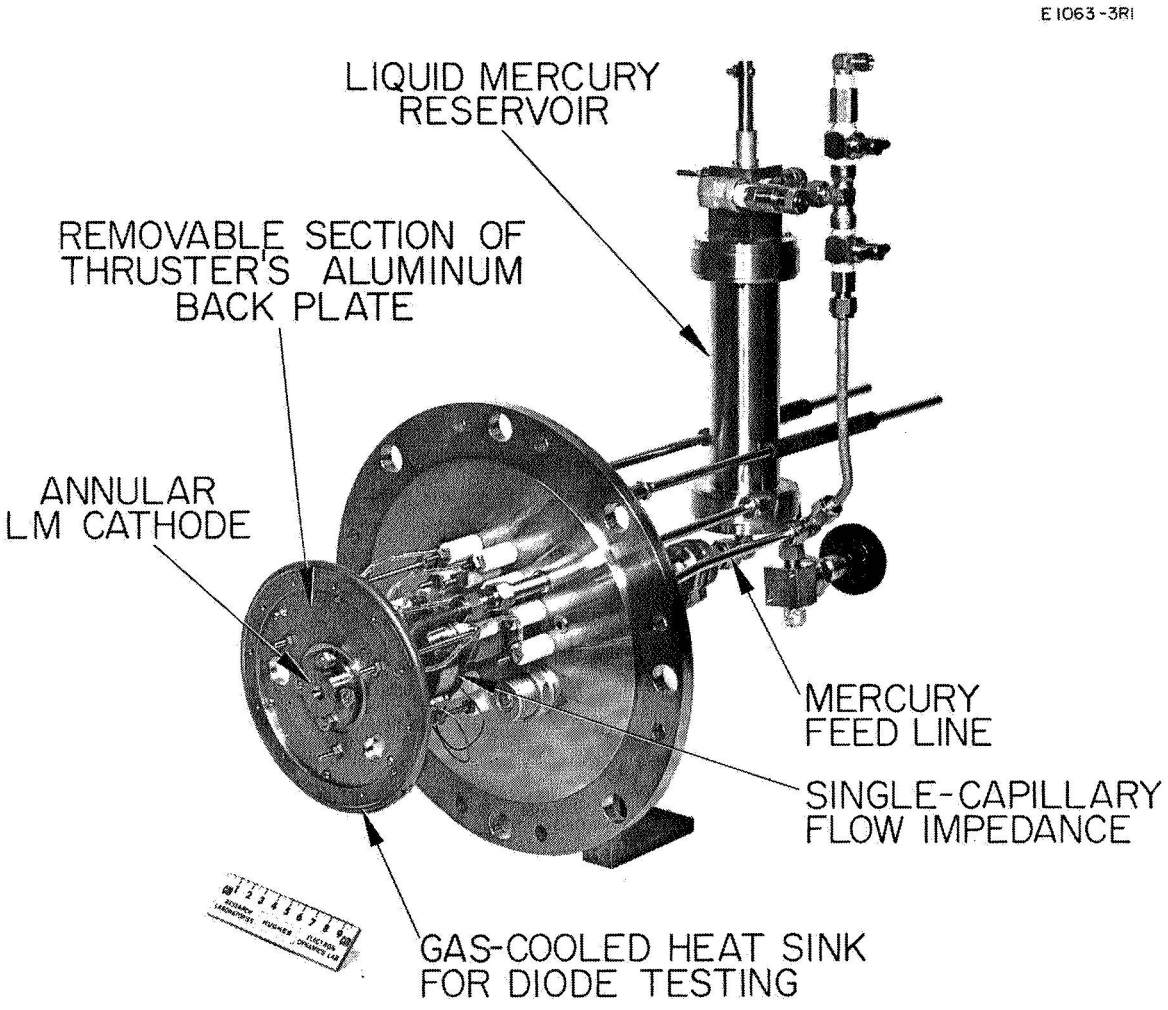

Fig. 22. Photograph of single-capillary-fed annular LM cathode K-51. (The cathode is mounted for testing in a diode discharge.)

features: they require neither heaters nor vaporizers, and their propellant consumption can be comparatively low. In diode tests electron-to-atoms emission ratios of 50 to 1 are obtained. This corresponds to a mercury flow-rate equivalent of 20 mA at an electron current of 1 A.

The design of the neutralizer cathode used during life test mentioned above is illustrated by Fig. 23. The basic difference between the neutralizer pool-keeping structure and that of the main thruster cathode is in the use of a bimetal structure in the case of the neutralizer. The upstream portion consists of a metal which is permanently wettable by mercury (such as copper or platinum), while the downstream portion is made of a refractory metal (such as molybdenum or tungsten) which requires the presence of an arc spot for each rewetting after consumption of a previous mercury layer. This combination results in the ability to contain a large-amplitude feed-rate fluctuation, while limiting the arc-spot pattern excursions under normal operating conditions to the upstream proximity of the dividing line between the two materials, thereby maximizing the obtainable electron-to-atom emission ratio.

Under the present contract, research has been undertaken to establish the limiting electron-to-atom flux ratio for the copper-molybdenum bimetal pool-keeping structure, and to investigate the performance of cathodes using materials other than copper for the upstream portion of the pool-keeping structure. New designs have been developed for LM cathode neutralizers which employ an all-molybdenum pool-keeping structure. In one design the level of the liquid mercury is stabilized by the use of a copper section, serving as a wick, which is located entirely upstream of the molybdenum pool-keeping structure and which has demonstrated the capability to smooth out flow fluctuations. The other new design contains no copper, but rather depends on the uniform flow characteristics of a single-capillary flow impedance to insure that no large-amplitude feed-rate fluctuations are present.

2. Research

a. Maximum Electron-to-Atom Emission Ratio

The results of a company-supported program at HRL[18] had led us to expect that considerably higher electron-to-atom emission ratios than previously achieved should be obtainable. It seemed reasonable to expect a maximum value of $K_e/K_a \sim 200$

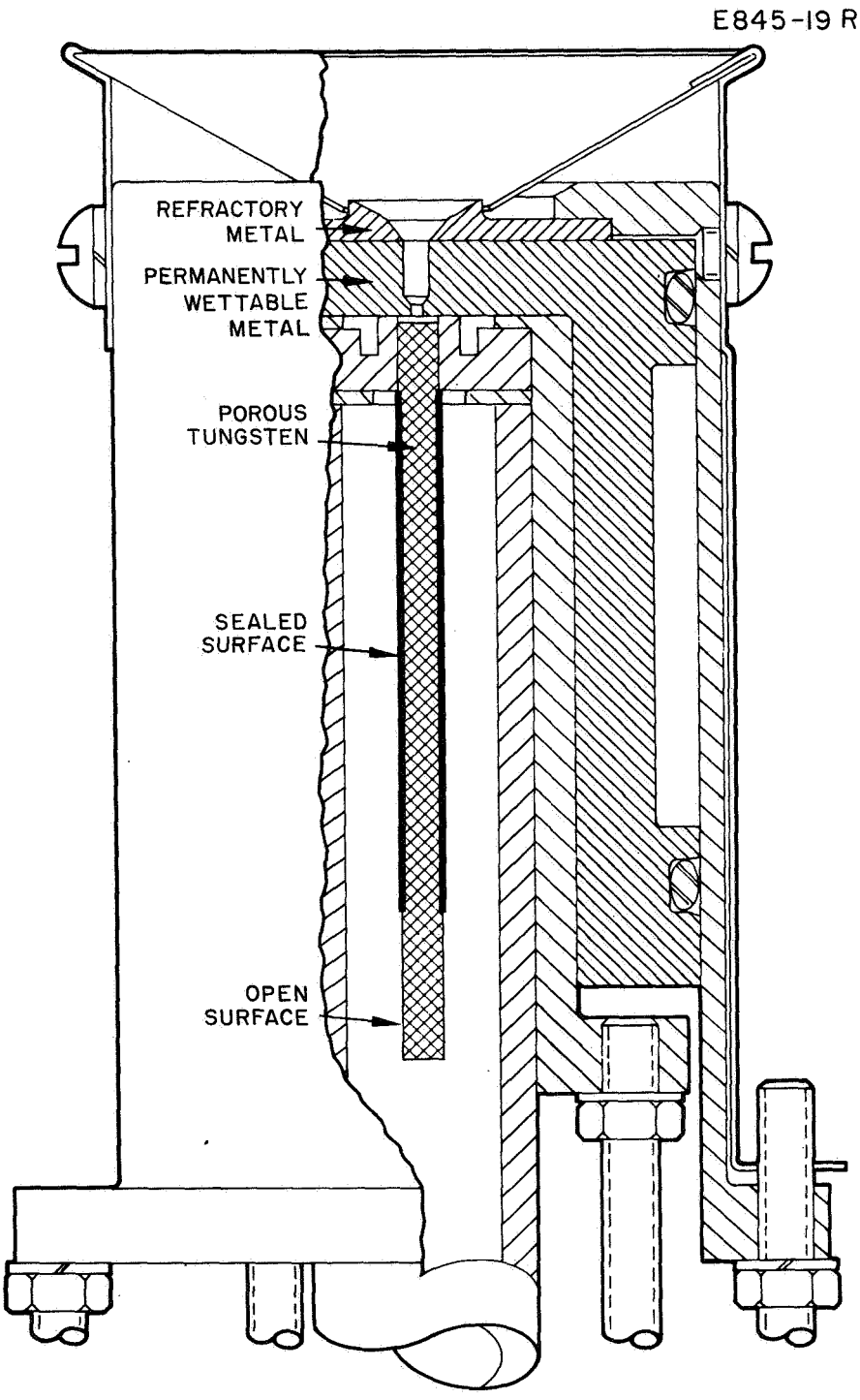

Fig. 23. Schematic cross section of an LM cathode neutralizer with a bimetal pool-keeping structure (not to scale).

for the neutralizer current range. A copper-molybdenum neutralizer, having a pool-keeping structure with 0.25 mm diameter cylindrical bore, was selected to test the validity of this prediction. An operating temperature of 40°C was found to give the best compromise between low mercury losses by evaporation (requiring low temperature) and avoidance of mercury recondensation on the downstream portion of the pool-keeping structure (which requires a relatively high temperature). Such recondensation would lead to frequent arc extinctions in the neutralizer current range.

When all parameters were optimized, it was indeed found possible to operate this cathode at $K_e/K_a \sim 200$ (average for a 2-hour run), with a current of 1.9 A and a diode discharge voltage of $\lesssim$ 30 V. While this result was achieved under strictly laboratory conditions and does not represent performance readily available with a thruster in space, it does demonstrate the ultimate potential of this approach, and it confirms our prediction.

b. Materials Evaluation

The materials used previously with the LM cathode neutralizer design shown in Fig. 23 were copper (for the upstream portion) and molybdenum (for the downstream portion of the pool-keeping structure). Under this contract an effort was concentrated on investigating the performance of LM cathode neutralizers using other materials for the upstream portion. The results of this effort can best be represented by Table V. For the materials listed closest to copper, several days of continuous operation were required to reveal an inferiority compared with copper, while for the most extreme entries the deficiency became obvious after a few minutes of operation.

3. Development

a. LM Cathode Neutralizer with Copper Wick Section

A new LM cathode neutralizer design (K-48) has been conceived, implemented, and tested. It combines the advantages of the bimetal neutralizer structure (minimum variation of the arc-spot pattern diameter for a given feed-rate fluctuation) with those of the main thruster cathode (arc-spot pattern always located on non-permanently-wettable material, hence no arc erosion of structural material). In this design an all-molybdenum pool-keeping structure is coupled to the downstream

TABLE V

Evaluation of Materials for Pool-Keeping Structure[a]

Platinum Aluminum	Excessive amalgamation, resulting in consumption of structural material.
Copper	Best over-all performance of materials tested.
50% porous tungsten, filled with copper Cold rolled steel Iron Stainless steel (304) Tungsten Nickel Tantalum	Insufficient permanent wettability resulting in instability of arc spot anchoring at low currents.

[a]The arrows indicate the direction of increasing importance of the stated properties.

end of the porous-tungsten flow impedance by means of a copper section, serving as a wick, which has demonstrated the capability to smooth out flow fluctuations. This neutralizer was operated in a diode discharge for periods of several hours at electron currents within the range of ion-beam current of a 30-cm thruster, and good stability (e.g., an average of 1.5 spontaneous extinctions per hour, automatically reignited by a stationary pulse igniter) has been demonstrated. Typical data points which were obtained with K-48 are given in Table VI.

TABLE VI

Diode Performance of LM Cathode Neutralizer Having a Copper Wick Section Followed by an All-Molybdenum Pool-Keeping Structure (arc-spot pattern always located on molybdenum)

Neutralizer Current, A	Discharge Voltage, V	K_e/K_a	Run Duration, Hours
2.5	25.5	95	1.1
1.82	25	67	3.5
1.06	24.5	43	5.3
1.05	24	45	6.7
0.78	25	33	2
0.5	22.5	20	4.5

Because the arc-spot pattern is always located on molybdenum, no arc erosion is anticipated with this neutralizer design. The ultimate life limitation, which may result from amalgamation of the copper wick section, is not yet firmly established, but would appear to be in excess of 6,000 hours. This conclusion is based on the fact that, after having been in storage for $\sim$ 6,500 hours with the wick section in contact with liquid mercury, K-48 was put back into service to provide ion-beam neutralization with the 30-cm thermally integrated thruster, and no performance deterioration was observed.

The electrical circuitry used for thruster operation of the LM cathode neutralizer was identical to that employed during the earlier 500-hour thruster test[5] (described in the Summary Report for Contract NAS 3-6262), except for the replacement of the automatic mechanical igniter by an automatic stationary pulse igniter. In order to avoid any possible

impingement of the neutralizer plasma jet on the accel electrode, the neutralizer was at first mounted ∿ 4 cm from the beam edge with its axis inclined at 30° with respect to the beam axis. This combination of distance and angle was found to be too conservative: the neutralizer discharge was difficult to maintain. Hence the angle between the neutralizer and beam axes was then increased to 45° in an effort to achieve better neutralizer-beam coupling. This improved the stability of the neutralizer discharge to the point where extinctions were essentially limited to beam outages due to high-voltage breakdown. Ion beam neutralization was obtained under typical thruster operating conditions (see Section II-C-3) with a total coupling voltage between neutralizer and collector V_{N-C} ∿ 30 V, and with electron-to-atom ratios (K_e/K_a) up to 26, corresponding to a neutralizer mass flow fraction $\eta_{m,N}$ = 3.0 ... 3.3%.

It is expected that the neutralizer can be operated at considerably higher values of K_e/K_a (as is the case in diode operation) if still better neutralizer-to-beam coupling is provided by reducing the radial distance between the neutralizer and the beam edge. (Note that such a reduction of distance, at constant angle between the axes, does not increase the possibility of accel electrode impingement by the highly directional plasma jet of an LM cathode neutralizer.) No trace of neutralizer or accel electrode erosion has been observed after 50 hours of thruster operation.

b. All-Molybdenum LM Cathode Neutralizer

As an additional step in the series of basic design modifications aimed at the elimination of potentially life-limiting factors, a third type of neutralizer cathode has been designed, fabricated, and tested. This cathode (K-50) does not contain permanently wettable materials in any location where they are operationally exposed to liquid mercury. Hence, this neutralizer type should have practically no life limitation, but its performance depends on a flow impedance which is capable of providing by itself a high degree of flow uniformity.

The design of K-50 permits the use of either a porous-tungsten or a single-capillary flow impedance, and it was hoped that a capillary in the appropriate impedance range for neutralizer operation would become available before the end of the contract period. This was not the case, however, and hence K-50 has been tested only with a porous-tungsten impedance. In this feed mode, stable operation at an electron current of

$\sim$ 1 A was limited to electron-to-atom ratios up to 10. On the other hand, the ability of a single-capillary flow impedance to provide highly stable mercury flow has been demonstrated (at higher flow rates) in a separate experiment, described in detail in Section V-B-3-d. The significant result is the observation that the diameter of the circular arc-spot pattern in a conical pool-keeping structure did not vary by more than $\pm$ 5%, even when the pattern diameter was only $\sim$ 0.25 mm.

Operation of the all-molybdenum neutralizer with a properly sized single-capillary flow impedance remains as a future task to which a high probability of success can be assigned, in the light of the results reported above.

SECTION V

LIQUID MERCURY FEED SYSTEM DEVELOPMENT

A. INTRODUCTION

The pneumatic reservoir system shown schematically in Fig. 24 has been used to replenish liquid mercury to the pool-keeping structure of the LM cathode. Pressurized nitrogen is applied above a piston pressing on the mercury surface to serve as the driving force. The piston position is indicated with a dial indicator (calibrated to 0.001 in. or 0.0001 in.) contacting the top of the piston shaft, and its change as a function of time serves as an indication of mercury consumption and yields an accurate measure of the flow rate. In the past, mercury flow was regulated by passing mercury at the required pressure through a porous tungsten plug used as a flow impedance. This impedance was placed immediately upstream of a small plenum leading to the feed channel of the LM cathode pool-keeping structure, as shown schematically in Fig. 25.

Under the subject contract, the single-capillary flow impedance has been qualified as a useful component for control of liquid-mercury flow in the range of interest for solar electric propulsion.[19] Throughout the range which was investigated, from a flow-rate equivalent of 50 mA to 6.5 A, the flow of liquid mercury through a single-capillary impedance has been shown to depend linearly on the drive pressure to within an experimental standard deviation of 5%.

Management of liquid mercury flow in an LM cathode thruster system extends beyond the capability for control over the flow rate. In a related contract effort[20] (Contract NAS 7-539) the design of liquid-mercury feed systems was explored in detail. A number of unique components were built and their operating characteristics were established in order to better evaluate the various systems considered. Two of these components, an electromagnetic (EM) pump and a high-voltage isolator, have since been incorporated into a breadboard flow system which was assembled under this contract for a demonstration of the proper operation of each of the components and of the mutual compatibility of all of the components of the feed system performing together with an LM cathode thruster.

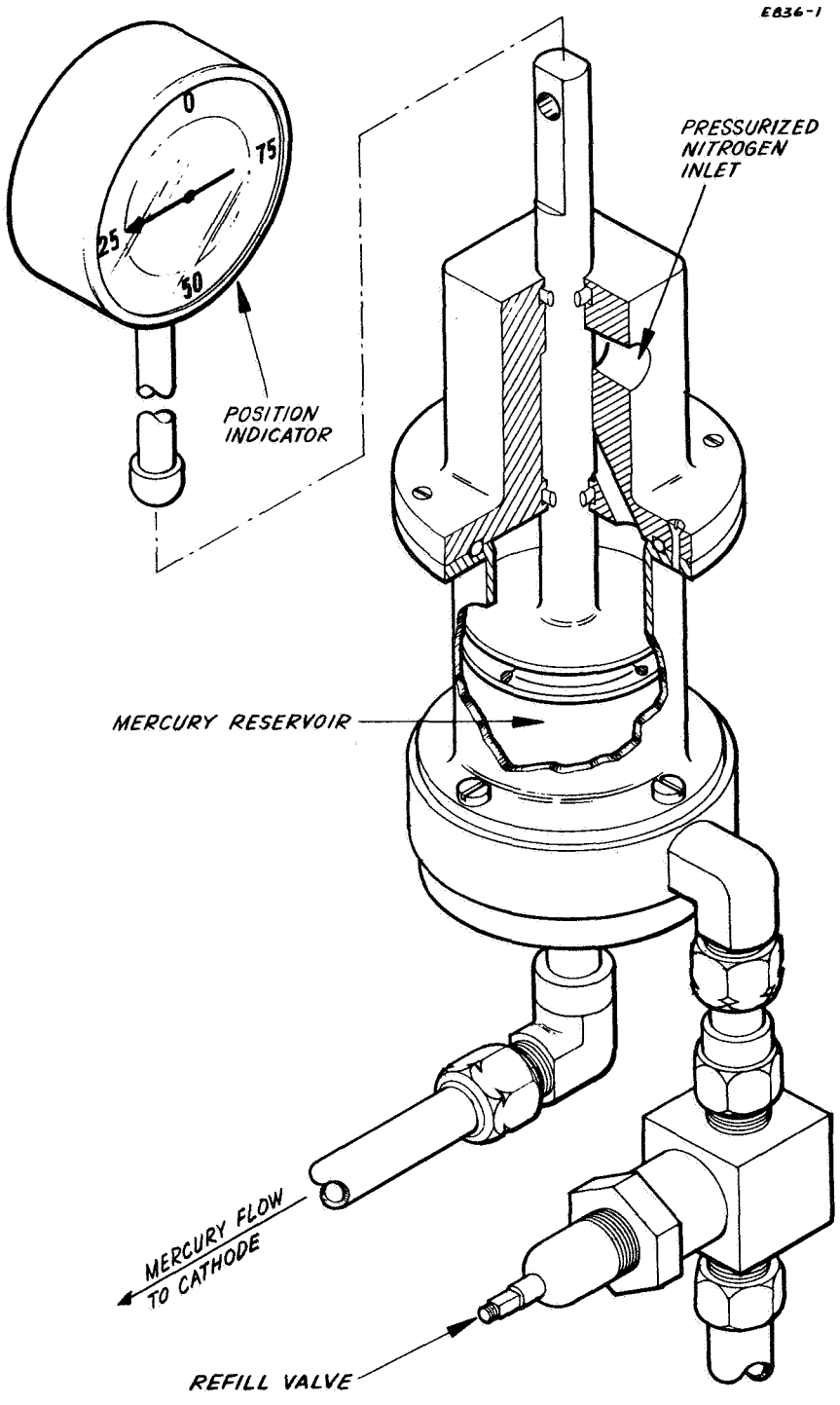

Fig. 24. Gas pressurized mercury reservoir.

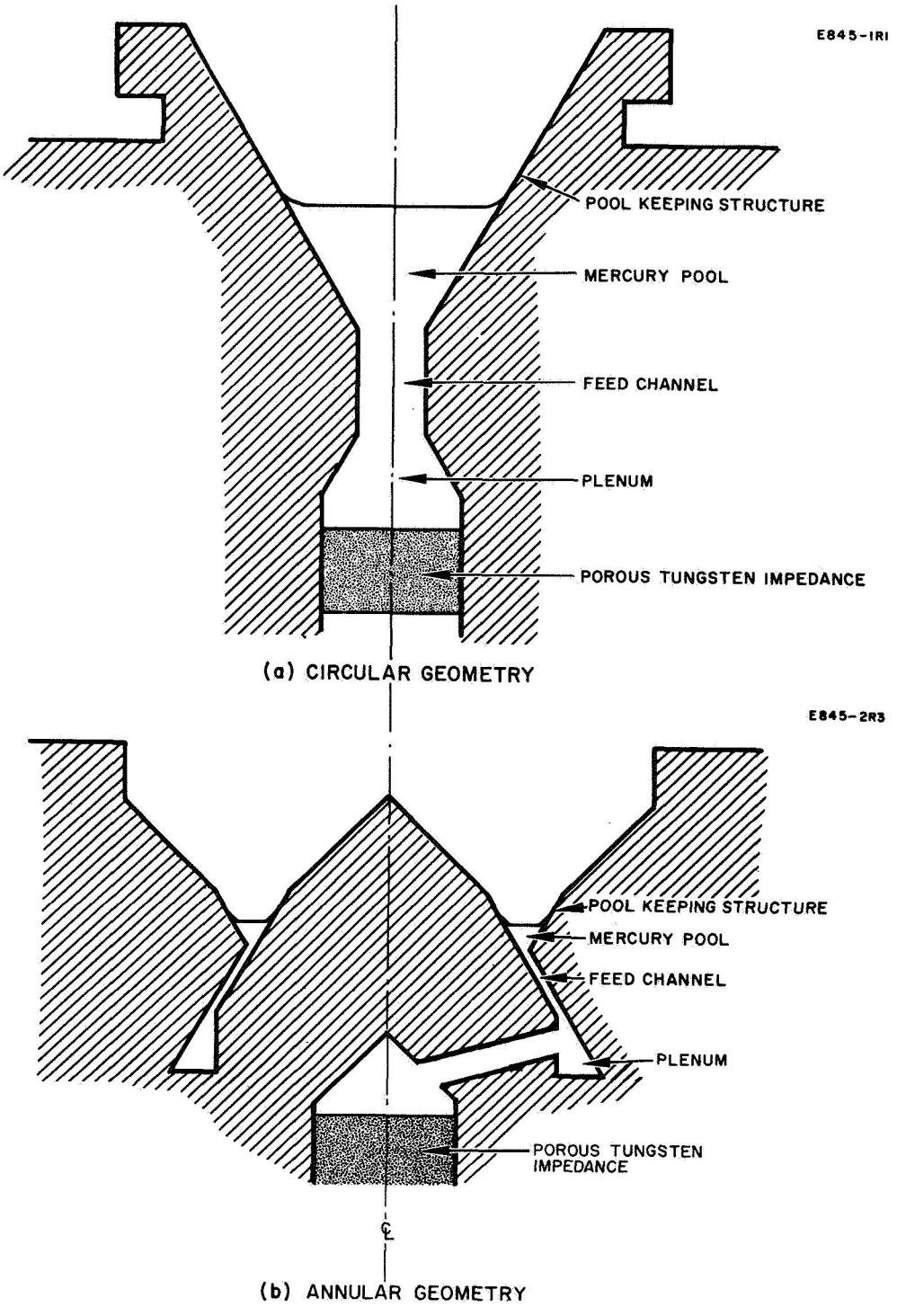

Fig. 25. Circular and annular LM cathode geometries with porous-tungsten flow impedances.

The system consists of (1) a gas-pressurized positive-expulsion mercury reservoir, (2) the EM pump, (3) the liquid-mercury high-voltage isolator, (4) a single-capillary flow impedance, and (5) the 30-cm thermally integrated thruster operated with high-temperature LM cathode K-51 (which was designed to take full advantage of the single-capillary feed system).

B. SINGLE-CAPILLARY FLOW IMPEDANCE

Past experience with porous-tungsten impedances has indicated that variations in fabrication are too numerous to permit exact impedance design; hence these impedances must be fabricated first and then calibrated to find which ones meet given requirements. It has also been found that the flow calibrations change as a function of the past history of a given porous-tungsten impedance with regard to heating, exposure to air, degree of wetting with mercury, etc. These disadvantages have been overcome by use of the single-capillary impedance, because with these the rate of flow is a linear function of the applied pressure and can be readily calculated. This permits the exact design of specific flow impedances to match the requirements of a given application. The single-capillary flow impedance can also be used to translate a pressure readout unequivocally into a direct, instantaneous flow-rate readout, because of its constant flow calibration.

Because only a small part of the active length of the single-capillary flow impedance must be in the intimate proximity of the cathode, the bulk of the impedance remains at reservoir temperature, while the downstream terminus of the tube can rise to whatever cathode temperature is required for thermally integrated thruster operation. The resulting thermal isolation between the cathode and the flow impedance results in a repeatable and predictable relationship between mercury flow rate and applied pressure which is independent of thruster operating conditions. In the discussion below it is shown that the single-capillary flow impedance offers still another advantage for use with the LM cathode through a reduction of the amplitude of mercury flow fluctuations which occur due to surface-tension forces.

1. Flow Uniformity

In order to appreciate the full benefits derived from use of the single-capillary flow impedance, one must first understand a phenomenon which leads to fluctuations in the rate of

mercury flow into the pool-keeping structure. Let us assume that a steady mercury flow is provided at the entrance of the minimum-diameter section (feed channel) through which the mercury passes into the pool-keeping structure shown in Fig. 26 and that mercury wets the walls of the pool-keeping structure but not those of the feed channel. The liquid in the pool-keeping structure is at a very low pressure determined by surface tension forces, by the momentum change imparted by surface evaporation of mercury atoms, and by arc pressure. Because the pressure exerted by surface tension is inversely proportional to the radius of curvature of the liquid surface,* the magnitude of this pressure rises greatly to a value P_{FC} at a location within the feed channel where the radius of curvature is a minimum (the radius of curvature being equal to that of the feed channel). In the upstream direction, the pressure p_{FC} is balanced by the driving pressure of the flow system. In the downstream direction, however, p_{FC} may not be balanced, and thus the downstream segment of the minimum-diameter mercury column is unstable and tends to be expelled into the pool-keeping structure. Such expulsion leaves a void, and no further mercury flow enters the pool-keeping structure until the void is filled by flow from the source, at which time the system is again unstable and the mercury contained in the feed channel may again be expelled into the pool-keeping structure.

It is apparent from this description that there is a tendency for the flow of a nonwetting liquid through a small capillary to exhibit fluctuations as the liquid emerges from the capillary. It should be noted, however, that the point of separation of the column can be no farther upstream of the pool-keeping structure than the upstream terminus of the minimum-diameter feed channel: thus the magnitude of the flow fluctuations is limited to the volume of the minimum-diameter feed channel. The effect of these flow fluctuations can be made to be negligible so long as the volume of the feed channel is made small compared with the volume of mercury normally contained in the pool-keeping structure. The designs of LM cathode K-41 (shown in Fig. 27) and of annular LM cathode K-51 (shown in Fig. 21) are both based on this principle.

---

*This simple relationship is correct if the angle of contact of the liquid with the wall is assumed to remain constant.

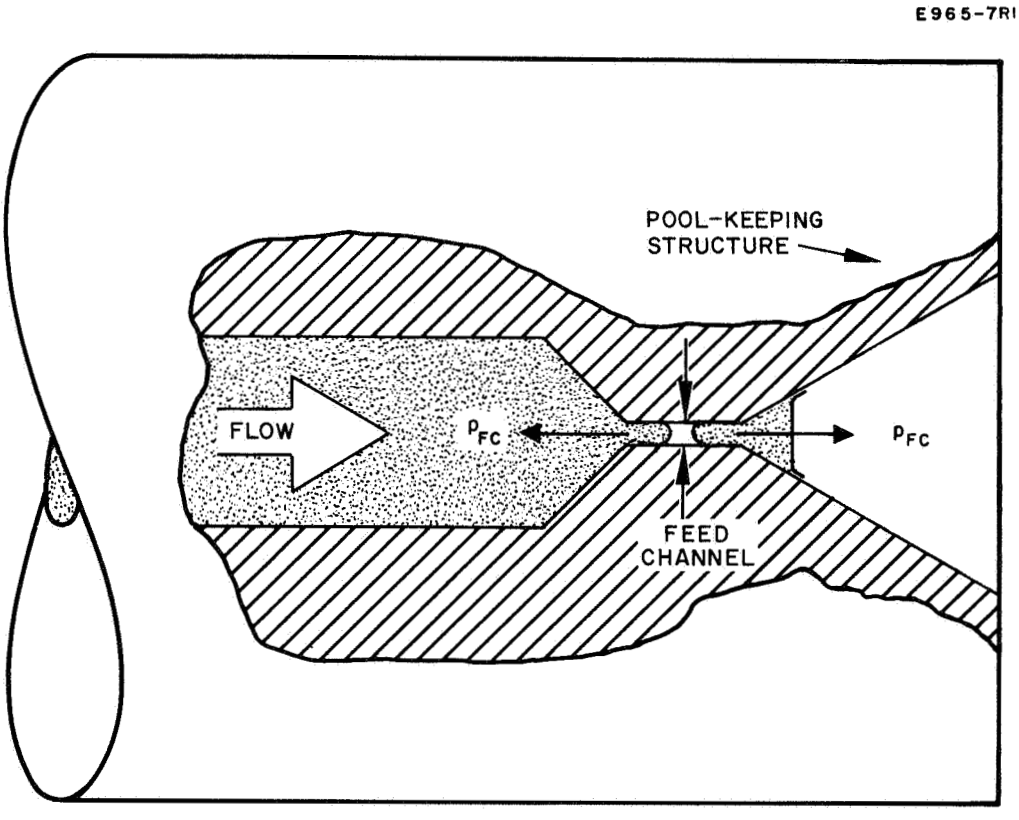

Fig. 26. Flow fluctuations due to surface-tension forces.

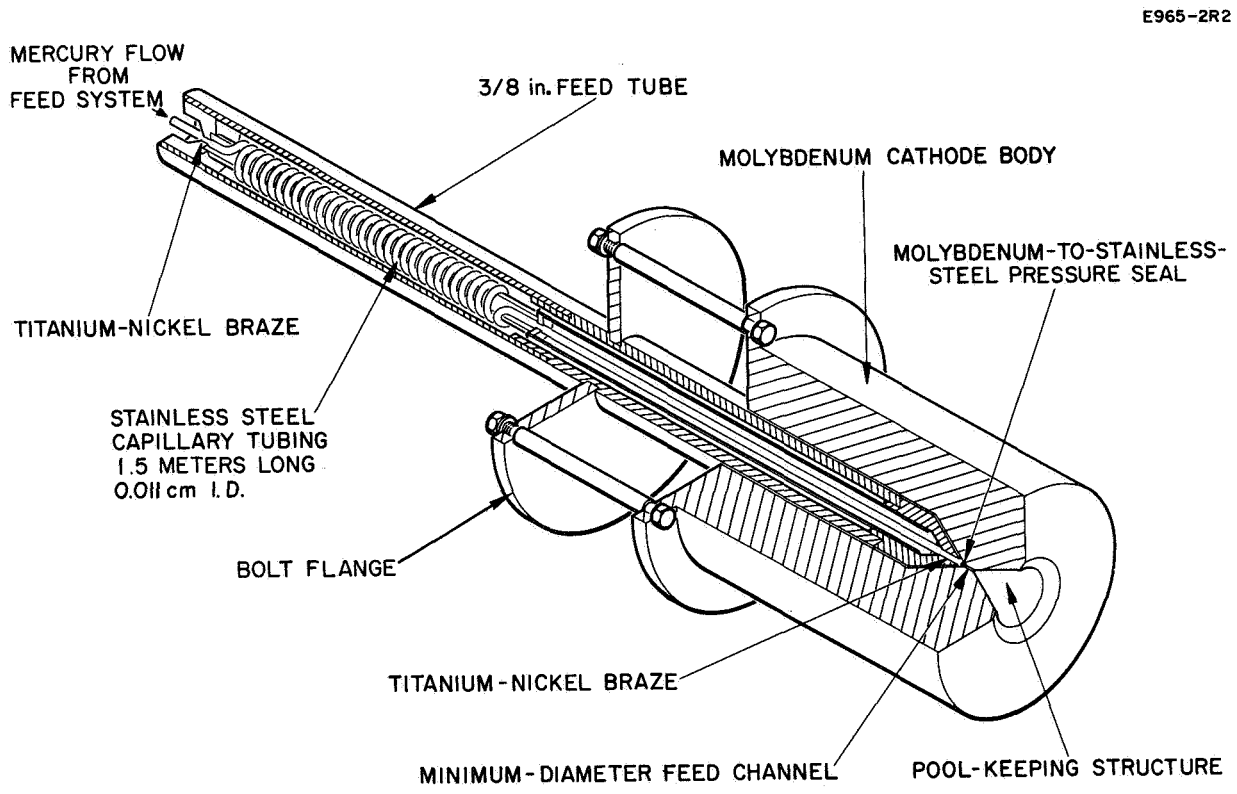

Fig. 27. Circular LM cathode K-41 with single-capillary flow impedance SC-2.

Only by feeding mercury to the cathode through a passage with a diameter which is everywhere larger than that of the feed channel can the fluctuation amplitude due to surface-tension forces be reduced to the minimum value imposed by the feed channel itself. If a porous-tungsten flow impedance is used, as shown in Fig. 25, the feed channel does not present the minimum flow diameter to the mercury stream. Rather, the minimum flow diameter would occur within the pores of the impedance. Consequently, the mercury flow entering the feed-channel would not be steady as was assumed, but would already exhibit fluctuations introduced by the porous-tungsten impedance. These primary fluctuations would simply add to those introduced by the feed channel. Use of the single-capillary impedance not only satisfies the criterion just stated, but also fulfills an even more stringent requirement: it feeds the mercury to the cathode through a passage of monotonically decreasing diameter, thereby preventing the trapping of gas bubbles. The single-capillary flow impedance also places the minimum volume of mercury in close proximity to the thermal fluctuations which can occur in the pool-keeping structure, and so minimizes the other major cause of flow fluctuations.[5]

2. Impedance Design

It is convenient to operate a liquid-mercury flow system at an absolute pressure in excess of 1 atm. The drive pressure should also be large compared with any fluctuating pressure drop which might exist in the system, in order to maintain a constant relationship between drive pressure and mercury flow rate.

A possible source of pressure fluctuation is related to the reluctance of a nonwetting liquid (mercury on stainless steel) to enter a capillary tube which arises from surface-tension forces. This reluctance must be overcome by a drive pressure equal to the pressure due to surface tension (p_{ST}) which is related inversely to the tube diameter (D) by the formula[21]

$$p_{ST} = \frac{4\gamma \cos \theta}{D}$$

where γ is the coefficient of surface tension and θ is the contact angle between the liquid and the tube wall. From Ref. 21 we have (for mercury on most metals)

$$\theta = 130°$$

$$\gamma = 473 \text{ dynes cm}^{-1}.$$

In convenient units the above formula can be re-expressed as

$$p_{ST} \text{ (psi)} = \frac{1.75 \times 10^{-2}}{D(\text{cm})} .$$

Over long periods of time, the exact value of the pressure p_{ST} may be expected to fluctuate in response to changes in the degree of wetting of the tube wall surface by the mercury. To avoid any related fluctuations in impedance calibration or in mercury flow rate, the drive pressure should be large compared with the pressure due to surface tension. On the other hand, the drive pressure must be as low as possible in order to impose minimum constraints on other components of the system and to keep system weight low. Both goals can be achieved by choosing a capillary tube of sufficiently large diameter.

The flow rate through a single-capillary impedance is limited by viscous forces to a value given by Poiseuille's law:

$$\dot{v} = \frac{\pi D^4}{128 \eta L} p,$$

where $\dot{v}$ is the volume flow rate, D is the diameter of a circular capillary tube, L is its length, η is the coefficient of viscosity of the liquid ($\eta_{Hg} = 1.55 \times 10^{-2}$ Poise), and p is the drive pressure. In convenient units this formula can be re-expressed as

$$I_a \text{ (A)} = 7.1 \times 10^8 \cdot \frac{[D(\text{cm})]^4}{L(\text{cm})} \cdot p(\text{psi}),$$

where I_a is the mercury flow-rate equivalent. To insure that the pressure due to surface is small compared with the drive pressure, capillary tubes have been chosen with the diameter D sufficiently large to insure that $p >> p_{ST}$. The length of the impedance is then specified by the value required to yield the desired flow impedance.

3. Impedance Testing

Four single-capillary flow impedances, designated SC-1...4, have been tested under this contract. In the first two tests, involving SC-1 and SC-2, the impedances were operated in the condition in which they were received from the supplier. The rate of mercury flow through these impedances was a linear and repeatable function of the applied pressure to within an experimental standard deviation of 5% of the maximum values of pressure and flow rate for all pressures in excess of zero psig (14.7 psia). Greater scatter, however, was apparent at pressures below 14.7 psia.

To avoid the possible effects of contamination of either the capillary tubes or the liquid mercury, flow tests of single-capillary impedances SC-3 and SC-4 were conducted under well-controlled experimental conditions. The interior of the capillary tubes was cleaned chemically to remove any surface contamination which might be present. Both the mercury and the interior of the capillary tubes were thoroughly outgassed in vacuum at elevated temperature prior to flowing the mercury through the impedances. In the tests conducted under such controlled conditions, the mercury flow rate was found to be a linear and repeatable function of the applied pressure within an experimental standard deviation of 5% over the entire range which was investigated, extending from 3 psia to 200 psia. This corresponds to a mercury flow-rate equivalent extending from 50 mA to 6 A.

a. Impedance SC-1

Single-capillary flow impedance (SC-1) consisted of a 25-cm length of type 304 stainless steel tubing having an outside diameter of 0.018 cm and an inside diameter of 0.0076 cm. The upstream end of this tube was fastened to a 1/16 in. diameter mercury feed line by means of epoxy cement. This feed line in turn was supplied with mercury by a standard piston-driven mercury feed system. The downstream end of the capillary tube discharged into a vacuum chamber. Prior to operation, the capillary tube was evacuated to $\sim 10^{-3}$ Torr by pumping both at the open downstream end and at the mercury feed system prior to its being filled with mercury. The feed system was subsequently filled with mercury under customary vacuum conditions.

Mercury was driven through the single-capillary flow impedance by applying nitrogen pressure above the piston of the feed system. The flow rate of mercury was accurately determined by measuring the displacement of the piston of the feed

system as a function of time. Typical flow data points were acquired over periods of 30 min each. The flow rate of mercury through the single-capillary impedance is plotted in Fig. 28 as a function of the pressure applied across the impedance. For changes in driving pressure to either higher or lower values within the operating range of 20-75 psia, the mercury flow increases linearly with pressure at a rate of $I_a/p = 0.078$ A/psia. Compared with a theoretically anticipated value of $I_a/p = 0.092$ A/psia this value is well within the tolerance anticipated from variations in tube diameter. Flow readings were both linear and repeatable as a function of pressure in this range to within an experimental standard deviation of ± 5% at the center of the range. The data points, indicated by circles in Fig. 28, exhibit no hysteresis or other systematic variations in the flow rate.

Excursions outside the stated range resulted in certain systematic variations in the flow rate. Zero flow was observed for driving pressures of less than 10 psia, and the flow was substantially reduced for a period of about 30 min when the driving pressure was subsequently raised to the region of 15 to 25 psia following such a zero-flow condition. This trend is exhibited by the data points indicated by upward-pointing triangles in Fig. 28. Similarly, when the driving pressure was returned to the operating range after having been set at 150 psia, substantially higher (+ 20%) flow rates were recorded for as long as 30 min thereafter. The latter trend is exhibited by the data points indicated by downward-pointing triangles in the graph. These systematic variations have since been eliminated with impedances SC-3 and SC-4 by observing more exacting experimental procedures.

b. Impedance SC-2

Based on the encouraging performance of the experimental impedance SC-1, a second single-capillary impedance (SC-2) was constructed which could be attached to an LM cathode. This impedance, shown earlier in Fig. 27, consisted of a 150-cm length of 0.0112-cm i.d. type 304 stainless steel tubing which was wound about a spool and totally enclosed within a rigid 3/8 in. tubular housing. Both the upstream and downstream ends of the capillary were attached to the 3/8 in. tubular housing with a nickel-titanium eutectic braze. The downstream end of the capillary impedance was pressed against the cathode adjacent to the upstream end of the minimum-diameter flow channel which precedes the pool-keeping structure. A leak-tight seal was made between the stainless steel capillary tube and molybdenum cathode body by pressing one against the other by means of a bolt flange.

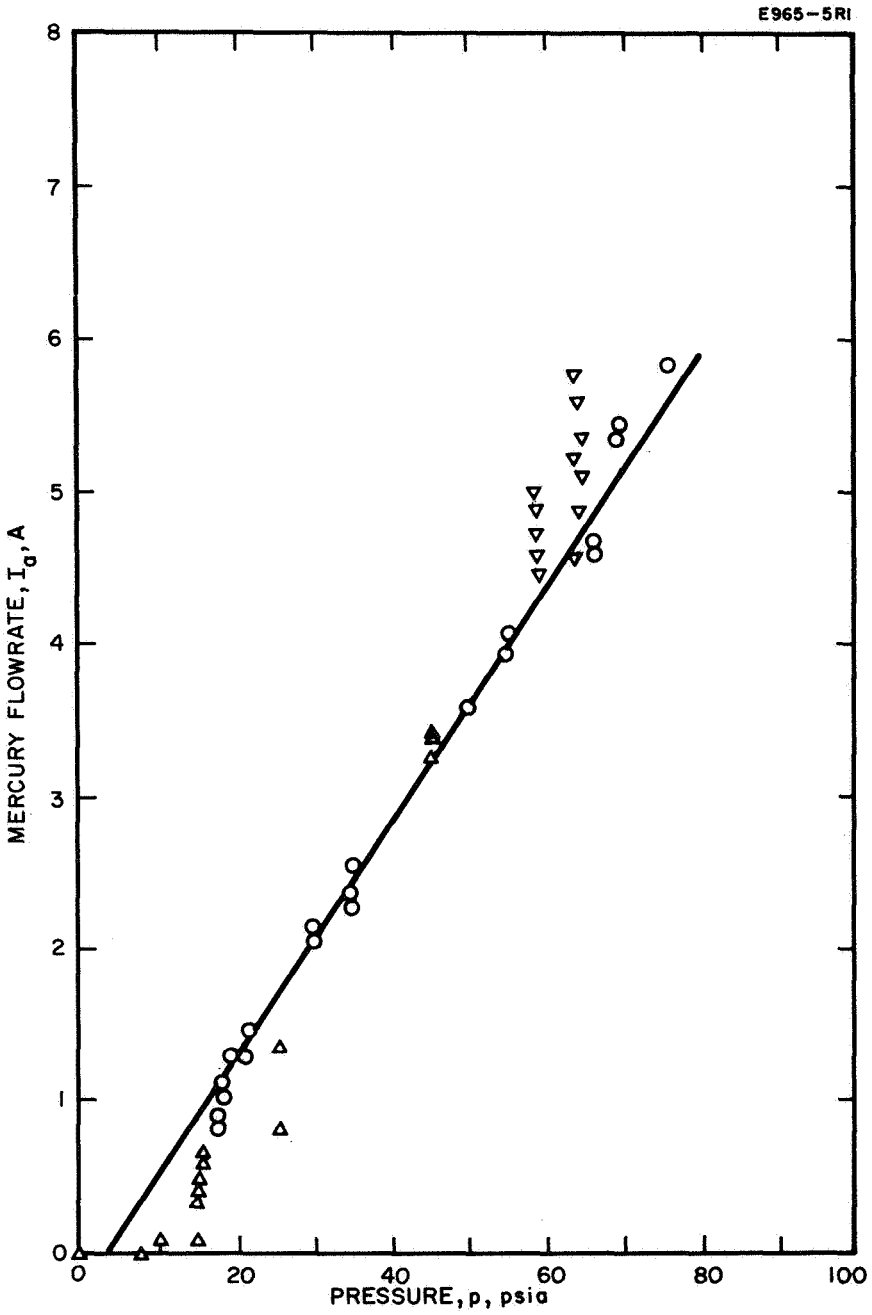

Fig. 28. Dependence of the mercury flow-rate equivalent (I_a) on drive pressure (p) for single-capillary flow impedance SC-1.

Data plotted in Fig. 29 relate the mercury-flow-rate equivalent (I_a) to the driving pressure (p) across the impedance alone in one case, and across the impedance with the cathode attached in the other. The incremental increase in flow with driving pressure is the same in either case: I_a/p = 0.08 A/psi. Within experimental error, the measured flow impedance is identical to the predicted value based on the best known dimensions of the stainless steel capillary tubing. Similar to the results reported previously with capillary SC-1, the rate of flow through this impedance was linear and repeatable over a period of one week to within the experimental accuracy of ± 5% of the full-scale reading for all pressures in excess of zero psig (= 14.7 psia). As in previous single-capillary tests, greater scatter of the data points was apparent at and below 14.7 psia.

Although the flow rate at a given pressure decreases when the cathode is attached to the capillary, $\Delta I_a/\Delta p$ does not change. Attachment of the cathode does not significantly increase the impedance, but rather introduces a constant pressure increment. The source of this pressure increment is related to the minute flow fluctuations which occur in the region of minimum diameter of the cathode feed channel. As described earlier, the downstream segment of the mercury column within the cathode feed channel is unstable and tends to be expelled into the pool-keeping structure. Such expulsion leaves a void, and no further mercury flow enters the pool-keeping structure until the void is filled by flow from the source, at which moment the system is again unstable and the mercury contained in the feed channel may again be expelled into the pool-keeping structure. Since such a void generally exists within the feed channel (which is part of the cathode), a pressure p_{ST} is generated opposing the driving pressure when the cathode is attached to the single-capillary flow impedance. This back pressure must be canceled by an equal driving pressure increment to maintain a given flow rate through the single-capillary flow impedance when the cathode is attached. The experimentally measured pressure increment of 5 psi is consistent with the value calculated in accordance with this model.

c. Impedance SC-3

The flow characteristics of impedances SC-1 and SC-2 indicate the presence of phenomena other than those accounted for by the basic theory of single-capillary flow presented in Section V-B-1. This lack of correspondence between theory and experiment was felt to result from experimental conditions which differed from the idealized conditions assumed by the theory.

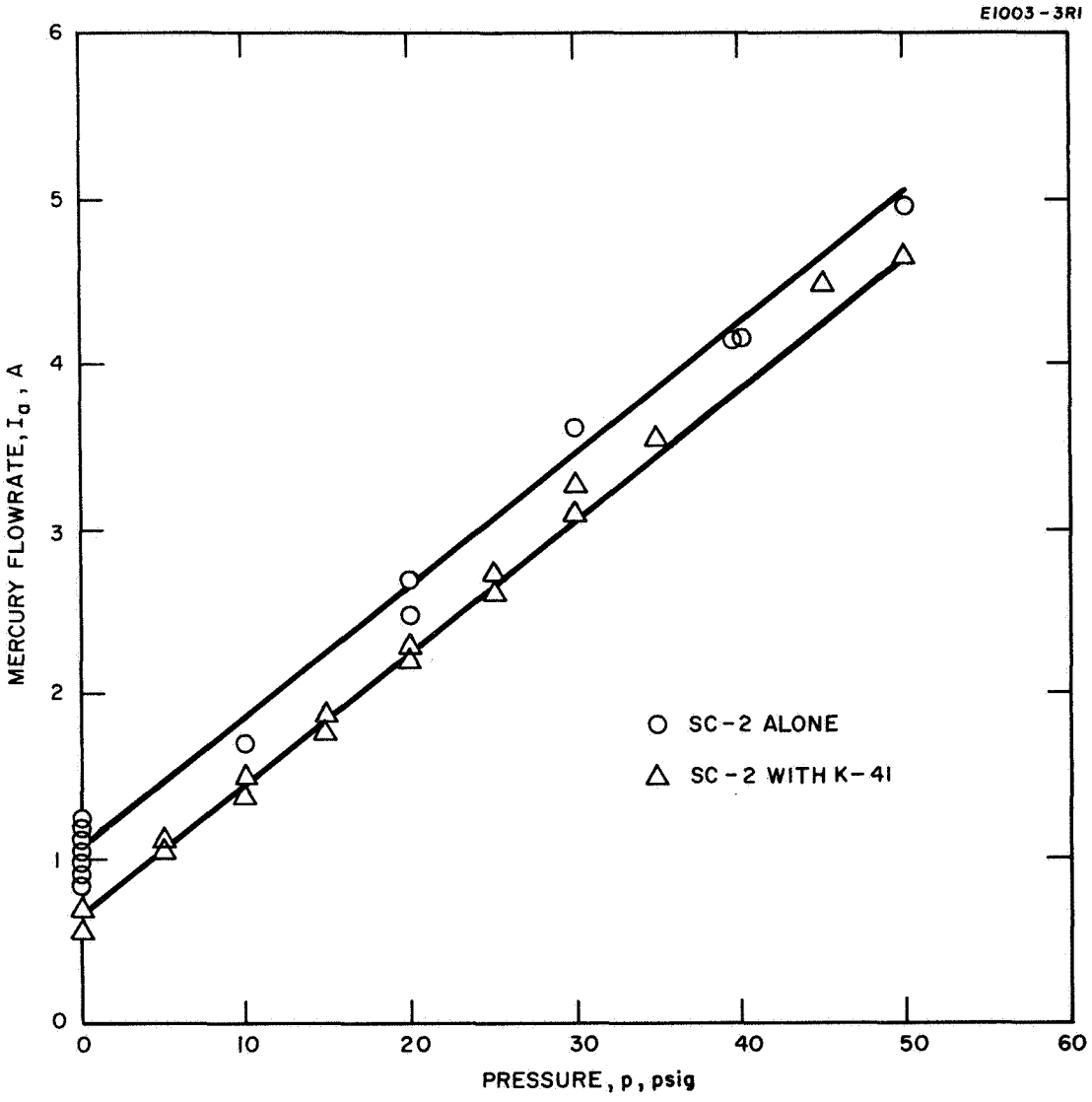

Fig. 29. Dependence of the mercury flow-rate equivalent (I_a) on drive pressure (p) for single-capillary flow impedance SC-2, showing the effect of attaching LM cathode K-41.

In order to more closely approach these idealized experimental conditions, a mercury flow research apparatus was assembled which permitted more controlled testing of single-capillary flow impedances by avoiding possible uncertainties which might be associated with the effects of contamination of either the capillary tubes or the liquid mercury.

For the first tests with the mercury flow research apparatus, a new single-capillary flow impedance was prepared (denoted as SC-3), consisting of a 1;100-cm length of 0.014-cm i.d. type 304 stainless steel tubing. The interior of this capillary was chemically cleaned in the sequency of operations described below:

1. Washed in acetone
2. Washed in detergent and water
3. Etched in a mixture of equal parts HF, HNO_3, and H_2O
4. Washed in deionized water
5. Washed in acetone.

For some time the acid solution of step No. 3 discharged from the capillary, carrying a black suspension of contaminants which were apparently lodged within the tube. After about 1 hour, the discharge was clear. The chemical etch was continued for an additional 1/2 hour after that.

The capillary tube was wound about a 10-cm diameter mandrel. A resistance heater attached to this mandrel was used to heat the single-capillary tube in vacuum to 200°C in order to drive out any trapped gases or vapors prior to operation with mercury. The single-capillary impedance was connected to the flow research apparatus shown in Fig. 30. In this setup mercury is held in a piston-driven positive-displacement feed system from which it can either be driven directly through the flow impedance at pressures from 14.7 to 200 psia, or this system can be used only as a reservoir to deliver mercury to a precision-bore glass capillary serving as a manometer. Mercury from the manometer can then be used under the pressure of the mercury head alone for measurements in the range of 0 to 15.5 psia. At the higher driving pressures, the rate of displacement of the piston permits the measurement of the mercury flow rate, while the rate of displacement of the mercury meniscus in the glass capillary indicates the mercury flow rate at the lower pressures. The O-ring seals of the piston-driven feed system were lubricated with Apiezon-H vacuum grease

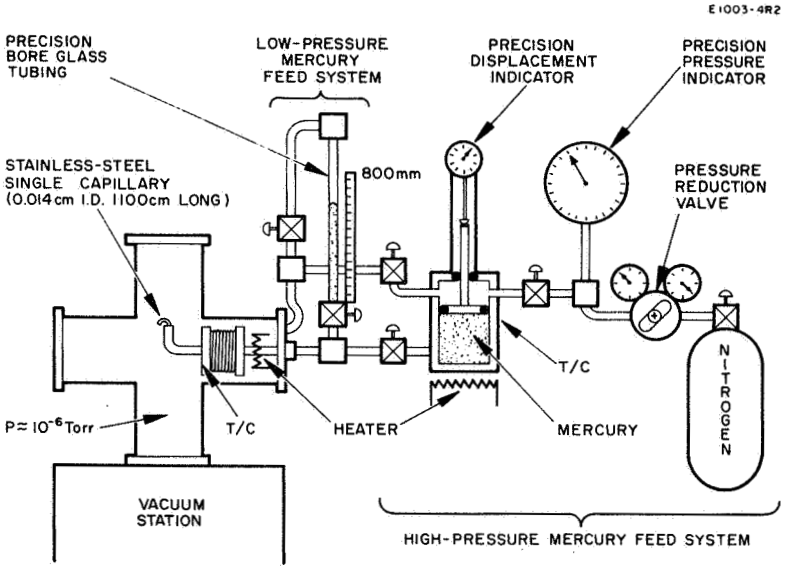

Fig. 30. Single-capillary-flow research apparatus. (T/C is thermocouple).

which permited the mercury, contained in the piston-driven feed system, to be outgassed — under vacuum — at temperatures up to 150°C. The capillary was baked at 180°C in a vacuum of 3×10^{-6} Torr for several days. The mercury in the reservoir was heated under vacuum at 150°C. During this time, the entire reservoir was agitated by a vibrator to help expel any gas trapped in the mercury.

No anomalous variations of the mercury flow rate have been observed with impedances prepared and operated according to the experimental procedures described above. At this time, however, it is not known which of these steps are truly necessary to realize the desirable characteristics of the single-capillary impedance.

In the range from 3.4 to 15 psia, the pressure required to force the mercury through the stainless steel capillary was established by the head of a column of mercury held within a section of precision-bore glass tubing. The mercury flow rate was determined by the rate of change in the position of the mercury meniscus within the precision bore tubing. Data shown in Fig. 31, obtained consecutively over a period of three weeks, exhibit a linear dependence of the mercury flow-rate equivalent (I_a) on the absolute driving pressure (p) with a standard deviation of less than 5%. The rate of increase of the flow rate with increasing mercury head agrees with the predictions of the theory of Poiseuille to within experimental error. An extrapolation of the data indicates that the flow rate drops to zero at a mercury head pressure of 1.86 psia, which corresponds (within 20%) to the pressure due to surface tension (p_{ST}) which is predicted by theory for this capillary diameter. To measure the high-pressure flow characteristics, the manometer feed system was replaced by the piston-driven feed system. Experimental results are presented in Fig. 32 for the change in mercury flow rate as the drive pressure was varied from 14.7 to 215 psia. As in the lower-pressure tests, the mercury flow rate was found to depend linearly on the drive pressure with a standard deviation of less than 5%. The slope was $\Delta I_a/\Delta p = 3.13 \times 10^{-2}$ A/psi, the same as obtained in the low pressure regime to within the experimental error.

To determine the effect of temperature, the drive pressure was varied from 15 to 200 psia with the temperature of the capillary set at 116°C. The mercury flow rate relation remained linear while the slope increased due to changes in mercury density and viscosity. After heating, the room-temperature measurements were repeated, and no variation was observed from the original room temperature data.

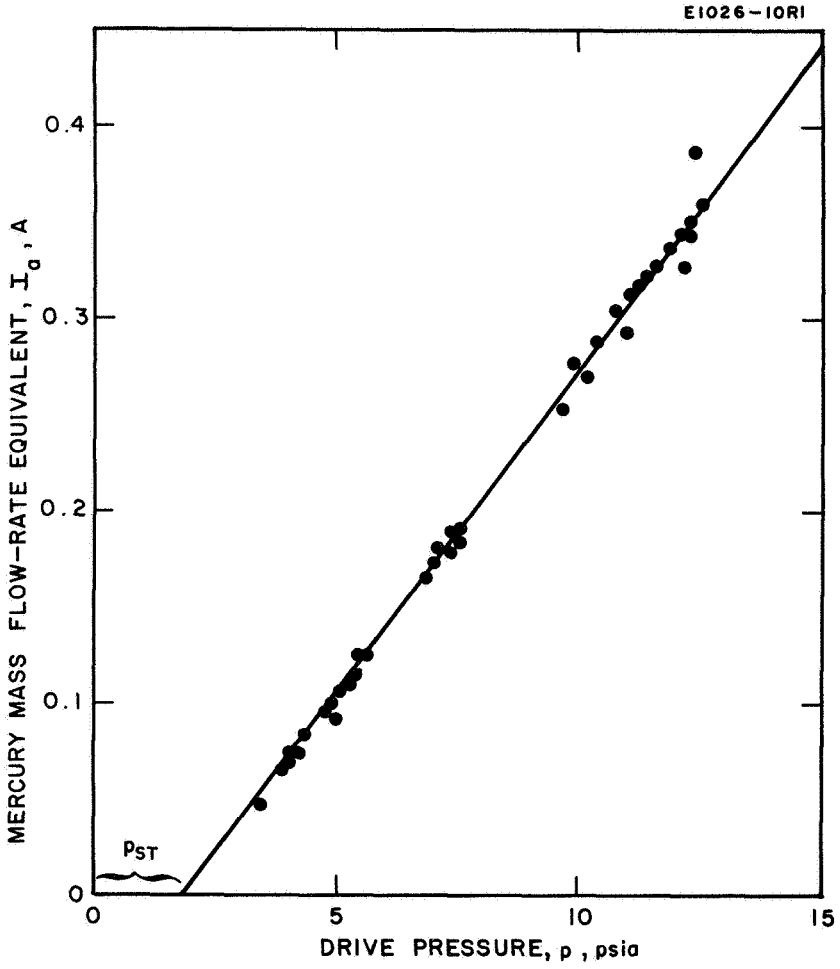

Fig. 31. Dependence of the mercury flow-rate equivalent (I_a) on drive pressure (p) for single-capillary flow impedance SC-3 at low drive pressures.

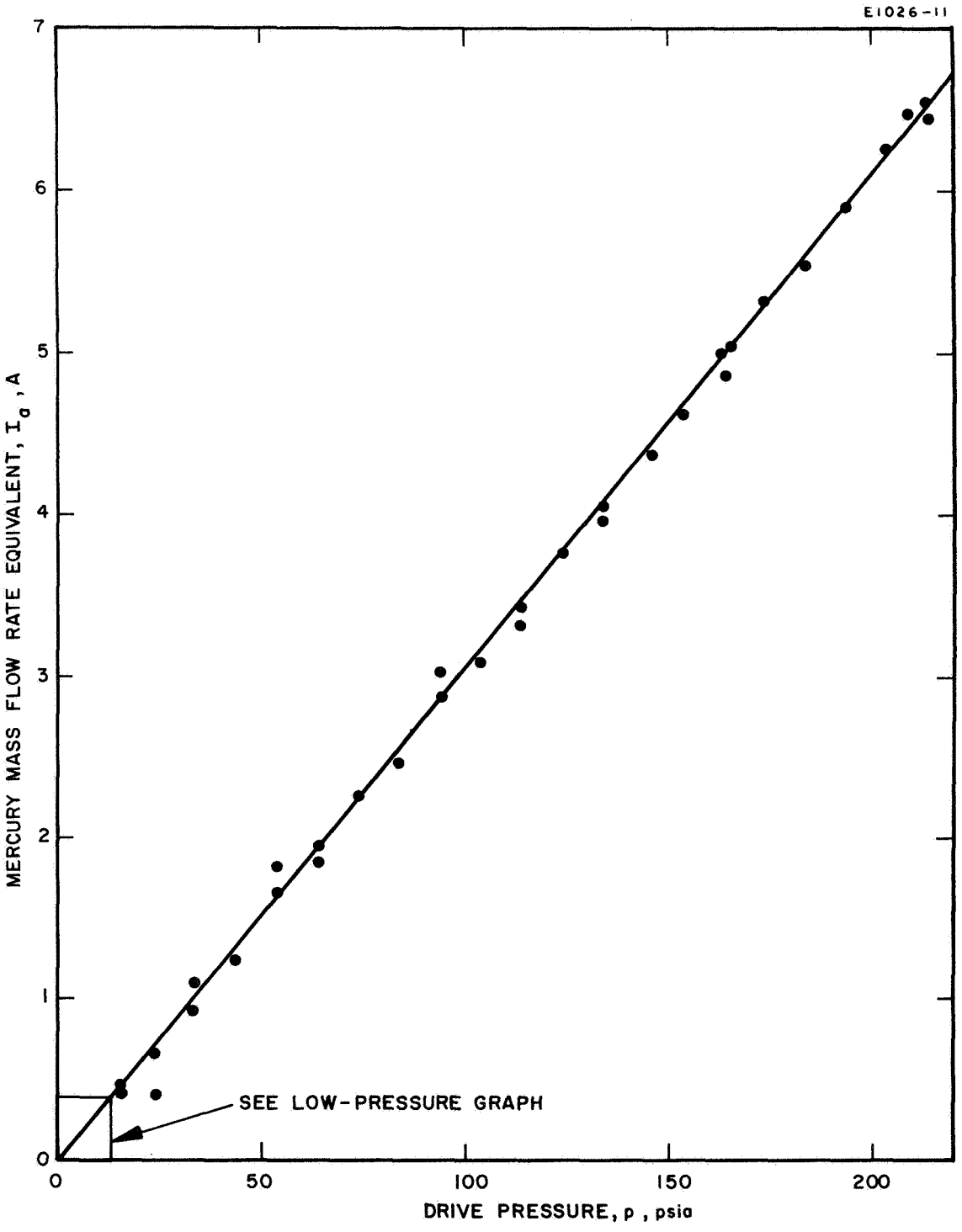

Fig. 32. Dependence of the mercury flow-rate equivalent (I_a) on drive pressure (p) for single-capillary flow impedance SC-3.

In summary, mercury flow-rate equivalents ranging from 50 mA to 6.5 A have been obtained for drive pressures ranging from 3.4 to 215 psia. The flow rate is linearly dependent on drive pressure, the results are repeatable over long periods of time, and the nature of the characteristics is not fundamentally altered by changes in impedance temperature.

At the time of the writing of this report, impedance SC-3 has been in operation for over 4000 hours.

d. Impedance SC-4

A new single-capillary impedance (SC-4) has demonstrated the superior flow characteristics which are expected from this type of impedance when it is attached to an LM cathode. This flow impedance consists of approximately 1,000 cm of 0.014-cm i.d. type 304 stainless steel tubing, wrapped on a stainless steel mounting spool. A section of capillary approximately 10 cm long extends from the mounting spool to a conical adapter with which the capillary can be connected directly to the cathode. The method of attachment, shown in Fig. 33, is similar to the technique which was used with impedance SC-2, where the capillary-to-cathode seal was made by pressing the stainless steel capillary tube directly against a molybdenum seat on the cathode body. In the present configuration, the nickel-titanium eutectic braze used with SC-2 has been replaced by an electron-beam weld, thus eliminating any possibility of mercury contact with a braze material. At the upstream end of the impedance, a section of capillary approximately 20 cm long is connected to the mercury supply by means of a teflon Swagelok fitting. A filter (consisting of a 0.0125 cm thick stainless steel diaphragm having ten 0.0025-cm diameter holes through it near the center) is placed between the mercury reservoir and the impedance to eliminate any possibility that foreign substances might clog the capillary or the cathode feed channel. The bulk of the capillary, which can be baked at temperatures up to 300°C in vacuum, is thermally isolated from the cathode and from the pressurized mercury feed system. Impedance SC-4 was cleaned and processed in vacuum using procedures similar to those employed with impedance SC-3.

Prior to being joined to an LM cathode, flow impedance SC-4 was operated alone to determine its flow characteristics; they were found to be similar to those of single-capillary SC-3. Impedance SC-4 was then connected to circular LM cathode K-41, and the assembly was operated in a diode discharge. The remarkable stability exhibited by the liquid-mercury surface (see Section IV-B-3-b) has demonstrated the freedom from

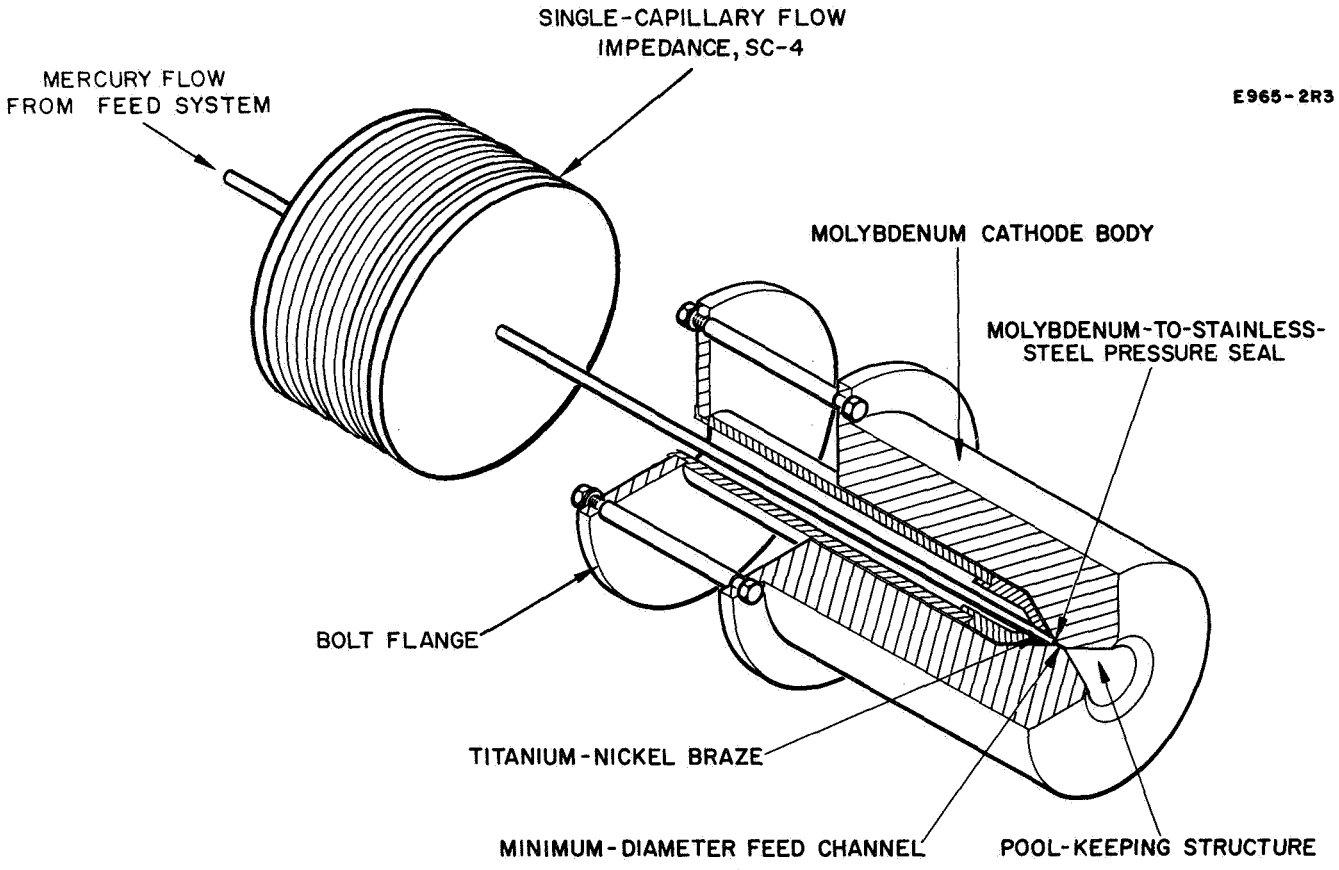

Fig. 33. Circular LM cathode K-41 with single-capillary flow impedance SC-4.

flow fluctuations which was expected of the single-capillary flow impedance. Impedance SC-4 has since been joined to annular LM cathode K-51 which was thermally integrated with the 30-cm thruster. With this cathode-impedance combination it is interesting to note from the data of Fig. 34 that the mercury flow rate approaches zero as the drive pressure is reduced to 9.5 psia. This reflects an increase in the pressure due to surface tension (p_{ST}), which results from the very small dimensions of the feed channel of K-51.

C. LIQUID MERCURY FEED SYSTEM

Performance of single-capillary impedance SC-4 has been entirely satisfactory for operation of LM cathode K-51 both during initial check-out in a diode discharge and when the cathode was subsequently thermally integrated and operated with the 30-cm thruster. The utility of the single-capillary flow impedance was sufficiently well established by the thruster test that it was then combined with an EM pump and a high-voltage isolator to form a prototype liquid-metal feed system.

1. Components Developed under Contract NAS 7-539

The liquid-mercury high-voltage isolator[20] is shown in Fig. 35. In this device (developed at HRL under Contract NAS 7-539) a hydrogen bubble is injected into a teflon section of the mercury feed line, where it forms an electrically insulating interruption of the mercury column. After the bubble has traveled a prescribed distance down the teflon tube, an electrical signal is generated by an electronic circuit connected with a bubble-sensing coil, and a new bubble is injected. The first bubble then proceeds to a porous-tungsten hydrogen vent, where it diffuses out of the feed line into the surrounding vacuum. Thus at least one hydrogen bubble is present in the teflon tube at all times.

Under the same contract an EM pump was designed, constructed, and tested.[20] This device, pictured in Fig. 36, is capable of generating pressure changes of the order of 1 atm with a power expenditure of only a few watts. The pressure head produced has been shown to be greater than 80% of the theoretical maximum calculated from a knowledge of the pump dimensions, magnetic field, and the measured driving current.[20] The ohmic heat generated in the mercury was readily dissipated by conduction. (Convective heat transfer is negligible, because the mercury flow rate is small.) Details of the EM pump performance are shown in Fig. 37.

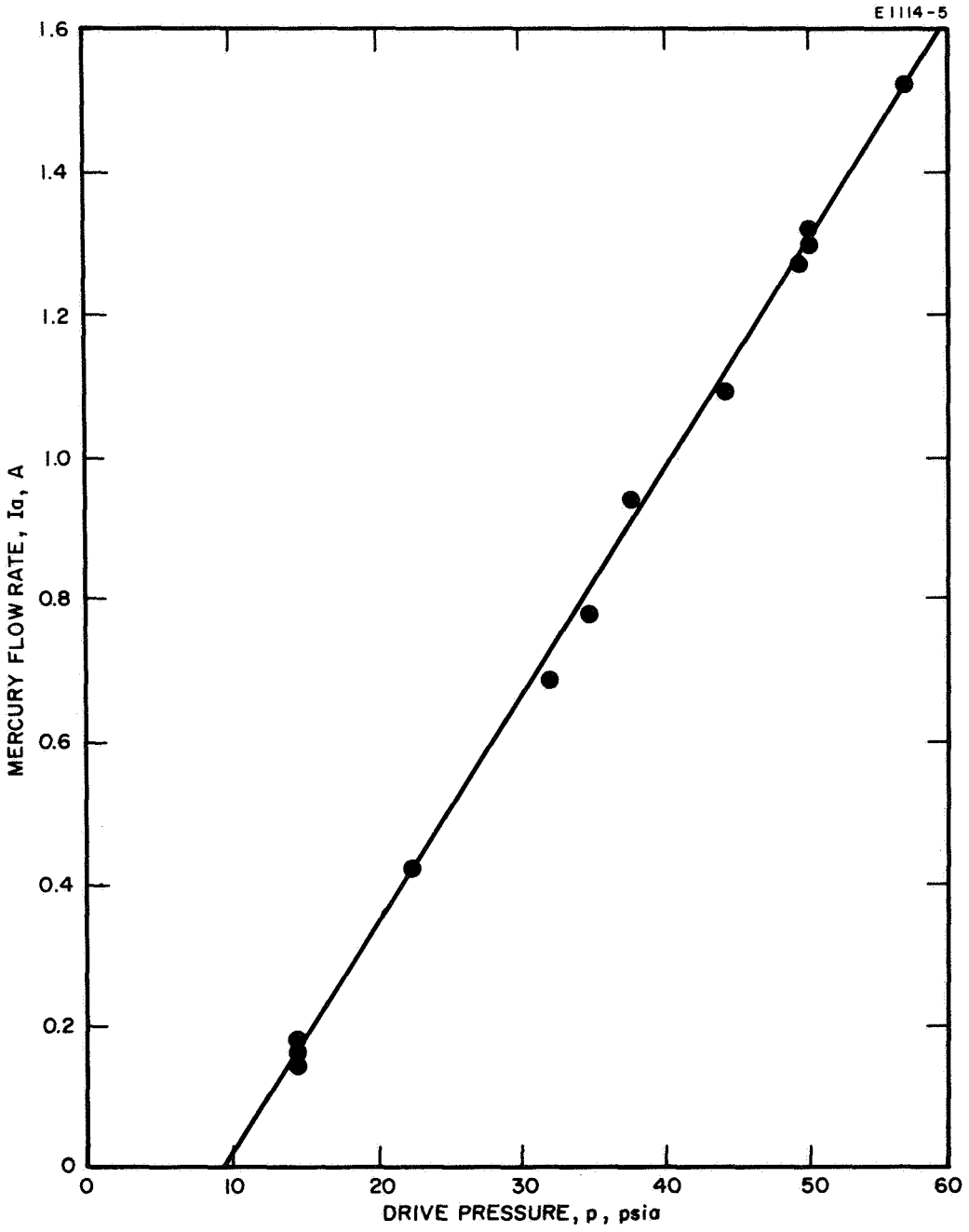

Fig. 34. Dependence of the mercury flow-rate equivalent (I_a) on drive pressure (p) for single-capillary flow impedance SC-4 with LM cathode K-51 attached.

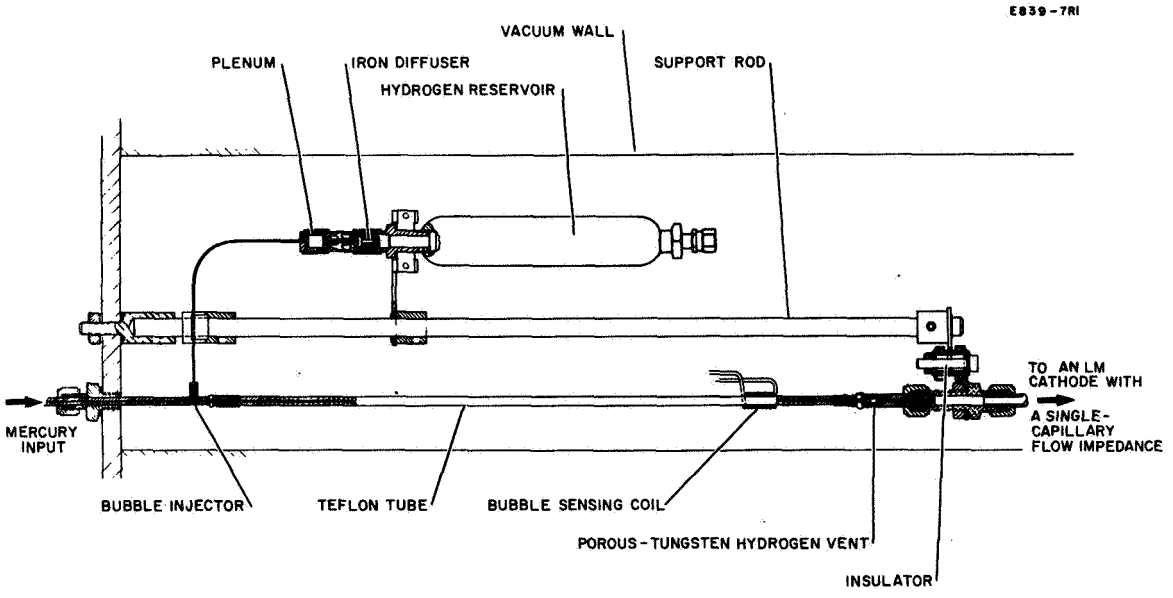

Fig. 35. High-voltage hydrogen-bubble isolator system.

M 5593

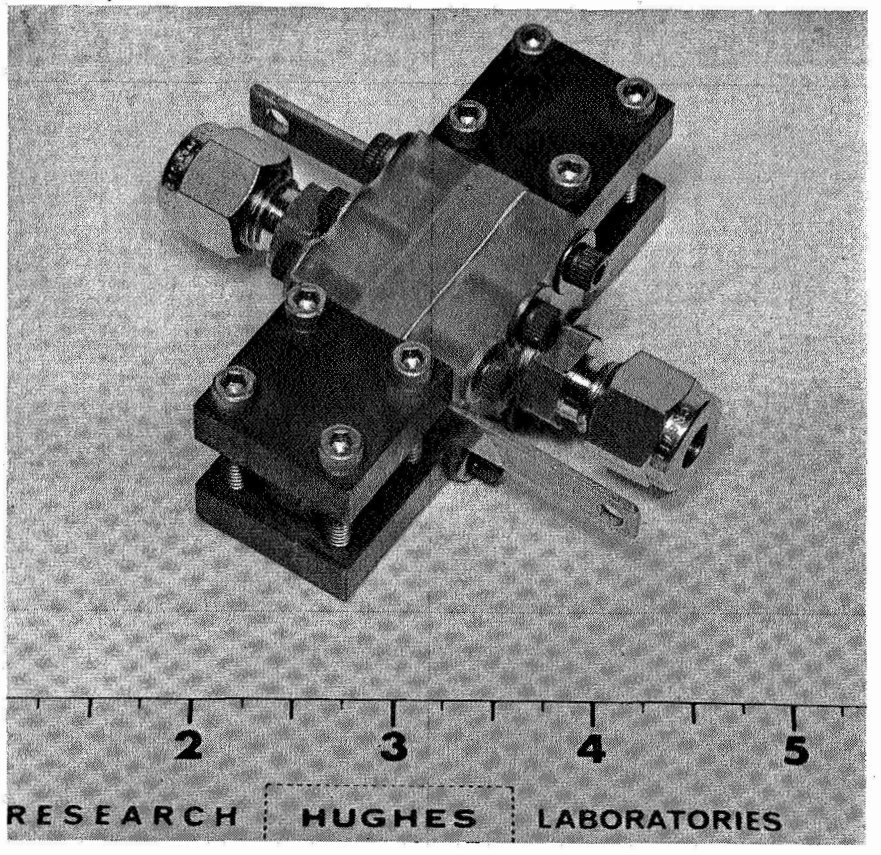

(a)

M 5595

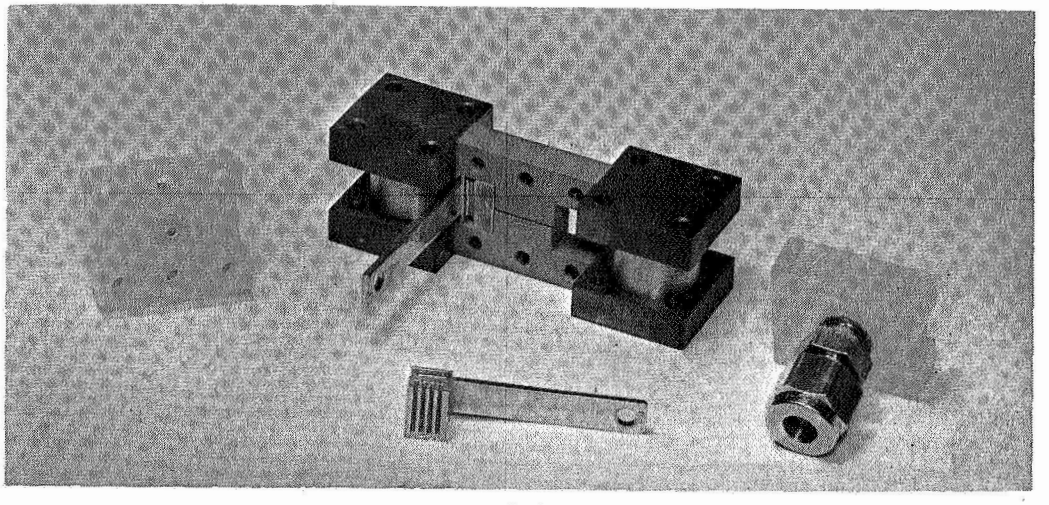

(b)

Fig. 36. Photograph of electromagnetic mercury pump. (a) Complete pump. (b) Pump components.

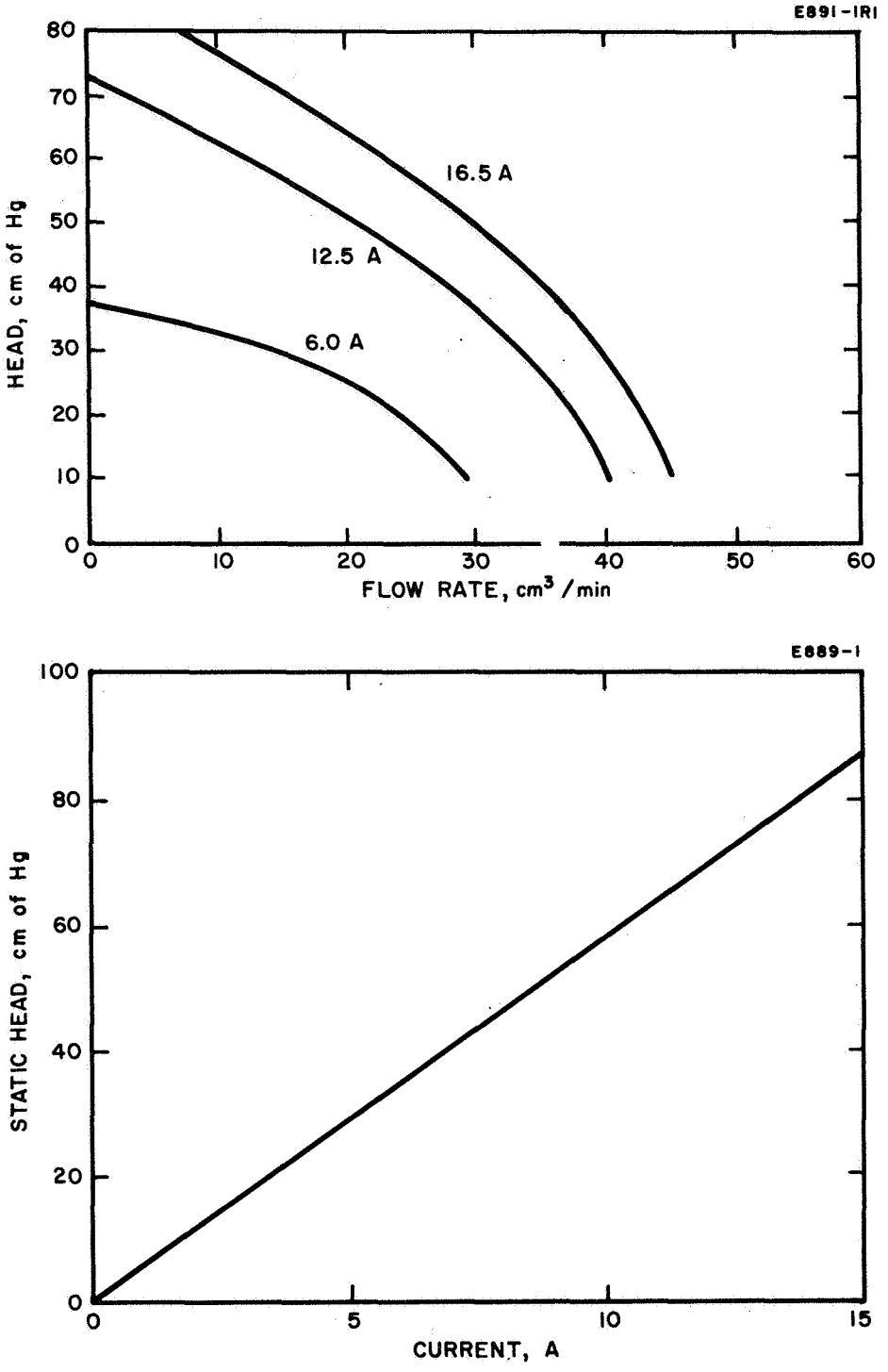

Fig. 37. Electromagnetic pump performance curves.

Both the EM pump and the high-voltage isolator were requalified under the subject contract to gain familiarity with their operation. The EM pump was sealed against mercury or vacuum leaks, filled with mercury, and attached to a mercury manometer. Measurements with the manometer confirmed that pressure differences were generated in proportion to the electrical driving current. The hydrogen-bubble high-voltage isolator was operated in conjunction with single-capillary-fed LM cathode K-41. Uninterrupted automatic operation of the LM cathode discharge under the condition of high-voltage isolation was demonstrated for periods of several hours at voltages up to 4.5 kV. The LM cathode functioned normally when operated in conjunction with the hydrogen bubble isolator. With the single-capillary flow impedance SC-2 located downstream of the isolator, the mercury driving pressure to the cathode remained constant in spite of the alternate injection and evacuation of hydrogen bubbles from the flow line. No fluctuations were observed in the flow of mercury to the cathode in response to hydrogen bubble formation or evacuation at the isolator.

During the period of component requalification, the control circuitry of the hydrogen-bubble high-voltage isolator was modified in an effort to improve its operational capabilities. In normal operation of the high-voltage isolator, hydrogen bubbles are forced into the mercury stream by thermal-expansion pressure which is developed when a plenum chamber is heated intermittently by a pulsed electrical resistance heater. In its original design, the control circuit for the pulsed heater employed a mechanical relay. A modified configuration has been operated satisfactorily in which the relay is replaced by a transistor switching circuit, thereby eliminating the only moving part of the entire isolator system. Furthermore, two new modes of operation have been demonstrated. In the first mode, the bubble-sensing coil and associated electronic circuitry are replaced by a clock-timer which pulses the plenum heater to eject bubbles at a sufficient rate to assure that at least one bubble is present in the insulating section of the mercury feed line in spite of possible variations in the mercury feed rate over the range of operation of the thruster system. The second new mode of operation considerably reduces the number of active elements in the isolator system and reduces or possibly eliminates the power requirements for this component. In this mode of operation, the pulse heater is not used; instead, the hydrogen gas flows at a constant rate into the plenum chamber which is maintained at a constant temperature. In order for the hydrogen gas to penetrate the mercury column within the liquid mercury feed line, the gas pressure must rise to a value which exceeds the sum of the hydrostatic

pressure of the mercury and the pressure which opposes gas penetration arising from surface-tension forces. Once this pressure is exceeded and the hydrogen bubble begins to expand into the mercury feed line, the pressure due to surface-tension forces is reduced, because the mercury feed line is of a larger diameter than the hydrogen feed line. As the mercury column is penetrated fully by the expanding bubble, the flow of gas is no longer opposed by pressure due to surface-tension forces, and the bubble expands freely until the gas pressure in the plenum is reduced to the hydrostatic pressure of the mercury liquid. At this point expansion of the gas ceases, the liquid mercury column again seals off the hydrogen gas inlet line, and the plenum pressure begins to rise to the higher value which is required to inject the next bubble. The only power required for this mode of operation is that which heats the iron plug through which the hydrogen gas diffuses into the plenum chamber. If, in a future design, this iron plug can be replaced by a diffusion element which operates at normal ambient temperature, the hydrogen-bubble high-voltage isolator can be operated with no expenditure of electrical power.

2. Breadboard Flow System

A breadboard flow system was assembled for a final demonstration of component utility and system compatibility. The system is shown in Fig. 38 and consists of (1) a gas-pressurized positive expulsion mercury reservoir, (2) an EM pump, (3) a hydrogen-bubble high-voltage isolator, (4) single-capillary flow impedances SC-3 or SC-4, and (5) the 30-cm thermally integrated thruster operated with high-temperature LM cathode K-51. The function of the components of this system is described below.

To assure complete utilization of liquid-mercury propellant in a zero-gravity environment, some form of positive expulsion reservoir will probably be required. In practice, the appearance of the reservoir would undoubtedly be different[17] from that shown schematically in Fig. 38, but its function would be quite similar. To serve as a driving force, pressurized nitrogen is applied above a piston pressing on the mercury surface. The piston position is measured with a dial indicator (calibrated to 0.001 in. or 0.000,1 in.) contacting the top of the piston shaft. This serves as an indication of mercury consumption and yields an accurate measure of the mercury flow rate.

The liquid mercury is expelled at a pressure approximately equal to that of the nitrogen gas on top of the piston. As

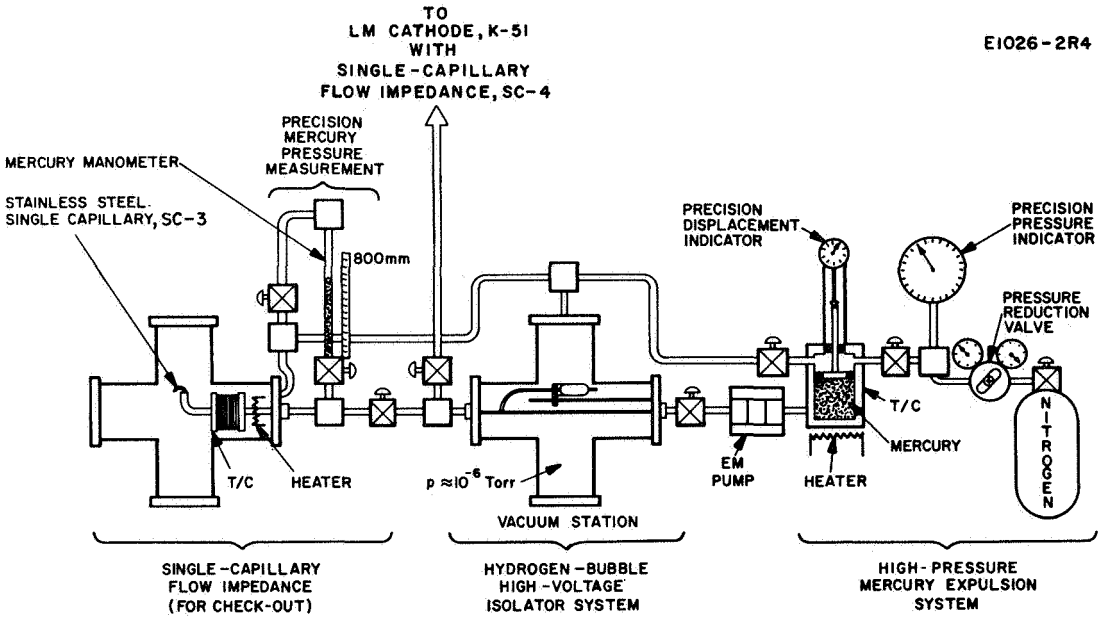

Fig. 38. Breadboard liquid-mercury flow system.

needed to vary the mercury flow rate, the mercury pressure can be varied by means of the EM pump located downstream of the positive-expulsion reservoir.*

Before reaching the single-capillary flow impedance, the mercury passes first through the hydrogen-bubble high-voltage isolator, which electrically isolates the thruster from its expellant supply. This capability is of importance where several thrusters in an array share a common expellant feed system.[19] The hydrogen-bubble high-voltage isolator must be placed upstream of the flow impedance to guarantee uniform flow at the LM cathode in spite of the alternate injection and evacuation of hydrogen bubbles from the flow line.

The single-capillary flow impedance was described in detail in the preceding section. Its function is to establish a mercury flow rate which bears a linear relation to the applied pressure. The characteristics of the single-capillary flow impedance are sufficiently linear and repeatable to be used both for flow control and flow measurement, although in this application it was used only for control. A filter (consisting of a 0.0125 cm thick stainless steel diaphragm having ten 0.0025 cm holes through it near the center) is placed upstream of the single-capillary impedance.

---

*Operation of the breadboard flow system revealed that location of the EM pump upstream of the hydrogen-bubble high-voltage isolator had been an inopportune choice. The hydrogen-bubble high-voltage isolator is designed to operate close to a delicate balance between the pressure of the liquid mercury and the pressure of the hydrogen gas. If the EM pump is located as shown in Fig. 38, the isolator reacts to a pressure decrease by issuing a plurality of bubbles, and to a pressure increase by failing to issue a bubble for a considerable length of time (possibly causing a temporary short-circuit condition). Unfortunately, it was too late to relocate the EM pump within the duration of the contract, and thus the EM pump was not electrically actuated while the system test was in progress. In future systems, the EM pump will be located between the high-voltage isolator and the single-capillary flow impedance.

Single-capillary flow impedance SC-3 was used to establish the fact that all components of the liquid-mercury breadboard feed system were operating together properly. Simultaneously, in a separate vacuum enclosure, the 30-cm thermally integrated thruster was operated with single-capillary-fed LM cathode K-51. Mercury flow to LM cathode K-51 was regulated by single-capillary impedance SC-4 driven by a separate gas-pressurized mercury expulsion system. After both the thruster (with its own mercury feed system) and the breadboard mercury feed system had demonstrated separately that they were functioning properly, the pressurized mercury from the breadboard system was diverted into the feed system of the 30-cm thruster.

For testing the LM cathode thruster system, the hydrogen-bubble high-voltage isolator was operated in the clock-timer mode with the plenum heater pulsed on every 7-1/2 min for a duration of 1-1/2 min. At this rate, a bubble would travel about one-half of the length of the insulating section of the mercury feed line when the next bubble was generated. The flow system has demonstrated reliable operation, and the cathode-impedance combination has continued to operate repeatably at all times. The successful operation of the LM cathode thruster with the prototype liquid-metal feed system constitutes a new level of readiness for the LM cathode thruster system.

SECTION VI

CONCLUSIONS

The LM cathode electron-bombardment thruster has demonstrated the various capabilities which are required for the creation of a viable thruster system. Proceeding from now existing technology, a laboratory thruster system can be built which imposes minimal requirements on external circuitry for accurate control while simultaneously imposing minimal constraints on its external environment. The thruster has been shown to be thermally self-sufficient with demonstration of efficient operation of the 30-cm thruster incorporating a single-capillary-fed thermally integrated LM cathode. By joining the 30-cm thermally integrated thruster with a breadboard liquid-mercury feed system and an LM cathode neutralizer, an over-all thruster system efficiency $\eta_T = 72.6\%$ has been demonstrated at a specific impulse $I_{sp,eff} = 3990$ sec. This efficiency equals the performance originally anticipated for the operation of other electron-bombardment thruster types for the year 1970, and as such represents highly competitive performance.

SECTION VII

RECOMMENDATIONS AND FUTURE PLANS

The devices and technology which now exist serve as a firm basis upon which to extend the level of sophistication of each of the components and to bring the components together into a reliable and useful thruster system. The existing 20-cm LM cathode thruster and the existing 30-cm thermally integrated LM cathode thruster together have demonstrated the capability for operation of a thermally integrated LM cathode thruster which is optimized for operation over a range of beam current. The efficacy of the thermal design of the 30-cm thruster should be evaluated by comparison of the predictions of thermal analysis with measured thruster temperatures. This comparison will be useful for improving the procedures of thermal analysis which will be employed in the design of new LM cathode thrusters. Wherever deficiencies have been uncovered in past operation of any system component, the component should be redesigned and refabricated with emphasis placed on reliability, thruster system compatibility, and ease of operation.

The LM cathode neutralizer has shown promise that it is capable of long lifetime similar to that exhibited by the main thruster cathode, while operating under conditions which subtract little from the over-all efficiency of the thruster system. In the past, LM cathode neutralizers have utilized a copper feed channel to stabilize the mercury flow upstream of the molybdenum pool-keeping structure. Although neutralizer operating life in excess of 500 hours and shelf life (in contact with mercury) in excess of 6,500 hours has been demonstrated, amalgamation of the copper may result in an insufficiently long life for this configuration. Research is necessary to establish, and possibly to extend, the lifetime of LM cathode neutralizer systems. In a promising new design, an all-molybdenum LM cathode neutralizer is expected to achieve adequate flow stability by virtue of being fed by a single-capillary flow impedance. This design is expected to result in a very long lifetime capability.

SECTION VIII

INVENTIONS AND NEW TECHNOLOGY

A. FIRST QUARTER

An invention, which had been conceived prior to the contract start date, has been reduced to practice with work which began during the first quarter of the subject contract effort.

LM Cathode with a Single-Capillary Flow Impedance (Patent Docket No. PD 68277)

Inventor: J. Hyman, Jr.

Progress Reports: First Quarterly Report on this contract, 15 May 1968, pp. 21-23; Second Quarterly Report on this contract, 15 August 1968, pp. 23-29; Third Quarterly Report on this contract, 15 November 1968, pp. 27-36; and this report.

B. SECOND QUARTER

During the second quarter of the subject contract effort, two items of new technology have been reduced to practice.

1. Linear-Slit LM Cathode

   Innovator: W. O. Eckhardt

   Progress Reports: First Quarterly Report on this contract, 15 May 1968, pp. 18 & 19; Second Quarterly Report on this contract, 15 August 1968, p. 14; Third Quarterly Report on this contract, 15 November 1968, pp. 9-11; and this report.

2. 30-cm Thermally-Integrated Electron-Bombardment Thruster Using an LM Cathode

   Innovator: J. Hyman, Jr.

   Progress Reports: First Quarterly Report on this contract, 15 May 1968, pp. 35-37; Second Quarterly Report on this contract, 15 August 1968, pp. 3-10; Third Quarterly Report on this contract, 15 November 1968, pp. 9-11; and this report.

C. THIRD QUARTER

No reportable items of new technology were identified during the third quarter of the subject effort.

D. FOURTH QUARTER

During the final quarter of the subject contract effort, an invention was conceived and reduced to practice.

Fluidic Bubble Injector (with application to High-Voltage Isolators for Liquid Metal Feed Lines), (Patent Docket No. PD 69113)

Inventor: J. Hyman, Jr.

Progress Report: This report.

All inventions and items of new technology have been reported to the NASA Western Operations Office.

REFERENCES

1. W.R. Kerslake, D.C. Byers, and J.F. Staggs, "SERT II Experimental Thruster System," AIAA Paper No. 67-700.

2. R.T. Bechtel, "Discharge Chamber Optimization of the SERT II Thruster," AIAA Paper No. 67-668.

3. R.T. Bechtel, G.A. Csiky, and D.C. Byers, "Performance of a 15-cm Diameter Hollow-Cathode Kaufman Thruster," NASA Lewis Research Center, Cleveland, Ohio, NASA TM X-52376, 1968.

4. W.O. Eckhardt, K.W. Arnold, G. Hagen, J. Hyman, Jr., J.A. Snyder, and R.C. Knechtli, "High-Temperature Liquid-Mercury Cathodes for Ion Thrusters," Summary Report, Contract NASW-1404, July 1967.

5. W.O. Eckhardt, H.J. King, J.A. Snyder, J.W. Ward, G. Hagen, W.D. Myers, and R.C. Knechtli, "Liquid-Mercury Cathode Electron-Bombardment Ion Thrusters," Summary Report, Contract NAS 3-6262, October 1966.

6. J. Hyman, W.O. Eckhardt, R.C. Knechtli, and C.R. Buckey, "Formation of Ion Beams from Plasma Sources: Part I," AIAA J. 2, 1739 (1964).

7. Liquid Metals Handbook, U.S. Government Printing Office, 2nd Ed., 165, (June 1954). J. Nejedlik and E. Vargo, "Material Resistance to Mercury Corrosion," Electrochemical Technology, Vol. 3, pp. 9-10, 250 (1965). W. Latimer and J. Hildebrand, Principles of Chemistry and Reference Book of Inorganic Chemistry (Macmillan, New York, 1940), p. 90. H. Logan, The Stress Corrosion of Metals (Wiley, New York, 1966), p. 193. H. Uhlig, The Corrosion Handbook (Wiley, New York, 1948), p. 618. B. Power and F. Robson, "Experiences with Demountable U.H.V. Systems," Tech. Rep. of Edwards High Vacuum Ltd., Crawley, Sussex, England.

8. J. Hyman, Jr., W.O. Eckhardt, J.W. Pfeifer, and J.A. Snyder, "High-Temperature LM Cathode Ion Thrusters," Quarterly Report No. 1, Contract JPL 952131, Hughes Research Laboratories, May 1968; NASA Accession No. N68-27741.

9. J. Hyman, Jr., W.O. Eckhardt, and J.A. Snyder, "High-Temperature LM Cathode Ion Thrusters," Quarterly Report No. 2, Contract JPL 952131, Hughes Research Laboratories, August 1968; NASA Accession No. N68-36658.

10. J. Hyman, Jr., J.R. Bayless, J.A. Snyder, and W.O. Eckhardt, "High-Temperature LM Cathode Ion Thrusters," Quarterly Report No. 3, Contract JPL 952131, Hughes Research Laboratories, November 1968.

11. N.B. Kramer and H.J. King, "Extraction of Dense Ion Beams from Plasmas," J. Appl. Phys. 38, 4019 (1967).

12. T.D. Masek and E.V. Pawlik, "Thrust System Technology for Solar Electric Propulsion," AIAA Paper No. 68-541, AIAA 4th Propulsion Joint Specialists Conference, Cleveland, Ohio, June 1968.

13. G.R. Brewer, K. Amboss, G. Nudd, H.J. King, R. Seliger, and S. Kami, "Ion Engine Thruster Vector Study," Quarterly Report No. 1, Phase II, Contract JPL 952129, Hughes Research Laboratories, December 1968.

14. E.A. Richley and W.R. Kerslake, "Bombardment Thruster Investigations at the Lewis Research Center," AIAA Paper No. 68-542, AIAA 4th Prop. Joint Specialist Conf., Cleveland, June 1968.

15. E.A. Richley and R.T. Bechtel, Cleveland, Ohio, June 1968, personal communication.

16. W. Knauer, R.L. Poeschel, H.J. King, and J.W. Ward, "Discharge Chamber Studies for Mercury Bombardment Ion Thrusters," Final Report, Contract NAS 3-9703, September 1968.

17. T.D. Masek and J.R. Womak, "Experimental Studies with a Clustered Ion Engine System," AIAA Paper No. 67-698, AIAA Electric Propulsion and Plasma Dynamics Conference, Colorado Springs, Colorado, September 1967.

18. G. Eckhardt, "Efflux of Mercury Atoms from the Cathode Spots of the Low-Pressure Arc," Research Report No. 395, Hughes Research Laboratories, Malibu, July 1968.

19. "Solar Powered Electric Propulsion Spacecraft Study," Final Report, JPL Contract No. 951144, Hughes Space Systems Division, December 1965; NASA Accession No. N66-19626.

20. J.H. Molitor, H.J. King, and S. Kami, "A Study of Liquid Mercury Isolator Development," Hughes Research Laboratories, Final Report, Contract No. NAS 7-539, September 1967.

21. F.W. Sears, Principles of Physics, I (Addison-Wesley, Reading, Mass., 1947).